Graphene-Modified Pencil Graphite Bismuth-Film Electrodes for the Determination of Heavy Metals in Water Samples Using Anodic Stripping Voltammetry

A thesis submitted in fulfilment of the requirements for

the degree of

Magister Scientiae in Nanoscience (Chemistry)

Department of Chemistry: SensorLab

University of the Western Cape

November 2013

Supervisor: Dr. N. Jahed

Co-supervisor: Prof. E.I. Iwuoha

by

Keagan Pokpas

BSc (Hons) Chemistry (University of the Western Cape)

Graphene-Modified Pencil Graphite Bismuth-Film Electrodes for the Determination of Heavy Metals in Water Samples Using Anodic Stripping Voltammetry

Keagan Pokpas

KEY WORDS:

Square-wave Anodic Stripping Voltammetry

Trace Metal Analysis

Heavy Metal Detection

Bismuth-Film

Pencil Graphite Electrode

Graphene

Electrochemical Reduction

Nafion

Nanocomposite

Chemical Sensor

ABSTRACT

Electrochemical platforms were developed based on pencil graphite electrodes (PGEs) modified with electrochemically deposited graphene (EG) sheets and Nafion-graphene (NG) nanocomposites in conjunction with an *in situ* plated bismuth-film (EG-PG-BiE and NG-PG-BiE). The EG- and NG-PG-BiEs were used as sensing platforms for determining Zn^{2+}, Cd^{2+} and Pb^{2+} by square wave anodic stripping voltammetry (SWASV). EG sheets were deposited onto pencil graphite electrodes by cyclic voltammetric reduction from a graphene oxide (GO) solution, while a dip coating method was used to prepare the NG-PG-BiE. The GO and graphene, with flake thicknesses of 1.78 (2 sheets) and 2.10 nm (5 sheets) respectively, was characterized using FT-IR, HR-SEM, HR-TEM, AFM, XRD and Raman spectroscopy. Parameters influencing the electroanalytical response of the EG-PG-BiE and NG-PG-BiE such as, bismuth ion concentration, deposition potential, deposition time and rotation speed were investigated and optimized. The EG-PG-BiE gave well-defined, reproducible peaks with detection limits of 0.19 µg L^{-1}, 0.09 µg L^{-1} and 0.12 µg L^{-1} for Zn^{2+}, Cd^{2+} and Pb^{2+} respectively, at a deposition time of 120 seconds. The NG-PG-BiE showed similar detection limits of 0.167 µg L^{-1}, 0.098 µg L^{-1} and 0.125 µg L^{-1} for Zn^{2+}, Cd^{2+} and Pb^{2+} respectively. For real sample analysis, the enhanced voltammetric sensor proved to be suitable for the detection and quantitation of heavy metals below the US EPA prescribed drinking water standards of 5 mg L^{-1}, 5 µg L^{-1} and 15 µg L^{-1} for Zn^{2+}, Cd^{2+} and Pb^{2+} respectively.

DECLARATION

I declare that the study **"Graphene-Modified Pencil Graphite Bismuth-Film Electrodes for the Determination of Heavy Metals in Water Samples Using Anodic Stripping Voltammetry"** is my own work. It has not been submitted for any degree or examination in any university, and all the resources I have used or quoted have been indicated and acknowledged by complete references.

Keagan Pokpas November 2013

Signed…….

ACKNOWLEDGEMENTS

Firstly I would like to thank God the Almighty for providing me with endless opportunities, strength and encouragement. Thank you for being my pillar.

To my supervisor, Dr. Nazeem Jahed, I wish to extend my sincerest gratitude. Thank you for your guidance, endless insight, encouragement and continuous support.

I would like to extend my gratitude to Prof. Emmanuel Iwuoha and Prof. Priscilla Baker, the co-chairs of SensorLab as well as UWC chemistry department staff. Thank you for the opportunity and trust placed in me. Thank you for your continuous support.

Sincere thanks to all SensorLab members and staff. Thank you for the endless discussions and laughs shared. Your support means a great deal to me.

A special thanks to Department of Science and Technology (DST) and National Research Foundation (NRF) for financial support.

Lastly, to my family and friends; thank you for all the sacrifices, support and good times. Thank you for the encouragement in difficult times. Without you this would not be possible. Words cannot express what it has and continues to mean to me.

“Nothing in the world is more flexible and yielding than water. Yet when it attacks the firm and the strong, none can withstand it, because they have no way to change it. So the flexible overcome the adamant, the yielding overcome the forceful. Everyone knows this, but no one can do it.”

- Lao Tzu.

LIST OF PUBLICATIONS

CONFERENCE PROCEEDINGS

Poster presentations

1. Pokpas, K.; Zbeda, S.; Jahed, N.; Baker, P.G.L. and Iwuoha, E.I. "*Electrodeposited Graphene Modified Pencil Graphite Bismuth-film Electrodes (EG-PG-BiFE) for the determination of Trace Metals by Anodic Stripping Voltammetry*" at the 13th Topical Meeting of the International Society of Electrochemistry, Advances in Electrochemical Materials Science and Manufacturing, 7-10 April, **2013**, CSIR, Pretoria, South Africa.
2. Pokpas, K. and Jahed, N. "*Electrodeposition of Reduced Graphene Oxide Pencil Graphite Bismuth-Film Electrodes for the Determination of Trace Metals by Anodic Stripping Voltammetry*", Belgian Economic Mission, 25 October **2013**, University of the Western Cape, Cape Town, South Africa
3. Pokpas, K.; Zbeda, S.; Jahed, N.; Baker, P.G.L. and Iwuoha, E.I. "*Electrodeposited Graphene Modified Pencil Graphite Bismuth-film Electrodes (EG-PG-BiE) for the determination of Trace Metals by Anodic Stripping Voltammetry*", Postgraduate Research Open Day, 30 October **2013**, University of the Western Cape, Cape Town, South Africa

JOURNAL PUBLICATION

1. K, Pokpas, S. Zbeda, N, Mohammed, N. Jahed, P. Baker and E. Iwuoha, "Electrochemically Reduced Graphene Oxide Pencil Graphite *in situ* Plated Bismuth-film Electrode for the Determination of Trace Metals by Anodic Stripping Voltammetry" *International Journal of Electrochemical Science,* vol. 8, Accepted **2013**.
2. S. Zbeda, K. Pokpas, S. Titinchi, N. Jahed, P. Baker and E. Iwuoha, "Few-layer Binder Free Graphene Modified Mercury Film Electrode for Trace Metal Analysis by Square Wave Anodic Stripping Voltammetry," *Int. J. Electrochem. Sci., V*ol. 8, pp. 11125-11141, **2013**.

TABLE OF CONTENTS

LIST OF FIGURES

LIST OF TABLES

LIST OF ABBREVIATIONS

2D	Two Dimensional
3D	Three Dimensional
AAS	Atomic Adsorption Spectroscopy
ABS	Acetate Buffer Solution
AdSV	Adsorptive stripping voltammetry
AE	Auxiliary Electrode
AFM	Atomic Force Microscopy
ASV	Anodic Stripping Voltammetry
ATR	Attenuated Total Reflectance
BiE	Bismuth Film Electrode
BiF	Bismuth Film
CE	Counter Electrode
CNT	Carbon Nanotube
CSV	Cathodic Stripping Voltammetry
CV	Cyclic Voltammetry
CVD	Chemical Vapour Deposition
D.L.	Detection Limit
DMF	N,N-Dimethylformamide
DNA	Deoxyribonucleic Acid
DPP	Differential Pulse Polarography
DPV	Differential Pulse Voltammetry
DPSV	Differential Pulse Stripping Voltammetry
EC	Electrochemical

EDS	Energy Dispersive X-Ray Spectroscopy
EG	Electrodeposited Graphene
EG-PG-BiE	Electrodeposited Graphene Pencil Graphite Bismuth Film Electrode
EPA	Environmental Protective Agency
Eqn.	Equation
FAAS	Flame Atomic Absorption Spectrophotometry
FET	Field-Effect Transistor
FT-IR	Fourier Transformed Infrared
GCE	Glassy Carbon Electrode
GE	Gold Electrode
GFAAS	Graphite Furnace Atomic Absorption Spectroscopy
GO	Graphene Oxide
G-PG-BiE	Graphene Pencil Graphite Bismuth Film Electrode
HgFE	Mercury Film Electrode
HMDE	Hanging Mercury Drop Electrode
HRSEM	High Resolution Scanning Electron Microscopy
HRTEM	High Resolution Transmission Electron Microscopy
ICP	Inductively Coupled Plasma Spectroscopy
ICP-MS	Inductively Coupled Plasma Mass Spectroscopy
ICP-OES	Inductively Coupled Plasma Optical Emission Spectroscopy
L.O.D.	Limit of Detection
MCL	Maximum Contamination Level

MFE	Mercury Film Electrode
NG	Nafion-graphene
N-PG-BiE	Nafion Pencil Graphite Electrode
NG-PG-BiE	Nafion-graphene Pencil Graphite Bismuth Film Electrode
NPV	Normal Pulse Voltammetry
PG	Pencil Graphite
PGE	Pencil Graphite Electrode
ppb	Parts Per Billion
ppm	Parts Per Million
RE	Reference Electrode
RNA	Ribonucleic Acid
RSD	Relative Standard Deviation
SECM	Scanning Electrochemical Microscopy
SV	Stripping Voltammetry
SW	Square Wave
SWASV	Square Wave Anodic Stripping Voltammetry
SWCNT	Single Walled Carbon Nanotube
SWV	Square Wave Voltammetry
US	United States
USEPA	United States Environmental Protection Agency
WDS	Windows Deployment Services
WE	Working Electrode
XRD	X-Ray Diffraction

CHAPTER ONE:

Introduction to the Study

1.1. Problem Statement

1.1.1. Heavy Metal Contamination

Heavy metals are natural components of the earth's crust and are defined as any metal that is toxic at low concentrations, with density greater than 0.5 g cm^{-3} [1]. These metals have become important in industrial applications and ubiquitous in the environment. Furthermore they are kept under the environmental pollutant category due to their toxic effect on plants, animals and humans, even when present even in miniscule quantities [2, 3]. The release of heavy metals in biologically available forms, as a result of human activity, may damage or alter both natural and man-made ecosystems [4]. Heavy metals pose a very distinguishable problem which set them apart from other known contaminants, owing to their non-biodegradable nature [2, 5]. This feature leads to their bioaccumulation in vital organs and lead to the toxic nature of these metals. Of the large number of heavy metals in existence today, Lead, Cadmium, Mercury and Arsenic pose the most alarming concerns. Some of which have been known to lead to cancer, heart disease, anorexia, brain damage *etc.* [2]. In recent years, the increase in heavy metal contamination has become widespread around the world in the form of pollution as well as food sources and drinking water [6]. Pollution in the environment may occur in different forms including anthropogenic activities such as mining and industrial processing [7]. Contaminated drinking

water from lead pipes as well as pollution from the industrial sector are the most common sources in modern times [8].

Heavy metals can also appear in the form of inorganic and organic complexes. Appearance of different heavy metal chemical forms will depend also from chemical nature of a given heavy metal, conditions of environment, presence of complexation substances, colloid dispersion, etc. To what extent will heavy metals in water be mobile, depends from number of parameters:

• pH of water;

• Presence of carbonates and phosphates;

• Hydrated oxides of iron and manages;

• Content of organic matter;

• Sulphide ions and pirite (significant for mobilization process of heavy metals in water environment).

1.1.2. Toxicity of Heavy Metals

In considering the ever growing concern for heavy metal contamination of drinking and ground water sources, it is wise to become acquainted with the toxicological effects of lead, cadmium and zinc on the environment and higher living organisms. Severe illnesses, caused by exposure to heavy metal contamination have been well documented in medical journals in recent years. Although this is not a study on the toxicology of heavy metals, a brief description on their toxic effects are required for further emphasis.

Exposure to lead poisoning has decreased significantly over the last three decades due to the introduction of un-leaded petrol and low lead paints, however drinking water still remains a main source of lead contamination and was

responsible for 20 % of all lead contamination in the United States (US) in 2006 [9]. Inhalation, ingestion and absorption via the skin carry lead into the blood stream and allow for collection in soft tissue of the brain, liver and lungs. Symptoms of such poisoning by lead may include nausea, constipation and anorexia [10] and result in oxidative damage to brain, heart, kidneys, and reproductive organs [9, 11, 12] and may lead to miscarriages along with impaired nervous systems in unborn children [8]. Similarly cadmium emissions by man into the atmosphere and soil range from approximately 25000 – 29000 tons yearly and collect in rivers, drinking water supplies and agriculture [1, 5]. Significant links to lung cancer, lesions on the prostate, renal failure, kidney damage and hyper tension have been identified [8, 13, 14].Overexposure to zinc poses concern in infants and humans alike. Poisoning by zinc results in damage to the pancreas and causes harmful symptoms in unborn children [5].

Along with their toxic nature, beneficial health properties are also exhibited by many heavy metals. Copper and zinc as examples promote efficient metabolism and the lack of zinc in the blood stream of children and adults alike may lead to loss of appetite, decreased sense of taste and smell; slow wound healing and skin sores [8].

1.1.3. Environmental Monitoring

Water is largely regarded as the most essential natural resource on the planet and is essential in guaranteeing the basic quality of human life. A considerable increase in demand for clean rivers, lakes and ground water has been evident for some time. Access to improved drinking water in South Africa has shown a considerable increase between 1994 and 2012 [15] , while the initiative of Blue

Drop Certification developed in 2008 deals with decentralization of monitoring water sources [15]. The national government has implemented regulations and policies to deliver safe water to all. On site monitoring, technology for continuous surveillance and automatic monitoring are important aspects of water policies and may lead to real time results which secure product quality and waste water treatment. The United States Environmental Protection Agency (US EPA) has set a maximum contamination limit by which all water treatment facilities need to abide. The maximum contamination levels (MCL) of zinc, cadmium and lead are 5 ppm, 5 ppb and 15 ppb respectively [16].

The growing demand for clean water has led to the increased attention surrounding water purification and monitoring and as a result the need for determination and characterization of these contaminants. Determination of heavy metals has traditionally been carried out in laboratories, where time-consuming sampling, transportation, preparation and storage steps are employed. On site monitoring may reduce errors associated with contamination, losses and matrix changes along with time saved [17].

Techniques for metal determination center around spectroscopic techniques like atomic absorption spectroscopy (AAS) and inductively coupled plasma mass spectroscopy (ICP-MS) [18, 19] which are sensitive and can perform a wide range of elemental analysis. The major drawbacks however, include complicated equipment, high costs which may only determine total concentrations. Speciation is possible by extraction and separation procedures but increases the risk of contamination [6]. Historically, electrochemical (EC) techniques have been at the forefront of metal analysis and have in certain instances been developed for this

particular purpose. Anodic stripping voltammetry (ASV) is one such example. Inexpensive instrumentation and the possibility of metal speciation as well as accuracy in determination at the trace levels are advantages of electrochemical methods [20].

1.2. Motivation to the Study

Electrochemical anodic stripping voltammetry (ASV) has, in recent years been widely regarded as an extremely powerful technique for the determination and measurement of several metals, including Pb, Cd, Cu and Zn [21]. The electroanalytical technique provides quantitative and qualitative information of a particular species by measuring current as a function of potential. Its high sensitivity due to the built-in preconcentration step, good selectivity, inexpensive and portable instrumentation and its ability of measuring four to six analytes in a sample simultaneously in the sub parts per billion (sub-ppb) ranges are of the many intrinsic advantageous properties [22]. The main spectroscopic counterparts (GFAAS and ICP-OES) offer similar sensitivities but at high cost of analysis and instrumentation up-keep. The small size and low power demand of the stripping analysis instrumentation proves to be beneficial.

The working electrode material is of crucial importance to voltammetric analysis. The choice of material determines the species which may be measured as well as the degree of inferences and additional chemicals needed. Electrode properties include a wide potential window, high sensitivity and reproducible response [23]. Mercury electrode has for many years been the dominating electrode material in voltammetric analysis due to its high intrinsic overvoltage

towards the hydrogen evolution reaction. Both hanging mercury drop electrode (HMDE) and mercury film electrode (MFE) are utilized forming liquid metal amalgams during the reduction process limiting intermetallic compound formation resulting in well-defined peaks.

A major criticism often leveled at the stripping voltammetric technique is the use of mercury working electrodes which pose a health hazard and as a consequence there is a shift towards the search for more environmentally friendly mercury free working electrodes [24, 25]. Much work and research has been invested into the search for alternative electrode materials resulting in the use of antimony and bismuth working electrodes as alternatives to mercury working electrodes. The thin bismuth-film electrode shows similar or comparable results to that of mercury-film electrodes since bismuth is capable of forming "fused" alloys with trace metals which is analogous to the amalgams formed with mercury [26, 27]. Moreover, bismuth coated electrodes offer many attractive properties including, the simple preparation [24], high sensitivity, good stripping signal and excellent resolution of peaks [28].

Carbon based solid electrodes are suitable for a wide range of applications due to their wide potential window and low background current. Pencil graphite has been previously used as an electrode substrate material in different applications of stripping analysis. These applications include chemical and biosensors for determination of trace metals [29, 30], DNA and RNA [31] and uric acid in urine and blood samples [32]. The attractive features of PG distinguish it from other solid electrode materials. Pencil graphite has been evaluated as alternative to the common glassy-carbon and gold electrodes (GCE

and GE) due to its good conductivity, little pretreatment steps, low cost, low background current and large scale availability.

Coating the pencil graphite electrodes with Nafion has shown to increase the detection sensitivity and alleviate the interference from the surfactants [33]. Nafion is a perfluorinated ionomer containing negatively charged sulfonic groups [34, 35]. Its many applications include proton-conducting membrane material for fuel cells [36] and determination of cadmium and lead in conjunction with graphene [37, 22, 8]. The Teflon like hydrophobic backbone and highly hydrophilic ionisable sulfonic groups are responsible for Nafion's excellent chemical stability and ionic conductivity [38]. The unique ion- exchange, discriminative and biocompatibility properties have made Nafion-films useful for modifying electrode surfaces. The polar side chain of Nafion allows for CNTs and Graphene to be easily suspended in solutions of Nafion in phosphate buffer and alcohols [39].

The most common material on earth, carbon, forms the basis of all organic chemistry. Because the bonding is extremely flexible it forms a wide variety of structures and therefore also a wide variety of properties. Graphene, a 2D allotrope of carbon, is a very important material not only for fundamental research but also for device applications. It has its sp^2 hybridized carbon atoms arranged in a honeycomb structure of hexagons [8]. Graphene has been attracting a lot of attention since it was first produced in 2004 and has shown to significantly improve the sensitivity in various applications [40]. In addition to the possibility of low power, high density, and high-speed switches, graphene- based devices may also be applied to other areas as a storm- thick membrane for sensing

pressure as components in nano-electrochemical systems or in chemical sensing because of their high surface area [37].

Many techniques have been incorporated to improve the sensitivity for the analysis of metal ions, namely, chemically modified electrode, heated electrodes *etc*. [40, 41]. Methods of developing active materials on electrode surfaces are crucial in the creation of sensitive high performance sensors. Commonly used coating methods include drop casting, dip coating and passive adsorption [8, 40, 42, 43] of graphene solutions, prepared via the chemical reduction of graphene oxide [44, 45, 46, 47, 48]. The lack of control of film thickness and harsh reagents, which contaminate samples are a major downfall. Electrochemical reduction has been seen as a promising alternative due to its fast and green synthesis approach [49, 50, 51, 52]. Guo *et al*. and Chen *et al*. have proposed a direct electrochemical reduction method of preparing reduced-graphene films at electrode surfaces in order to control film thickness and limit structural defects in graphene sheets [49, 50].

1.3. Objectives

The objectives of this project are:

- To investigate and understand the Square wave anodic stripping voltammetry technique;
- To prepare thin film electrodes of Bismuth and investigate their responses towards Cd^{2+}, Pb^{2+} and Zn^{2+};
- To do a comparative study of Bi-films based on their instrumental parameters;
- To investigate the ability to improve the sensitivity of the electrodes by coating them with Nafion- graphene nanocomposites and electrodeposited graphene without the use of a binder; and
- To develop an analytical procedure for the determination of metals in water

1.4. Research Questions

- Would pencil graphite electrodes be suitable for use in trace metal analysis?
- Would coatings such as Nafion and graphene improve electrode sensitivity in analysis or determination of trace metal concentrations?
- Do bismuth film electrodes offer comparable results to other thin-metal films electrodes in terms of limits of detection and recoveries for real water samples?

1.5. Hypothesis

It is possible to improve the sensitivity and detection limits of relatively cheap pencil graphite electrodes to below the USEPA standards of 0.5 ppm, 5 ppb and 10 ppb of Zn^{2+}, Cd^{2+} and Pb^{2+} respectively using graphene based composites in conjunction with bismuth metal-films using square-wave anodic stripping voltammetry (SWASV).

1.6. Research Approach

A number of experiments were designed in order to understand the effect of:

- Methods of Graphene Synthesis;
- Coating Techniques of PGEs;
- Instrumental Parameters on stripping voltammetry process;
- Graphene based Bismuth film electrodes for improved sensitivities and detection limits towards trace metals;
- Standard Addition Method on Recovery Studies of Test Solutions;
- Real Sample analysis of graphene-based chemical sensor.

In this study commercially bought Graphite powder, obtained from Sigma-Aldrich, simulated water as well as real water samples collected from tap water from the Bellville Municipality area in Cape Town, South Africa was used.

The chemistry involved during the synthesis of graphene was evaluated by analysis of solid, graphite-based structures, along the chemical synthesis process

by morphological and structural characterization techniques. These techniques included: FT-IR, EDS, Raman Spectroscopy, XRD, HRTEM, HRSEM and AFM Square-wave anodic stripping voltammetry (SW-ASV) was utilised using a Metro 797 VA Computrance to evaluate the viability of graphene-based composites as enhanced detection material towards the detection of trace metals. This was achieved by investigation of instrumental parameters, calibration data, test solution analysis and real water samples.

1.7. Scope and Delimitations

The study involved the use of tap water samples from the Bellville Municipal region in Cape Town, South Africa and starting reagents for synthesis from Sigma Aldrich and Kimix Chemicals. The water sample was used for investigation of trace metals, Zn^{2+}, Cd^{2+} and Pb^{2+}.

For tap water samples, numerous metal species present themselves such as Cu, Fe, Al, Mn, As, Se, Pb, Cd, Zn and Sb. Cd^{2+} and Pb^{2+} were selected as they are naturally occurring oxidation states of commonly occurring heavy metal contaminants with oxidation states more negative than Bi^{3+} and maximum contamination levels (MCL) in the low parts per billion range. Zn^{2+}, with MCLs in the ppm range shows the ability of modified electrodes to determine analytes in various concentration ranges. Further heavy metals such as copper and antimony were excluded as to alleviate known intermetallic interferences and were deemed to have MCLs outside of the low ppb range. Lake water samples were not collected due to the need for further purification before analysis.

Pentel 0.5 mm HB black lead with HI polymer were used in the production of the pencil graphite electrodes as they provided good stability and reproducibility. Other makes of "graphite-rods" were not tested.

Chemical and electrochemical synthesis approaches were utilized in preparation of graphene for enhanced electrode sensitivity. The two methods provide reproducible and good quality graphene sheets without the need for expensive instrumentation which is not readily available for point-of-care detection.

Figure 1.1: Geographic location of water sampling region under investigation in the study.

1.8. EG-PG-BiE Conceptual Diagram

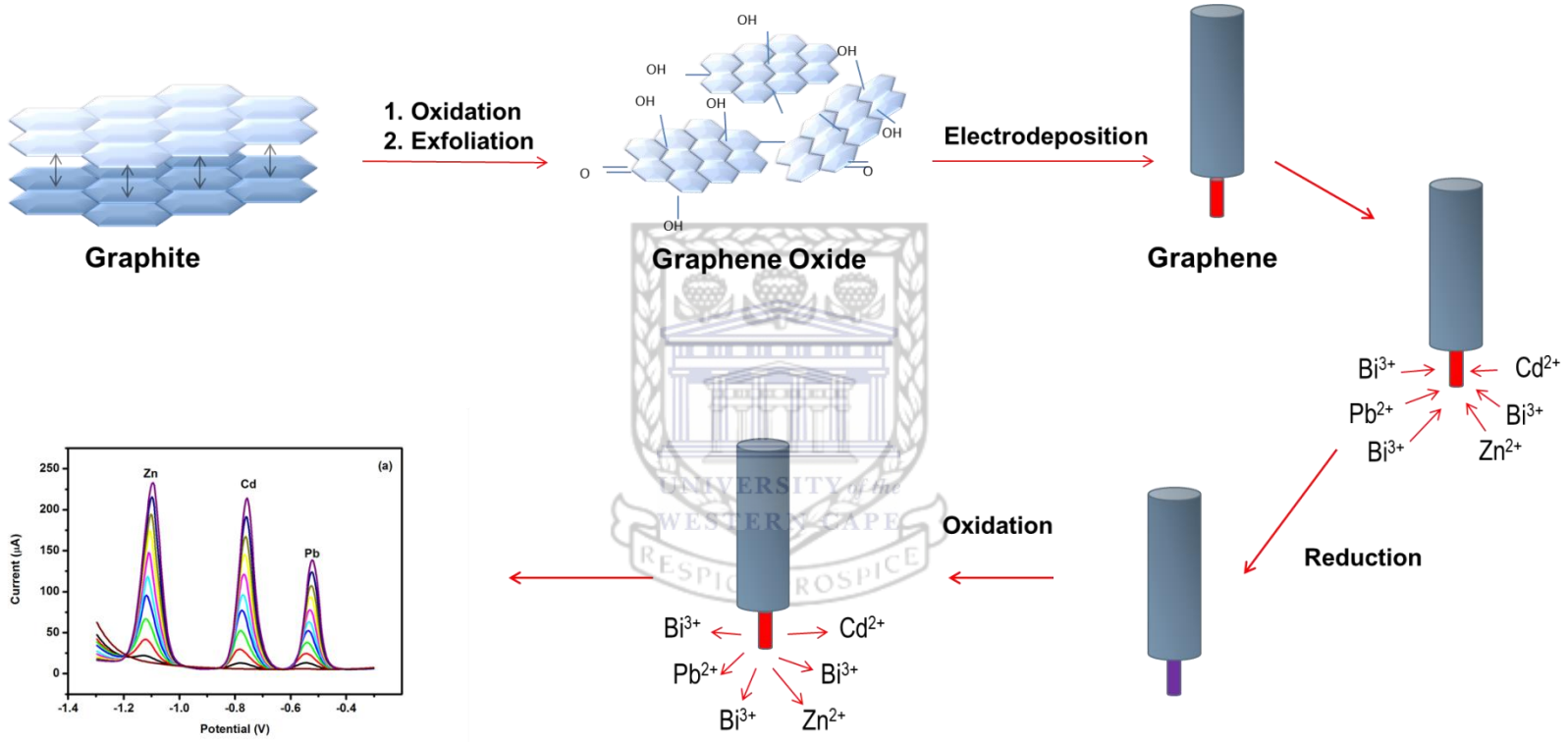

Figure 1.2: Conceptual diagram of the development of an Electrodeposited Graphene Pencil Graphite *in situ* plated Bismuth-film Electrode for the Determination of Heavy Metals by Anodic Stripping Voltammetry.

1.9. NG-PG-BiE Conceptual Diagram

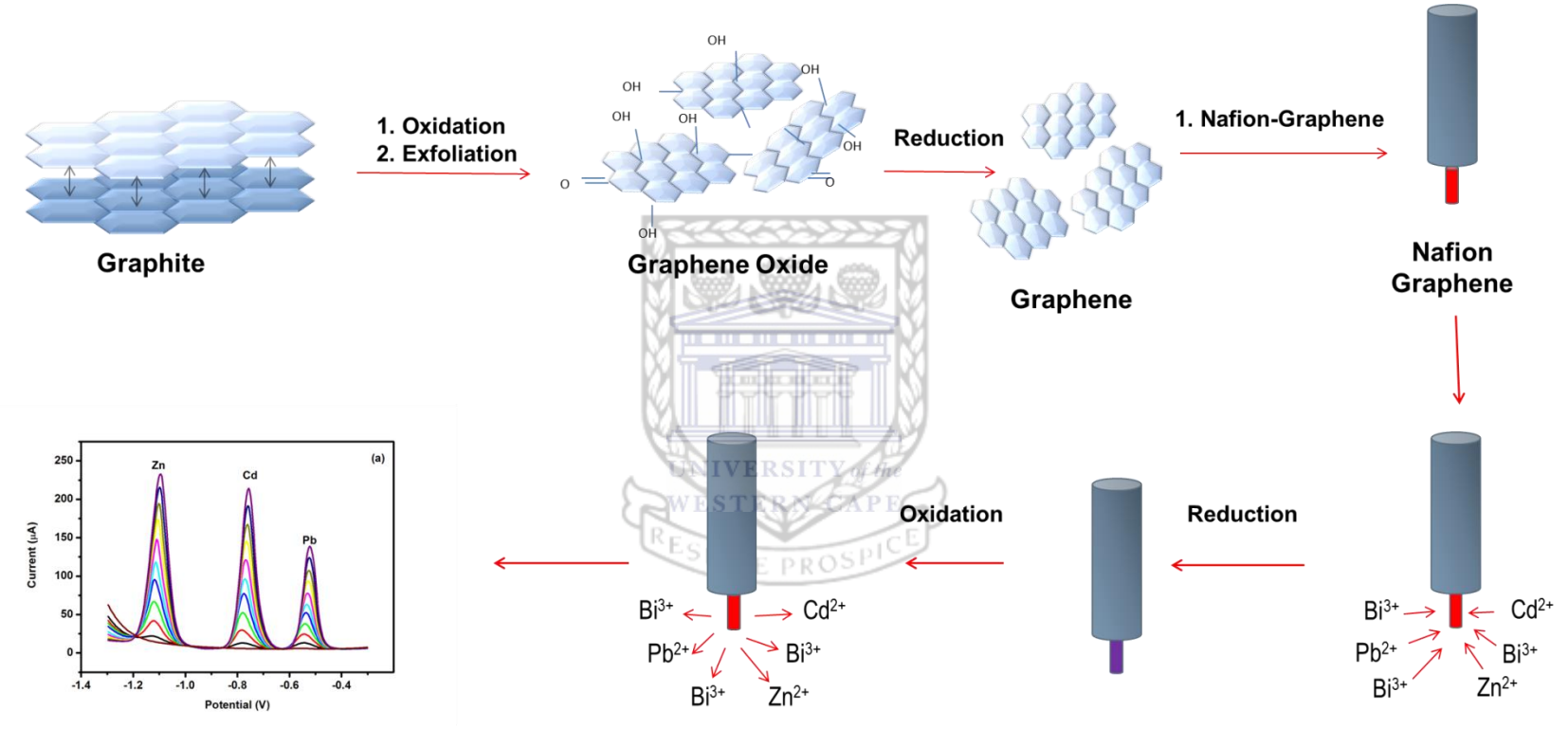

Figure 1.3: Conceptual diagram of the development of a Nafion-Graphene Nanocomposite Pencil graphite Bismuth-film Electrode for the Determination of Heavy Metals by Anodic Stripping Voltammetry.

1.10. Thesis Outline

The thesis to follow is comprised of seven chapters which cover various aspects of the work covered.

Chapter One: Introduction to the study

Chapter One provides a brief introduction to heavy metal detection and their toxicity as well as provides a rationale and motivation of techniques and chemicals utilized in the study. The main objectives to be met, scope and delimitations, research approach and hypothesis are also provided.

Chapter Two: Literature review

A comprehensive survey of relevant literature pertaining to the study is discussed in Chapter Two. The review focuses on graphene, trace metals of interest and metal thin-films. For electrochemical analysis, a detailed background of electrodes, supporting electrolyte, voltammetric techniques such as stripping voltammetry and electrochemistry of metal ions are discussed. Analytical characterization techniques will also be introduced. Further, gaps in literature are identified and the relevance of this particular study highlighted.

Chapter Three: Methodology

Chapter Three outlines the use of equipment and techniques used in this work. Detailed descriptions of sample collection and preparation are highlighted.

All relevant protocols for analysis as well as synthesis and characterization are provided.

Chapter Four: Morphological and Structural Characterization of Graphene

In Chapter Four, the steps in the chemical synthesis, from starting reagents to produce graphene oxide (GO) and graphene is detailed. The chemistry involved in synthesis is reported and relevant findings from characterization techniques highlighted in order to confirm the production of good quality few-layer graphene sheets. Reference is made to relevant literature. Both spectroscopic and microscopic analysis techniques were used to scrutinize the graphene sheets produced.

Chapter Five: Electrodeposited Graphene Pencil Graphite *in situ* plated Bismuth-film Electrode (EG-PG-BiE)

Chapter Five provides further results and discussion. EG-PG-BiEs are prepared by electrochemical reduction of graphene oxide (GO) solutions. The main trends and significant findings are highlighted. Microscopic and electrochemical characterisation of the graphene-modified electrode is demonstrated. Recovery studies and calibration curves conducted on test solutions of known concentrations are shown as proof of concept. Real water sample analysis is performed at EG-PG-BiEs and concentrations calculated below the USEPA standards

Chapter Six: Nafion-graphene Pencil Graphite Bismuth-Film Electrodes (NG-PG-BiE)

Results and discussion related to NG-PG-BiEs are listed in Chapter Six. This chapter opens with the preparation of Nafion-graphene nanocomposites. The introduction is followed by the production of the modified electrodes, including methods of coating, parameter optimisation, electrolyte investigation, as well as calibration and recovery studies of test solutions. Comparison is made between N-PG-BiEs and NG-PG-BiEs. Any relevant correlation is made to literature. The modified electrode is applied to real water samples below the USEPA standards.

Chapter Seven: Conclusions and Future Work

In Chapter Seven the hypothesis of this research is verified based on the results and discussion of the previous three chapters. Conclusions are drawn based on the results obtained and future work is specified. Future work arising from the work is suggested.

CHAPTER TWO:

Literature Review

2.1. Introduction

This chapter describes the use of relevant materials for the preparation and application of electrochemical sensors for the detection of zinc, cadmium and lead. It highlights various electroanalytical techniques, as well as focuses on sensors modified with bismuth (Bi) as "green approaches" for detection. Further focus is placed on the use of nanomaterials and specifically graphene-composites for enhanced sensing capabilities. In addition, techniques for characterisation of graphene are reported and discussed.

2.2. Electroanalytical Techniques for Heavy Metal Detection

2.2.1. General Basis of Voltammetry

Electrochemical techniques are of great interest to researchers as alternatives to common processes in existence. Electrochemical techniques are used to study reaction mechanisms, as well as kinetics and thermodynamics of electron and ion transfer processes [53]. Cheap instrumentation, good sensitivity, a wide linear concentration range, rapid analysis times and simultaneous determination of several analytes offers electrochemical techniques to a wide range of applications for inorganic and organic compounds [22]. The word "voltammetry" is derived from the root word 'voltam-' which refers to both potential ("volt") and current ("am") [54]. The beginning of voltammetry was

facilitated by the discovery of polarography, which is a class of voltammetry where the working electrode is a hanging mercury drop electrode, in 1922 by the Nobel Prize winning chemist Jaroslav Heyrovský followed by expanded analytical methods which led to enhanced sensitivities obtained with voltammetric techniques. Voltammetric techniques involve the application of an applied potential difference, E, between the electrodes, while monitoring the resulting current, I [55, 56, 57].

Voltammetry measurements are performed with the aid of a two or three electrode system in simple electrochemical cells as illustrated in Figure 2.1 below. Common electrochemical cells consist of a working electrode (WE), reference electrode (RE) and auxiliary or counter electrode (AE or CE). The working electrode, at which the reaction or transfer under investigation takes place, is an electron conductor and governs the oxidation or reduction of analytes at the electrode surface [2]. The reference electrode is kept under constant potential and acts as a measure to which current responses are determined [2]. In a three electrode system, the auxiliary or counter electrode acts as a counter reaction to that of the working electrode [55]. The AE minimizes errors from cell resistance in measurements.

The application of a potential to the working electrode will result in a change in concentration of the electroactive species at the electrode surface. Mass transport and current occurs as a function of the change in concentration. As a result quantitative determination of various compounds is achieved in voltammetric analysis [55].

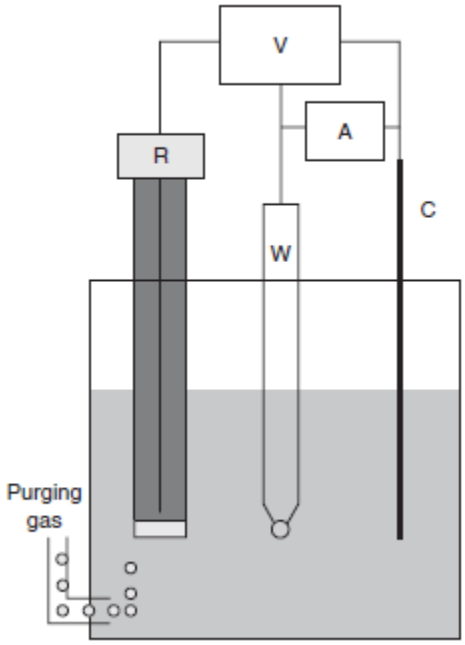

Figure 2.1: Schematic representation of a common 3 electrode system electrochemical cell. R, reference electrode; W, working electrode; C, counter electrode; V, voltammeter; A, amperemeter [55]

2.2.2. Theory and Definitions in Voltammetric Techniques

Considering the general reversible electrode reaction:

$$Ox + ne^- \rightleftharpoons Red\ (I), \qquad \text{(Eqn. 2.2.2.1)}$$

Two well-known laws may be applied for defining the relationship between the applied potential and surface concentrations of oxidation and reduction. Equation 2.2.2.1 is a typical redox reaction and its equilibrium state is governed by the Nernst equation. The Nernst equation, represented by Equation 2.2.2.2 holds for thermodynamically reversible electrochemical reactions. Here as the potential is changed, equilibrium is re-established.

$$E = E^0 + \frac{RT}{nF} ln \frac{c(Ox)_{x=0}}{c(Red)_{x=0}}, \qquad \text{(Eqn. 2.2.2.2)}$$

Where;

R is the gas constant, $R = 8.314\,472(15)\ \mathrm{J\,K^{-1}\,mol^{-1}}$

T is the absolute temperature (K)

n is the number of electrons exchanged

F is the Faraday constant, $F = 9.648\,533\,99(24)\times10^{4}\ \mathrm{C\,mol^{-1}}$

E^0 is the standard redox potential for the ox/red couple

For some techniques it is useful to know the relationship that links current, potential and concentration. The Butler-Volmer equation is an activation controlled reaction. Here the rate of a reaction is controlled only by the rate of the electrochemical charge transfer process. This equation is useful for estimating standard rate constant of electron transfer k_s. Equation 2.2.2.3 represents the Butler-Volmer equation:

$$\frac{i}{nFA} = k^0\{{c_{ox}}^0 \exp[-\alpha\theta] - {c_{red}}^0 \exp[(1-\alpha)\theta]\} \quad \text{(Eqn. 2.2.2.3)}$$

Where;

$\theta = nF(E-E^0)/RT$

k^0 is the heterogeneous rate constant

α is the transfer coefficient

A is the area of the electrode

2.2.3. Common Voltammetric Techniques

A wide range of dynamic methods in electroanalytical chemistry have been developed to solve various limiting factors of voltammetry. These techniques include the commonly used cyclic voltammetry, pulse methods as well as various

pre-concentration techniques. This section provides a brief discussion of voltammetric techniques used in heavy metal detection.

2.2.3.1. Cyclic Voltammetry

Cyclic voltammetry (CV) is a widely used technique in electrochemical analysis. It provides information of both oxidation and reduction half-cell reactions taking place at the working electrode [58, 59]. Starting from an initial potential (E_i), the potential is ramped to the switching potential (E_λ) before the direction of the potential scan is reversed. The scan rates between forward ($v_{forward}$) and reverse ($v_{reverse}$) are equal and always represented as positive values. If scanned from a negative potential, the forward part of the CV is oxidation. The shape of the cyclic voltammogram provides information as to the type of electrode reaction, the number of electrons involved as well as additional reactions like adsorption [58]. For reversible reactions the oxidation and reduction peaks are equal. The peak potential (E_p) and current (I_p) may be identified. The magnitude of the current is proportional to the concentration of the solution [54].

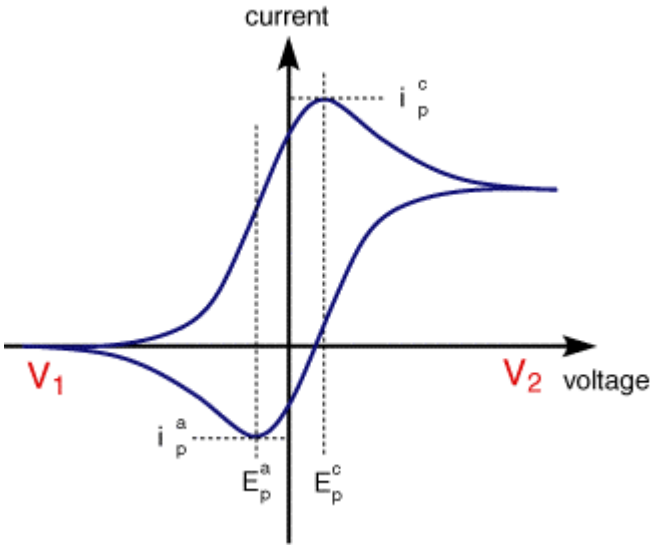

Figure 2.2: A typical cyclic voltammogram recorded for a reversible single electrode transfer reaction [60]

2.2.3.2. Normal Pulse Voltammetry

Normal pulse voltammetry (NPV) makes use of a series of single steps with constant width and permanent increased amplitude to apply potential to the electrochemical cell [61]. Current is measured as a function of the applied potential which ranges in duration and intervals [55].

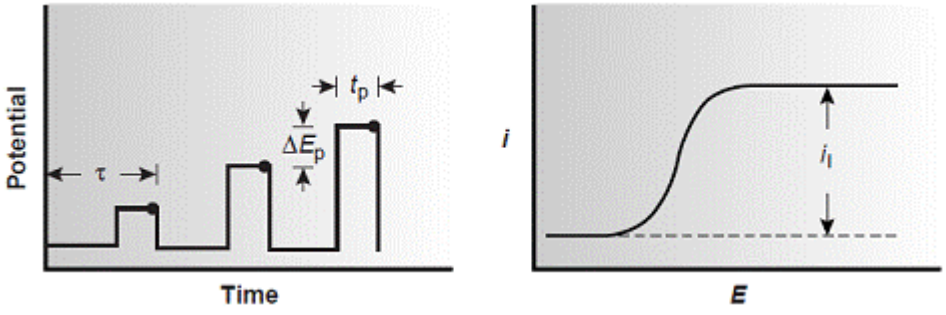

Figure 2.3: Potential form and resulting voltammogram in normal pulse voltammetry [153].

2.2.3.3. Differential Pulse Voltammetry

In differential pulse voltammetry (DPV), small pulses of constant amplitude (10-100 mV) are superimposed on a staircase-wave form [55]. Generally the potential scan rate in order to limit change in the ramp potential during pulse life. Differences in currents measured before and after the pulse are plotted as a function of potential. The resulting voltammogram has peak potential corresponding to rate of metal oxidation [2]. Figure 2.4 below represents a typical potential waveform and its resulting voltammogram in differential pulse voltammetry. The measured current is the difference between currents measured for each single pulse [55]. DPV offers improved signal-to-background response. Enhanced sensitivity is achieved by its slow scan rate. It may not be an attractive method for high concentration analysis where short deposition periods are sufficient [2]. The DPV currents are susceptible to interferences by surface-active materials [62]. Inexpensive instrumentation makes it an attractive application when measuring metals at the parts per billion ranges [63].

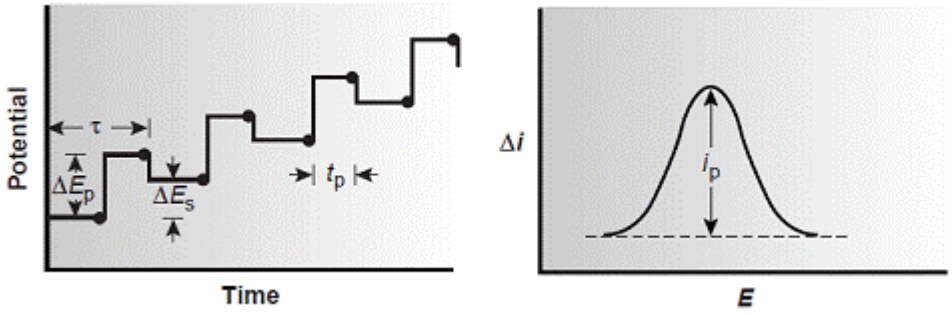

Figure 2.4: Potential form and resulting voltammogram in differential pulse voltammetry [153].

2.2.3.4. Square-Wave Voltammetry

Square-wave voltammetry (SWV) is a sophisticated technique in the pulse voltammetric techniques [64] and was first introduced by Barker [65]. SWV takes advantage of the differences in decay rates of the analytical and charge currents. It is defined by parameters including: step height, ΔE, and the step width, T. In SWV, a stair case potential sweep is employed. The current is measured at the end of each half-wave, prior to the potential change. The difference between forward half-cycle and reverse half-cycles are calculated and plotted as a function of potential and demonstrated by the voltammogram in Figure 2.5 below. High sensitivity and speed of analysis as well as insensitivity to dissolved oxygen make it an attractive option for heavy metal detection [66].

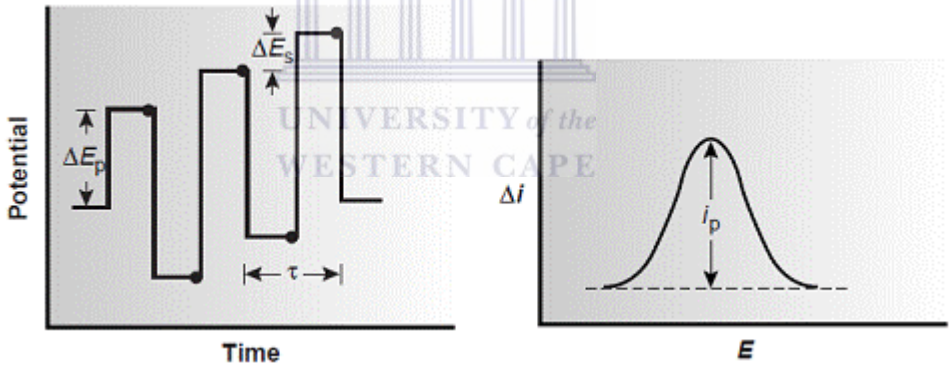

Figure 2.5: Potential form and resulting voltammogram in differential pulse voltammetry [153].

2.3. Pre-concentration Voltammetric Techniques (Stripping Voltammetry)

Analytical techniques aim to provide lower detection limits, good sensitivity and good selectivity. The nature of mass transport and features of the electrode and electroactive species affect the limit of detection in voltammetric techniques

[55]. Many compounds are capable of dissolving or reacting with the electrode material forming an amalgam (mercury electrode) or alloy (bismuth electrode) soluble complex. This phenomenon forms the basis of pre-concentration voltammetric techniques; adsorptive stripping voltammetry (AdSV), anodic stripping voltammetry (ASV) and cathodic stripping voltammetry (CSV).

2.3.1. Why use Stripping Voltammetry

Every analytical technique offers its own advantageous and disadvantageous properties. The choice of analytical technique is usually due to the chemist's preference and material type under investigation. As a result, this section discusses various techniques used for heavy metal detection. Graphite furnace atomic absorption spectroscopy (GFAAS), inductively coupled plasma spectroscopy (ICP) and stripping voltammetry (SV) are briefly compared.

Table 2.1: A summary of commonly available heavy metal detection techniques

Analysis Method	Advantages	Disadvantages
GFAAS	• Detection limits in the ng L^{-1} • Short atomisation time • Increased sensitivity • Small sample volumes	• Large number of lamps • Automated sample and injection system • Expensive • Wasteful of inert gas
ICP-OES	• Large number of samples • Detection limits in µg L^{-1} • Simultaneous analysis	• Wasteful of inert gas • Expensive • Time consuming
SV	• 4-6 trace metals simultaneously • Detection limits in µg L^{-1} • Inexpensive • Low power demand • Species characterisation	• Intermetallic interferences • Analysis limited to 6 metals simultaneously • Electrode modification often limits choice of analytes

2.3.1.1. Graphite Furnace Atomic Absorption Spectrometry (GFAAS)

Many compounds break apart into gaseous phase when heated to a sufficiently high temperature. GFAAS makes use of this feature. Samples are vaporized at very high temperatures and the concentrations of selected atoms are determined by measuring absorption at their characteristic wavelengths [67]. The technique makes use of small sample sizes which are compensated by long residence times. The need for sample injection systems, expensive lamps and low

reproducibility are major drawbacks of the GFAAS technique [68]. Low detection limits in the ng L^{-1} are found.

2.3.1.2. Inductively Coupled Plasma Spectrophotometry (ICP)

ICP spectrophotometry is capable of simultaneously measuring a wide variety of elements in the µg L^{-1} range. ICP analysis is often wasteful of sample, requiring sample preparation to be employed in many instances and requires an excess of argon or other gases.. Instrumentation requires regular maintenance and is expensive increasing cost of analysis.

2.3.1.3. Stripping Voltammetry (SV)

Recently, a great deal of attention has been place on stripping analysis as an alternative to the commonly used GFAAS and ICP techniques discussed in sections 2.3.1.1 and 2.3.1.2 respectively. The ability to measure four to six trace metals at concentrations in the sub ppb range simultaneously is the biggest draw card for stripping analysis. Instrumentation is readily available, small in size and has a low power demand. Species characterization and multi-element analysis with automated stripping analysis make it a quick and robust technique. Little intermetallic interferences are exhibited with stripping voltammetric techniques. Point-of-care or on site analysis is possible with stripping analysis using a wide range of substrate materials. [2]

2.3.2. Principles of Stripping Voltammetry

In stripping analysis an electrolytic step to pre-concentrate sample from solution onto working electrode is used. An electrochemical measurement is then conducted in the presence of electrolyte to minimize matrix interferences. Trace metal analysis is usually performed by ASV [2]. A brief description of the theory

and definitions of voltammetric techniques and particularly the Nernst equation governing the faradaic reversible process of the ASV procedure is discussed in section 2.2.2. Figure 2.6 below is a brief summary of the stripping voltammetric procedure.

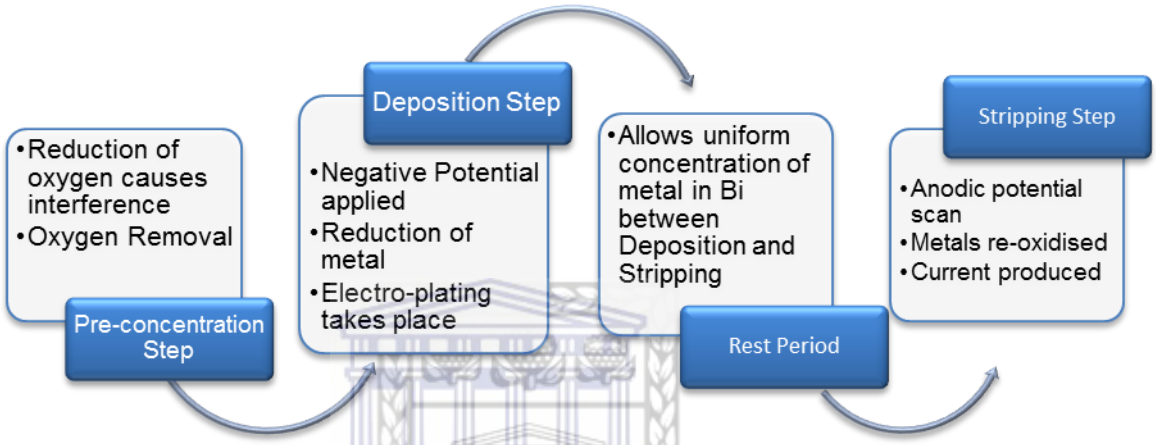

Figure 2.6: A Summary of the Stripping Voltammetric Procedure

2.3.2.1. Deposition Step

In stripping voltammetry the deposition step is employed by applying a fixed potential for a definite time under reproducible hydrodynamic conditions. This pre-concentration step is responsible for low detection limits in stripping analysis [69]. Here the electro-plating of the analytes along with the *in situ* plated metal-film is performed by the formation of "fused alloys" [26, 27], or amalgams [2]. Accumulation is evident in the anodic version while deposition is required for cathodic stripping voltammetry to occur. The deposition potential and time is chosen depending on the concentration of metal ion present [69].

2.3.2.2. Rest Period

Stripping steps in all forms of stripping voltammetry (section 2.3.2.3 below) require uniform concentration distribution of the metal at the electrode surface or metal-film. A rest period is employed to allow formation of uniform concentration allowing the stripping step to be performed in quiescent solution [2].

2.3.2.3. Stripping Step

The stripping step, which usually consists of an anodic potential sweep, is used to re-oxidize the deposited metal back into solution at specific standard potentials for the metal-metal ion couple [2]. Equation 2.3.2.3.1 below describes the ionic form:

$$M \rightarrow M^{n+} + ne^{-} \quad \text{(Eqn. 2.3.2.3.1)}$$

The resulting voltammogram provides the analytical information required. The peak potential occurs at standard redox potentials of the metal ion. The stripping peak current for each individual metal is proportional to the concentration in the solution. The various potential scan methods which may be employed in this step are discussed in section 2.2.

2.3.3. Adsorptive Stripping Voltammetry

Adsorptive stripping voltammetry is an extremely sensitive technique and has been used for the determination of a wide variety of compounds [70, 71, 72]. Upon application of an appropriate potential, oxidation or reduction of the accumulated compound by adsorption takes place. Sample preparation and contamination are important [55]. Chemically modified electrodes are often used.

2.3.4. Anodic Stripping Voltammetry

As previously mentioned the anodic stripping voltammetry process is commonly used in heavy metal detection. The reduction of the present metal ions from solution takes place. Once amalgamation or fused alloy production is completed the metals are re-oxidised into solution [2]. Peak currents of subsequent voltammograms are proportional to metal ion concentrations. Intermetallic interference is a concern but can be accounted for by application of complexing agents or adjusting the deposition potential [55]. The two-step mechanism is illustrated by equation 2.3.4.1 and 2.3.4.2 [2]:

Deposition: $M^{n+} + ne^- \rightarrow M$ (Eqn. 2.3.4.1)

Stripping Step: $M \rightarrow M^{n+} + ne^-$ (Eqn. 2.3.4.2)

2.3.5. Cathodic Stripping Voltammetry

Cathodic stripping voltammetry (CSV) is used in a wide range of organic and inorganic compounds which form insoluble salts. Potential sweeps are opposite to the ASV procedure. Here the deposition step involves oxidation of compounds. The mechanism of cathodic stripping voltammetry is represented by equations 2.3.5.1, 2.3.5.2 and 2.3.5.3 [2].

Deposition: $M \rightarrow M^{n+} + ne^-$ (Eqn. 2.3.5.1)

$M^{n+} + A^{n-} \rightarrow MA$ (Eqn. 2.3.5.2)

Stripping step: $MA + ne^- \rightarrow M + A^{n-}$ (Eqn. 2.3.5.3)

2.4. Bismuth-Film Electrodes for Trace Metal Analysis

2.4.1. Introduction

A major criticism often leveled at the stripping voltammetric technique is the use of mercury working electrodes which pose a health hazard and as a consequence there is a shift towards the search for more environmentally friendly mercury free working electrodes [24, 25]. Much work and research has been put into the search for alternative electrode materials resulting in the use of antimony and bismuth working electrodes as alternatives to mercury working electrodes. Since its introduction for electroanalytical purposes in 2000 the BiE has garnered a lot of attention [73]. The thin bismuth-film electrode shows similar or comparable results to that of mercury-film electrodes [74] since bismuth, is capable of forming "fused" alloys with trace metals which is analogous to the amalgams formed with mercury [26, 27]. Moreover, bismuth coated electrodes offer many attractive properties including, the simple preparation [24], high sensitivity, good stripping signal and excellent resolution of peaks [28].

2.4.2. Preparation of Bismuth Electrodes (BiE)

2.4.2.1. Substrate and Cleaning Procedures

Traditionally a wide range of carbon-based substrate materials are used as support for bismuth films. The size and shape of electrode does not affect electrode coating. Bismuth is plated on similar substrates to mercury. Many different types of materials have been used as substrates for BiFE; including glassy carbon [73], wax impregnated graphite [27], carbon paste [75], pencil-lead [40] etc. In many applications when pre-plating is used, the same bismuth-film is

required for subsequent analysis methods. A cleaning potential is applied for short time periods at potentials more negative for *in situ* [48] and more positive for *ex situ* [76] plating of the bismuth-film. The cleaning step allows for reproducible analysis to be performed.

2.4.2.2. Plating of Bismuth

Plating of the bismuth film is imperative for reproducible and accurate analysis in stripping voltammetry. Three common methods are employed for the preparation of bismuth electrodes. In *in situ* plating bismuth ions are co-deposited with metal ions under investigation [77, 8]. This method allows for shorter analysis times and reproducible results. Here, the concentration of Bi (III) controls the thickness of the bismuth film [78]. By varying the bismuth concentration peak heights or stripping peak currents are affected while peak position remains generally unchanged. At too high bismuth ion concentrations, saturation causes a reduction in sensitivity [75]. *Ex situ* deposition of bismuth-ions before electrode is transferred to solution under investigation is the second method of electro-plating [76]. Modification of electrodes with a bismuth precursor, such as Bi_2O_3 [79] is another method of bismuth electrode preparation and is confined to carbon-paste electrodes [80]. It has one major drawback in that it results in shifts in stripping peak potentials [79].

2.4.3. Applications and Interferences of Bismuth Electrodes

A major drawback of stripping voltammetry and analytical chemistry in general are interferences caused by loss of analytes, contamination and human

error. These interferences affect electrode sensitivity and accuracy of the stripping technique.

Interferences in bismuth-film electrodes are largely attributed to the adsorption of surface active compounds, contamination, formation of intermetallic interferences and poor resolution between adjacent peaks [80]. Fouling of the electrode and impeded sensitivity occur as a result of adsorption of surface active compounds on the electrode surface. , the permselective membrane has shown to increase the detection sensitivity [40, 8] and alleviate the interferences from surfactants at bismuth film electrodes [33]. Contamination usually arises from impurities in reagents and improper cleaning procedures. Blanks are performed to limit the error caused by cross-contamination and is largely used. The use of Teflon or polypropylene containers are also used and reduce the chances of adsoption onto the inner walls of containers. Numerous intermetallic compounds have been reported; these include the following combinations.: Ag-Cd, Ag-Cu, Ag-Zn, Au-Cd, Au-Ga, Au-Mn, Au-Sn, Au-Zn, Co-Zn, Cu-Cd, Cu-Ga, Cu-In, Cu-Mn, Cu-Ni, Cu-Sb, Cu-Sn, Cu-Tl, Cu-Zn, Fe-Mn, Mn-Ni, Ni-Ga, Ni-Sb, Ni-Sn, Ni-Zn, Pt-Sb, Pt-Sn and Pt-Zn [2]. Intermetallic interferences depress or shift stripping peaks of particular ions. These interferences are usually alleviated by the addition of an additional complexing ion such as Ga(III) to reduce the Cu-Zn interference [81].

The metal ions so far detected by stripping analysis include Cd, Pb, Zn, Tl, In and Cu by anodic stripping analysis and Ni, Co and Cr by adsorptive stripping analysis [80]. In the last decade a large shift has been made to the analysis of environmental, clinical and food analysis. Determination of heavy metals in tap

water [40, 27], urine [82], soil [83, 84] and hair samples [27] have all been previously reported at bismuth electrodes. Good sensitivity and reproducibility were reported for the 'green' electroanalytical approaches.

Further applications of Bismuth electrodes include their use in the analysis of organic compounds [85]. Carbon paste electrodes were used in conjunction with an *ex situ* plated BiF for the detection of neonicontinoid insecticides by DPV [86]. Kreft *et al*. reported the use of a bismuth-film electrode for the determination of Vitamin B12 by CV and square-wave adsorptive stripping voltammetry [87].

2.5. Nanoscience

Nanotechnology and nanoscience is a popular and largely emerging area of science in modern times. It spans a large variety of fields and has therefore attracted many researchers from physics, biotechnology, chemistry and engineering fields alike. It is for this reason that large amounts of public and private sector funding have been dedicated to research in this field [88]. Many nanomaterials are naturally occurring in nature and as a result scientists have set about trying to imitate these materials by biomimetics.

Nanotechnology is the term given to those areas of science and engineering where phenomena that take place at dimensions in the nanometre scale are utilised in the design, characterisation, production and application of materials, structures, devices and systems [89]. It is clear that being able to manipulate and control various materials at the nanoscale (chemistry and physics that are on the length scale of 1-100 nm) may have a significant impact on society and pose beneficial properties for a large range of applications.

Nanotechnology exploits benefits of ultra-small size, enabling the use of particles to deliver a range of important benefits. It may be used to attain transparent or thin film coatings as well as modification of surfaces with minimal material.

The phenomena intrinsic to the nanoscale are: Size confinement, Dominance of interfacial phenomena and Quantum Mechanics.

At the nanoscale we are concerned with the nature of matter between atoms and molecules, also known as quantum mechanics. It is this quantum effects which result in unique properties namely, functionality and structure [90]. These properties are achieved through four quantum mechanisms:

- *Quantum confinement*: is change of electronic and optical properties when the material sampled is of sufficiently small size - typically 10 nanometers or less. The bandgap increases as the size of the nanostructure decreases. Specifically, the phenomenon results from electrons and holes being squeezed into a dimension that approaches a critical quantum measurement, called the exciton Bohr radius [91].
- *Discretisation*: only defined energy levels are allowed for particles.
- *Superposition*: involves the overlapping of waves and shows the mathematical probability of how either constructive, destructive interference will occur.
- *Entanglement*: Quantum effects of two or more objects are linked together. One object can't be described without mention of the other.

Synthesis of nanomaterials may be divided into two main approaches distinguishable by their starting materials: Top- down and bottom- up approaches.

Top-down: Structures are etched into bulk materials in order to produced nano-sized materials.

Bottom-down: Bringing atomic and molecular building blocks together by covalent and non-covalent interactions to make self-assembled nanostructures [92].

2.6. Graphene

2.6.1. Carbon Allotropes

Carbon is one of the most abundant materials found on earth and is naturally occurring in many forms and substances. Not many materials exist entirely of carbon. These substances are known as allotropes. Allotropes are compounds that exist in forms with different chemical structures [93]. Some common examples of allotropes are phosphorus ("white" or "yellow", "red", and "black / purple"), oxygen (O_2 and O_3) and finally carbon (diamond, graphite, fullerenes and carbon nanotubes, or CNTs). Graphite and diamond are the two most commonly used forms of carbon over the centuries due to the ease of availability. Due to the hybridization (sp^3 and sp^2) and bonding of the carbon atoms different allotropes will exist. Carbon may also exist in an unordered arrangement known as amorphous carbon. Three nanoscale forms of carbon have attracted lots of attention; Buckeyballs, carbon nanotubes and Graphene due to their distinct properties at the nanoscale [94].

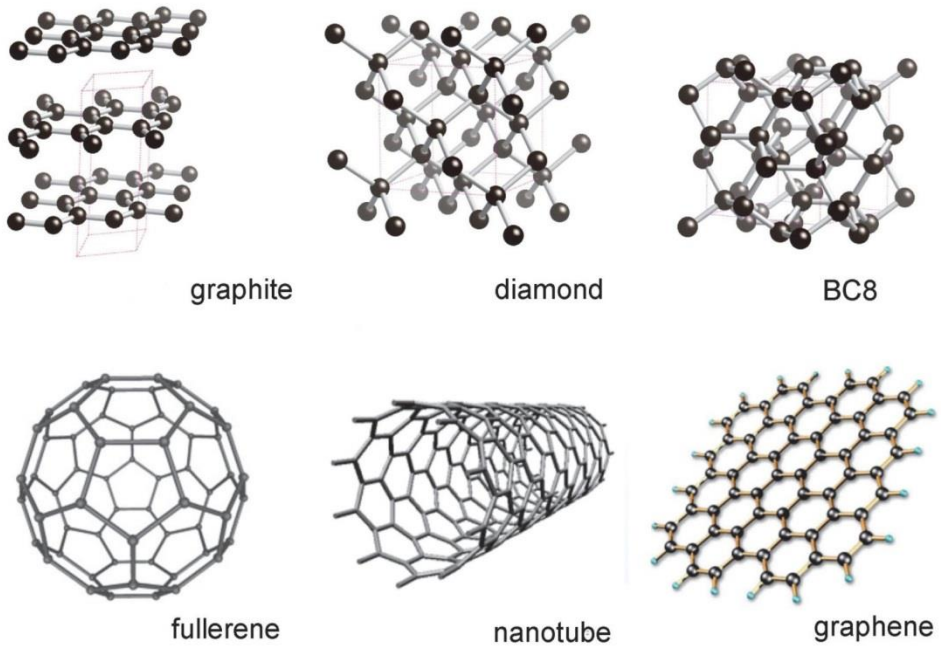

Figure 2.7: Structures of selected carbon allotropes [95]

2.6.2. Introduction to Graphene

Carbon is the most common material on earth; it forms the basis of all organic chemistry. Because the bonding is extremely flexible it forms a wide variety of structures and therefore also a wide variety of properties. Graphene, a 2D allotrope of carbon, is a very important material not only for fundamental research but also for device applications. It has its carbon atoms arranged in a honeycomb structure of hexagons with sp^2 hybridization [8]. These sp^2 hybridized carbon atoms are arranged in single sheets. It takes at least 10 such sheets stacked on top of each other for it to be considered bulk graphite [94].

The extra quantum confinement of the electrons due to the lack of a third dimension provides graphene with novel properties. Graphene is transparent, flexible and strong [96] and acts as a mobile charge carrier enabling enhanced

conductivity [97]. Graphene has shown to significantly improve the sensitivity in various applications [40]. In addition to the possibility of low- power, high density, and high-speed switches, graphene- based devices may also be applied to other areas as a storm- thick membrane for sensing pressure as components in nano-electrochemical systems or in chemical sensing because of their high surface area [37].

2.6.3. Discovery of Graphene

The discovery of graphene was based on the hypothesis of Andre Geim and Kostya Noveselov in 2003, that using scotch tape it was possible to peel away layers of graphite. The tape was dissolved in solution, leaving behind thin flakes of graphite (10 layers thick). This technique yielded the first graphene sheets in 2004 [98].

2.6.4. Structure of Graphene

As stated above, graphene is a quasi 2D sheet of carbon atoms arranged in a honeycomb lattice. Individual sheets are held together by sp^2 bonds [94]. The carbon-carbon bond length is approximately 0.142 nm. The electronic structure of 10 layer sheets resembles graphite [99]. Many definitions exist as to what is deemed graphene and what remains bulk graphite. It is possible to distinguish between single-, double- and few- (3 to < 10) layer graphene as three different types of 3D crystals [97]. The unit hexagonal cell of graphene contains two carbon atoms with an area of 0.052 nm^2.

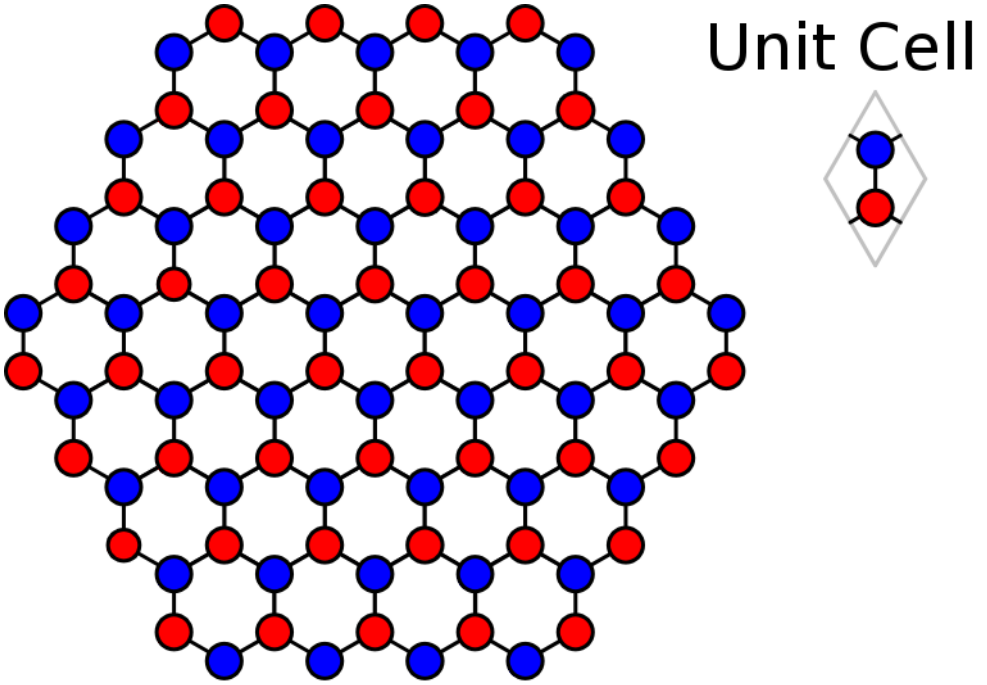

Figure 2.8: Diagram representing the graphene lattice unit cell [100].

2.6.5. Properties of Graphene

2.6.5.1. Electrical Properties of Graphene

In theory, graphene is known as a zero-gap semiconductor [98]. The valence and conduction bands of graphene do not overlap as in metals but touch at the Fermi level (the border between valence and conduction bands in conductors) [101]. This feature leads to an entirely new transport mechanism in graphene [94]. Electrons in graphene have a linear dispersion relation and behave like massless relative particles [102]. The conductivity of bulk graphene is $0.96 \times 10^{6} \Omega^{-1} cm^{-1}$. The quantum Hall Effect, discovered in 1980 is due to the unusual nature of charge carriers in graphene, behaving like massless particles and move with little scattering under ambient conditions.

2.6.5.2. Optical Properties of Graphene

Due to its transparency, graphene has attracted lots of attention in many fields including transparent displays in electronics. The rate of absorption of incident white light is πα or 2.3 % where α is the fine structure constant [103]. The D and G bands produced by Raman spectroscopy of graphene are optical bands which occur due to compressing and breathing modes respectively.

2.6.5.3. Mechanical Properties of Graphene

Graphene is an extremely light material and is known as one of the strongest materials ever tested. It weighs 0.77 mg m^2, with a breaking strength 100 times greater than steel. The breaking strength of graphene is 42 N m^{-1}. Many studies have been conducted to measure the tensile strength of single graphene sheets using atomic force microscopy (AFM).

2.6.6. Synthesis of Graphene

A wide range routes for the synthesis of graphene exist and are used and studied in modern times. The use of instrumentation, materials, cost of production and efficiency as well as the quality of graphene produced is major contributing factors to the choice of synthesis method.

The scotch tape method developed by Geim *et al*. [97] is one of the first and simplest methods of preparing thin graphene sheets. Here, scotch tape is used to separate or exfoliate thin sheets of graphite. The scotch tape is then folded repeatedly until transparent sheets are observed. The produced graphene sheets are transferred to silicon wafers for analysis. The method produces exfoliated graphene sheets without the use of expensive instrumentation.

Chemical synthesis to produce graphite oxide is commonly employed in research laboratories around the world. Three principle methods are used for the synthesis of GO: Brodie [104], Hummers [105] and Staudenmeier [106]. The produced GO is subsequently reduced to graphene via many routes. Chemical reduction using sodium borohydride or hydrazine, thermal reduction, photoreduction, electrochemical reduction etc. are commonly used. The formation of defects in the graphene structure is a major drawback of this technique.

Chemical vapor deposition (CVD) is the most promising method to produce graphene. The CVD methods results in high quality single graphene sheets on a large scale, without the need for further treatment [107]. As a result the method is one of the cheapest graphene synthesis methods. The CVD method can be employed to grow single sheets of graphene on arbitrary surfaces using transition metal catalysts [108].

Further methods of synthesis are epitaxial growth and the burning of magnesium ribbons to convert carbon dioxide to graphene [109].

2.6.7. Applications of Graphene

The novel electrical, thermal, mechanical and optical properties of graphene lend it to a wide range of applications. A great deal of research into graphene as alternatives to existing materials is being employed in laboratories around the world. Graphene has attracted lots of attention as a replacement to traditional electrode materials such as indium tin oxide in electrical and optical devices [110]. It is used as low cost display screens in mobile devices [111], lithium-ion batteries [112], ultracapacitors [113], fuel cells [114], hydrogen storage [115],

light weight gas tanks, solar cells, electrodes in electrochemical sensors [8, 48, 116].

Modifying carbon based electrodes with graphene and reduced graphene oxide has attracted lots of attention since its discovery. The intrinsic physiochemical properties (high surface area, excellent conductivity, high mechanical strength and ease of functionalization and mass production) make it a perfect platform for a wide range of applications. Graphene-based electrochemical sensors have often been employed as chemical and biological sensors for environmental analysis. The use of graphene-based electrodes for particular use in heavy metal determination is of particular interest to many scientists. Li et al. and Willemse et al. reported Nafion-Graphene composite films for Pb^{2+} and Cd^{2+} at a bismuth-film and $Zn^{2+,}$ Cd^{2+}, Cu^{2+} and Pb^{2+} at a mercury film using DPSV and ASV respectively [11,8]. These works show improved sensitivity due to increased surface area and better conductivity due to the inclusion of graphene compared to work performed by Kefala et al. and Demetriades et al. at Nafion-modified, bismuth-film pencil electrodes for Pb and Zn and Pb, Cd and Zn determination using SWASV [27,40]. The above mentioned graphene-based electrodes exhibit superior detection properties over their carbon nanotube [25,142] and graphite nanofiber [141] counterparts. Gong et al. reported an Hg^{2+} sensor with graphene and gold nanoparticles with detection limits as low as 6 ppt. The sensor inhibits the interference from other heavy metal ions such as Cu^{2+}, Cr^{3+}, Co^{2+}, Fe^{3+}, Zn^{2+} and I^{-} [154] and further supports the use of nanocomposites for enhanced detection capabilities.

2.7. Pencil Graphite Electrodes

Carbon based solid electrodes are suitable for a wide range of applications due to their wide potential window and low background current. Pencil graphite has been previously used as an electrode substrate material in different applications of stripping analysis. These applications include chemical and biosensors for determination of trace metals [29, 30], DNA and RNA [31] and uric acid in urine and blood samples [32]. The attractive features of PG distinguish it from other solid electrode materials. Pencil graphite has been evaluated as alternative to the common glassy-carbon and gold electrodes (GCE and GE) due to its good conductivity, little pretreatment steps, low cost, low background current and large scale availability.

A comprehensive spectroscopic characterization of pencil graphite electrodes was conducted by J. Kariuki [117].

Many techniques have been incorporated to improve the sensitivity for the analysis of metal ions, namely, chemically modified electrode, heated electrodes *etc*. [40, 41]. Methods of developing active materials on electrode surfaces are crucial in the creation of sensitive high performance sensors. Commonly used coating methods include drop casting, dip coating and passive adsorption [8, 40, 42, 43] of graphene solutions, prepared via the chemical reduction of graphene oxide [44, 45, 46, 47, 48]. The lack of control of film thickness and harsh reagents, which contaminate samples are a major downfall. Electrochemical reduction has been seen as a promising alternative due to its fast and green synthesis approach [49, 50, 51, 52]. Guo *et al*. and Chen *et al*. have proposed a direct electrochemical reduction method of preparing reduced-graphene films at

electrode surfaces in order to control film thickness and limit structural defects in graphene sheets [49, 50]. Dip coating of nanomaterials and Nafion [40] have also been previously reported.

2.8. Characterization Techniques

The quality of graphene oxide (GO) and graphene produced in any synthesis route is imperative in understanding the properties which individual sheets may poses. The applications of individual graphene sheets are governed by these properties. Various characterization techniques are employed to investigate the purity and defects of graphene. A brief discussion of Fourier transformed infrared spectroscopy (FT-IR), x-ray diffraction (XRD), Raman spectroscopy, atomic force microscopy (AFM), high resolution transmission electron microscopy (HRTEM) and high resolution scanning electron microscopy (HRSEM) are listed below.

2.8.1. Fourier Transformed-Infrared (FT-IR) Spectroscopy

The FT-IR spectroscopy technique is used to determine qualitative and quantative features of IR-active molecules in organic and inorganic solid, liquid or gas samples. Functional groups in various samples are investigated. It is an inexpensive and rapid method of detection [118]. In simple FT-IR analysis an interference wave interacts with a sample at a specific wavelength and the amount of light absorbed is measured [119].

2.8.2. X-ray Diffraction (XRD)

In XRD the atomic or molecular structure of a crystal can be determined. Samples cause an X-ray beam to diffract into many specific directions. The angles and intensities of incident light are measured and used to determine a picture of the molecule. Crystalline, amorphous and non-amorphous materials of the same element can be differentiated. Detailed information about the chemical composition and crystallographic structure of natural and manufactured materials can be observed [120].

2.8.3. Raman Spectroscopy

In Raman spectroscopy, photons of laser light are absorbed and re-emitted by a sample under investigation. The frequency of re-emitted phonons is measured in response to the original frequency. The spectra obtained provide information as to the vibrational, rotational and low frequency transition metals. Functional groups as well as changes in structure are obtained [121].

2.8.4. Atomic Force Microscopy (AFM)

The surface morphologies of various samples are measured by atomic force microscopy. It is a mechanical imaging instrument meaning it does not rely on electromagnetic radiation or electron beams. In AFM, a cantilever is moved along the surface of a specimen or material. The measured deflection of the cantilever is used to image the sample surface.

2.8.5. High Resolution Transmission Electron Microscopy (HRTEM)

Transmission electron microscopy (TEM) replaces optical light with an electron beam. The interaction of this beam with sample produces photons which

are collected on a photon screen. The energy of electrons striking this screen produce light creating an image. The morphology of a sample is determined.

2.8.6. High Resolution Scanning Electron Microscopy (HRSEM)

Like TEM, scanning electron microscopy is a type of electron microscope that produces and image by interaction with an electron beam. The signals produced provide information as to the surface topography and composition of a sample.

2.8.7. Summary of Characterization Techniques

Table 2.2: A summary of Characterization Techniques used in the study

Technique	Use
FT-IR	Structural Configuration
XRD	Structure/ Mineralogy
TEM, SEM	Morphology and Particle Size
XRF, ICP, AAS	Composition
AFM	Morphology
Raman Spectroscopy	Vibrational and Rotational Frequency modes/ Configuration
Cyclic Voltammetry	Electro activity
SECM	Electro activity, Corrosion, Morphology, Topography, Coating uniformity

CHAPTER THREE:
Experimental Approach

3.1. Introduction

This section details the instrumentation used and experimental procedures utilised in acquiring the relevant data utilized in this study. A step-by-step account of sample and electrode preparation is provided.

3.2. Apparatus

Square-wave anodic stripping voltammetric measurements were performed using a 797 VA COMPUTRACE instrument (Metrohm, Switzerland) controlled by a personal computer. A three electrode electrochemical system consisting of an electrodeposited graphene pencil graphite bismuth-film electrode (EG-PG-BiE) served as the working electrode. An Ag/AgCl (saturated KCl) and platinum wire served as the reference and counter electrodes, respectively. All experiments were performed in a one compartment 20 mL voltammetric cell at room temperature.

Fourier Transform Infrared (FT-IR) spectra were recorded using a (Perkin Elmer Spectrum 100) coupled to an Attenuated Total Reflectance (ATR) sample holder. FT-IR was used to obtain information and confirmation on graphene oxide. Scanning Electron Microscopy (SEM) measurements were performed using a LEO 1450 SEM 30 kV instrument equipped with Electronic Data System (EDS) and Windows Deployment Services (WDS); images were taken using the secondary electron detector. The samples were dried in a vacuum oven and deposited on the silicon grid surface before SEM observations. High Resolution

Transmission Electron Microscopy (HRTEM) measurements were carried out with a Tecnai G2 F20X-Twin MAT Field Emission Transmission Electron Microscope from FEI (Eindhoven, Netherlands) under an acceleration voltage of 200 kV. The samples were prepared by dropping a dilute suspension of graphene oxide in ethanol onto copper grids followed by air drying at room temperature. XRD measurements were carried out using a Bruker AXS D8 Advance diffractometer from BRUKER- AXS Germany with Cu-Kα radiation and Raman spectroscopy was obtained using a Dilor XY Raman spectrometer with a Coherent Innova 300 Argon laser with a 514.5 nm laser excitation. A tapping-mode atomic force microscope (Veeco Nanoman V) was employed to evaluate the morphology of graphite and graphene oxide, with special emphasis on estimating its thickness. The silicon tip [antimony (n) doped] had a curvature radius of 2.5 – 3.5 μm, a force constant of 1 – 5 N m^{-1} and a resonance frequency of 60 – 100 kHz. The samples for AFM were prepared by drop coating the graphite/water and graphene oxide/water (5 μL) dispersion onto a silicon wafer.

3.3. Reagents

All chemicals used in this study were analytical reagent grade and used without further purification. Standard stock solutions (1,000 mg L^{-1}, atomic absorption standard solution) were obtained from Sigma-Aldrich and diluted as required.

Acetate buffer (0.1 M, pH 4.6) was used as supporting electrolyte and prepared by mixing glacial acetic acid and sodium acetate followed by diluting the solution with ultra-pure distilled water (Millipore). A pH meter (Metrohm 827 pH

Lab.) was calibrated using pH 4 and pH 7 calibration buffer solutions and, then used to verify the pH of the acetate buffer (supporting electrolyte) solution

Chemicals	**Source**
1 wt. % Nafion	Aldrich
Isopropyl-alcohol	Sigma-Aldrich
Cadmium	Fluka
Lead	Fluka
Copper	Fluka
Zinc	Fluka
Bismuth	Fluka
Antimony	Fluka
Mercury	Fluka
Glacial Acetic Acid	Sigma-Aldrich
Sodium Acetate	Sigma
Double-distilled Water	-
96 % Ethanol	Saarchem
37 % Hydrochloric Acid	Saarchem
65 % Nitric Acid	KIMIX

3.4. Standard solutions

Standard solutions were prepared in polyethylene vials in order to limit absorption onto the inner walls of the vial. Atomic absorption stock solutions of Zn^{2+}, Cd^{2+} and Pb^{2+} (1000 ppm) were diluted with 0.01 M HCl.

3.5. Acetate buffer solution (Electrolyte solution)

Ultrapure water was mixed with appropriate amounts of sodium acetate and glacial acetic acid in order to prepare a 0.01 M acetate buffer solution (ABS) which was used as the electrolyte for all electrochemical experiments.

3.6. Nitric acid solution

Nitric acid (65 %) was diluted with high purity distilled water on a volume to volume basis to prepare a 6 M Nitric acid solution. The prepared solution was utilised for electrode and glassware cleaning.

3.7. Synthesis of graphene oxide (GO)

Graphite oxide was synthesized from graphite powder according to the Hummers method [105] with some modification. Graphite powder (2 g) and sodium nitrite (1 g) were mixed with sulfuric acid (50 mL) in a clean dry conical flask and stirred at room temperature for 30 minutes, followed by subsequent mixing in an ice bath for 20 min. Potassium permanganate (7 g) was added gradually over a 30 minute period with constant stirring. The resulting solution was allowed to reach room temperature prior to being placed in a water bath set at 35 ^{o}C and, left to stir for 2 hours. The flask was returned to the ice bath with constant stirring. Ultra-pure water, 150 mL, was added before the addition of approximately 5 mL hydrogen peroxide until effervescence ceased. The flask was removed from the ice bath and allowed to stir at room temperature overnight and centrifuged for 20 minutes. Three successive acid washes were performed followed by one with ultra-pure water. The resulting product was the dried for 48

hours in a vacuum oven. The prepared graphite oxide (10 mg) was exfoliated in 10 mL of ultra-pure water or Ethanol to give a 1.0 mg mL^{-1} GO solution.

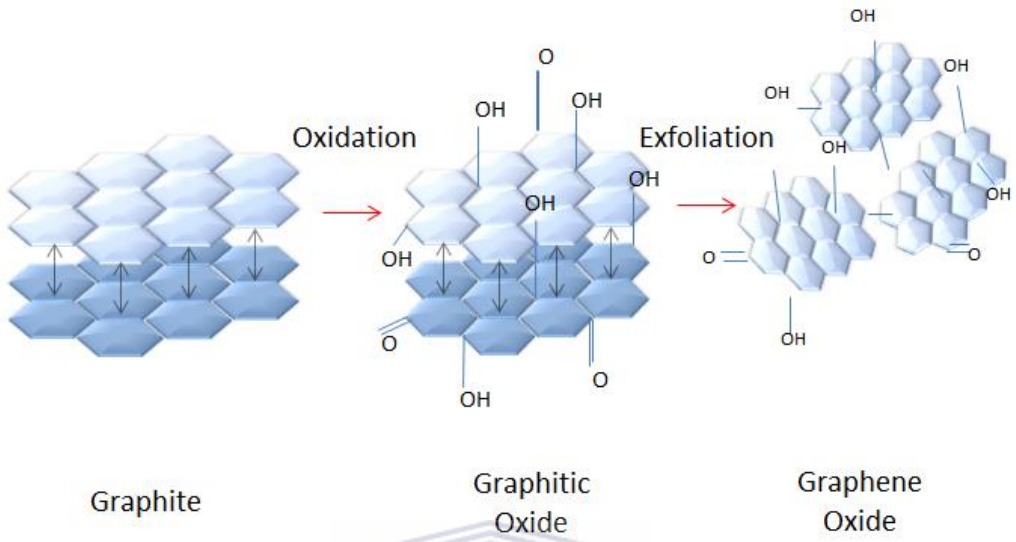

Figure 3.1: Graphic representation of GO synthesis from graphite powder

3.8. Synthesis of graphene powder

Synthesised graphene oxide (100 mg) was dispersed in a 100 mL portion of ultra-pure distilled water in a 250 mL round-bottom flask by ultrasonication for 1 hr. Following the ultrasonication, 200 mg $NaBH_4$ was added and stirred for 30 min. The resulting solution was allowed to cool to room temperature before refluxing over silicon oil at 135 ^oC for 3 hrs. Once cooled, the synthesis yields a 100 mL graphene in water solution. Separation of aqueous layer from the back solid was then performed by centrifugation, followed by resting the solution overnight. The top layer was then decanted and discarded. The graphene produced was dried at 60 ^oC for 3 days in a vacuum oven.

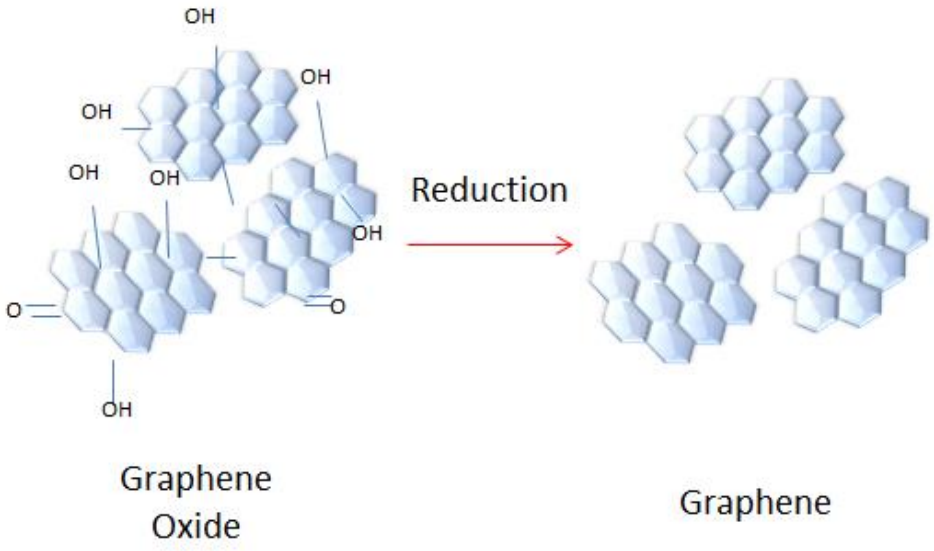

Figure 3.2: Graphic representation of reduction of graphene oxide (GO) to form graphene powder

3.9. Preparation of graphene oxide (GO) solutions for electrochemical reduction

The prepared graphite oxide (10 mg) was exfoliated in 10 mL of 0.1 M acetate buffer solution (pH 4.6) by ultrasonication for 1.0 hour to give a 1.0 mg mL^{-1} GO solution.

3.10. Preparation of graphene solutions

Graphene solutions were prepared by a weight-to-volume method. Appropriate amounts of graphene powder were accurately weighed out and dispersed in Ethanol prior to ultrasonication for 1.0 hour.

3.11. Preparation of Nafion solutions

3.11.1. 1 % Nafion Solution

A 1 mL portion of 5 wt. % Nafion was diluted using 5 mL ethanol in Ependorf tubes to yield a 1 % Nafion solution.

3.11.2. 0.2 % Nafion Solution

200 μL of 5 wt. % Nafion was diluted using 5 mL ethanol in Ependorf tubes to yield a 0.2 % Nafion solution.

3.12. Nafion-graphene (NG) solution

0.25 wt. % NG solutions were prepared by mixing 0.2 % Nafion solution with appropriate amounts of graphene powder followed by ultrasonication for 1 hour.

3.13. Preparation of Pencil Graphite Electrodes

The pencil graphite rods (Pentel, HB of 0.5 mm in diameter and 6 cm in length) were purchased from the local book store. A plastic syringe served as a holder into which the pencil rod was inserted exposing 1 cm of the rod tip at one end of the syringe. In order to establish electrical connection with the potentiostat a copper wire was attached to the other end of the pencil rod and passed through the top of the syringe.

3.14. Electrode cleaning

To achieve accurate and reproducible results in quantitative analysis impeccable electrode hygiene was applied. The pencil graphite electrodes were thoroughly cleaned before each use in a simple reproducible manner. A small quantity of ethanol was placed onto soft tissue paper and the surface of the electrode gently wiped followed by thorough rinsing with ultra-pure water. Successive dipping of the PGE in a 6 M HNO_3 solution and rinsing with ultra-pure water followed.

3.15. Nafion-graphene pencil graphite electrode (NG-PGE) preparation

Each pencil graphite electrode surface was electrochemically pretreated by applying a potential of +1.4V for 30 s in the blank supporting electrolyte (0.1 M acetate buffer solution (ABS) pH 4.6) without stirring in order to increase the hydrophilic properties of the electrode surface through the introduction of oxygenated functionalities, accomplished with oxidative cleaning as demonstrated in the work by Levent *et al* [122]. The pre-treated pencil graphite electrodes were immersed in vials containing NG solution for 5 min and air dried allowing for the evaporation of solvent. This process was repeated three times to produce uniformly coated NG-PGEs.

3.16. Electrochemical reduction of GO to form electrodeposited graphene pencil graphite electrodes (EG-PGE)

The cyclic voltammetric reduction was performed in 10 mL of GO dispersion (1 mg mL^{-1}) with constant stirring on a 797 VA COMPUTRACE instrument in the potential range between -1.4 and +0.3 V for seven successive cycles. The instrumental parameters used for the electrodeposition procedure were as follows; deposition time (120 s), frequency (50 Hz), amplitude (0.04 V) and voltage step (0.004 V).

3.17. Procedure SWASV analyses

The electrodes were immersed into the electrochemical cell containing, 10 mL of acetate buffer (0.1 M, pH 4.6), 10 µL of Bi^{3+} stock solution (1000 µg mL^{-1}), and the target metal ions. A reduction potential (-1.4 V) was applied to the working electrode (EG-PGE) with constant stirring at 1000 rpm for 120 seconds resulting in the *in situ* deposition of the bismuth film and target metal ions (Zn^{2+}, Cd^{2+}, and Pb^{2+}) onto the EG-PGE. After a brief rest period (10 seconds) the potential was scanned from -1.4 V to +0.3 V by applying a square- wave waveform to the EG-PGE. At the end of the scan the EG-PGE was electrochemically cleaned from the residual metals by applying a potential of 30 s at +0.3 V, with stirring.

The optimum instrumental parameters were determined for each film by varying one while keeping the remaining ones constant and investigating the

effects on the peak heights produced by the current. These optimum conditions were then utilized for all further experiments.

Before each experiment was performed a base line was recorded without any metals present in the cell in order to determine whether the electrode surface and cell was clean and to check for any spurious peaks.

Once an understanding of the technique as well as the electrode developed was achieved, the electrode was used for real life sample applications namely, for tap water analysis.

3.18. Quantitation

The method of standard addition was used to determine the concentration of the analytes. For reproducibility purposes, each analysis was repeated four times. The concentration of the analytes was calculated using the standard addition formula (3.18.1).

$$\mathbf{c\ (unknown)} = \frac{c(standard)\times v\times 1000}{(i'-i)\times(V+v)} \qquad \text{(Eqn. 3.18.1)}$$

Where,

c (unknown) = concentration of the final unknown solution.

c (standard) = concentration of the standard solution.

V = volume of the sample solution.

v = volume of the standard solution added.

i = peak height of the unknown solution.

i' = peak height of the unknown solution + standard.

3.19. Sample preparation

Tap water was collected in our laboratory after allowing water to run for 1 minute. For the determination of Zn^{2+}, Cd^{2+} and Pb^{2+}, an 8 mL sample of tap water and 2 mL of 2 M acetate buffer was added to the electrochemical cell and the analysis was performed as described by the procedure in Section 3.17.

3.20. Characterisation Techniques

3.20.1. Fourier Transformed Infrared (FT-IR) Spectroscopy

FT-IR spectroscopy was performed in order to distinguish between GO and graphene and confirms the inclusion of oxygen into the structure of graphite in the form of oxygenated functionalities. Little to no sample preparation was required for analysis. FTIR spectrum was recorded on the Perkin Elmer Spectrum 100 FT-IR spectrometer by placing approximately 10 mg of graphite, graphene oxide and graphene, ground in a pestle and mortar, on the Attenuated Total Reflectance (ATR) sample holder.

3.20.2. X-ray Diffraction (XRD)

Structural changes in graphite, graphene oxide and graphene were investigated along the chemical synthesis route through XRD analysis. A BRUKER AXS X-ray diffractometer with Cu-Kα radiation was utilised. Instrumental operating conditions are listed in Table 1 below.

Table 3.1: Operating parameters for XRD

XRD Operating Parameters	
Radiation Source	Cu-Kα
Radiation Wavelength (λ)	1.506 Å
Tube Voltage	40 kV
Tube Current	40 mA
Variable Slits	0.28 mm

3.20.3. Raman Spectroscopy

Raman spectroscopy was utilised to investigate any structural changes in graphite structure. A Dilor XY Raman spectrometer with a Coherent Innova 300 Argon laser with a 514.5 nm laser excitation was used. Samples for Raman spectroscopy were prepared by ultrasonicating 1.0 mg mL^{-1} solutions of graphite, graphene oxide and graphene in Ethanol. The exfoliated samples were drop cast onto glass slides in order to form thin films of sample for analysis.

3.20.4. High Resolution Transmission Electron Microscopy (HRTEM)

HRTEM analysis was used as a method of imaging any morphological and physical changes in graphite, graphene oxide and graphene. Samples diluted in ethanol were ultrasonicated in order to exfoliate sheets. Small quantities of the exfoliated solutions were drop cast onto S147-4 Holey carbon film 400 mesh Cu grids. Field Emission gun lens 1 was used with spot size 3, at 200 kV using Tecnai G2 F20 X-Twin MAT 200 kV Field Emission Gun Transmission Electron Microscope.

3.20.5. High Resolution Scanning Electron Microscopy (HRSEM)

HRSEM analysis was utilized as a method of characterizing the surface morphology of graphite, graphene oxide, graphene as well as morphological characterization of modified pencil graphite electrodes. Graphite, graphene oxide and graphene powders prepared as stated in section 3.7 and 3.8 were ground in a mortar and pestle in order to achieve a 'fine' powder. The ground samples were scattered onto carbon tape and investigated at various magnifications. For electrode characterization, modified electrodes were placed on carbon tape and analysed.

3.20.6. Atomic Force Microscopy (AFM)

The tapping-mode atomic force microscope (Veeco Nanoman V) was employed to evaluate the morphology of graphite oxide and graphene, with special emphasis on estimating its thickness. The silicon tip (Antimony (n) doped) had a curvature radius of 2.5-3.5 μm, a force constant of 1-5 N m^{-1} and a resonance frequency of 60-100 kHz. The samples for AFM were prepared by drop coating the graphene/water and graphene oxide/water (5 μL) dispersion onto a silicon wafer.

CHAPTER FOUR:

Morphological and Structural Characterization of Graphene

4.1. Introduction

The work demonstrated in this chapter describes and explains the morphological and structural changes along the chemical synthesis routes described in Chapter 3.7 and 3.8 above. FT-IR, EDX, Raman Spectroscopy, XRD, HRTEM, HRSEM and AFM were utilized to confirm the formation of good quality few-layer graphene sheets to be utilized as sensing platform for the detection of trace metals by anodic stripping voltammetry.

4.2. Fourier Transformed Infrared Spectroscopy (FT-IR)

Previous research has shown the scattering of a variety of oxygen containing functionalities along the graphene oxide surface namely hydroxyl, ethers, epoxides, carbonyl and carboxylic groups [48, 123, 124]. Figure 4.1 shows the Fourier transformed infrared (FT-IR) spectra of graphite and graphene oxide. As expected, graphite exhibits no significant characteristic IR features. However, for GO, the following characteristic IR peaks appear namely, the O-H stretching vibration at 3117 cm^{-1}, the C=O stretching vibration at 1760 cm^{-1} [125] and aromatic C=C stretching vibration at 1589 cm^{-1} [124]. The peak at 1401 cm^{-1} is associated with the bending C-O-H vibration [124], while the peaks at 1260 cm^{-1} [123] and 1026 cm^{-1} are due to the C-O stretching vibration occurring in epoxides and alcohols [125] within the graphite structure. Upon reduction using $NaBH_4$ as

reducing agent, a considerable decrease or complete removal of the above mentioned oxygen containing functionalities is noted demonstrating that all or most of the oxygen has been removed.

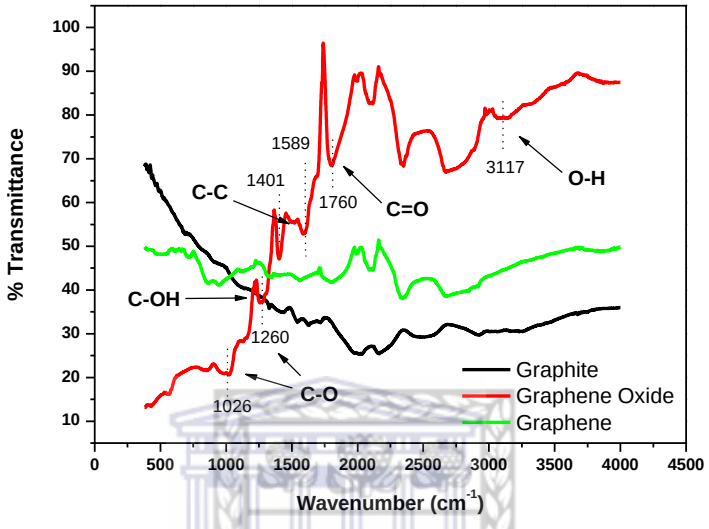

Figure 4.1: FT-IR spectra of Graphite, Graphene Oxide (GO) and Graphene

4.3. Energy Dispersive X-Ray Spectroscopy (EDS)

The EDS spectra of Graphite, Graphene Oxide and Graphene are represented in Figure 4.2 below. EDS corroborates the results obtained by FT-IR over small sample cross-sections. Similar Cu peaks are observed in all three samples under analysis. This inclusion is attributed to the choice of Cu mesh grids used for analysis. The grids used provide a sharp contrast between sample and grid as discussed in Chapter 3. Graphite, represented by Figure 4.2 (a), shows a large intensity of carbon present within the sample with no other significant peaks, as expected. In contrast, Oxygen, Sulphur and Chlorine peaks are observed for graphene oxide (Figure 4.2 (b)). The inclusion of oxygen within the graphite

structure indicates its effective oxidation. The sulphur and chlorine peak arise as a result of incomplete removal of starting materials after washing and drying and constitute contamination. Upon analysis of graphene (Figure 4.2 (c)) we note the reduction in intensity of oxygen peak indicating subsequent reduction of graphene oxide. The incomplete removal of oxygen is a draw-back to the chemical synthesis approach as well as the use of $NaBH_4$ as reducing agent but is to be expected. The presence of sodium indicates that further acid washing may be required to remove excess reducing agent.

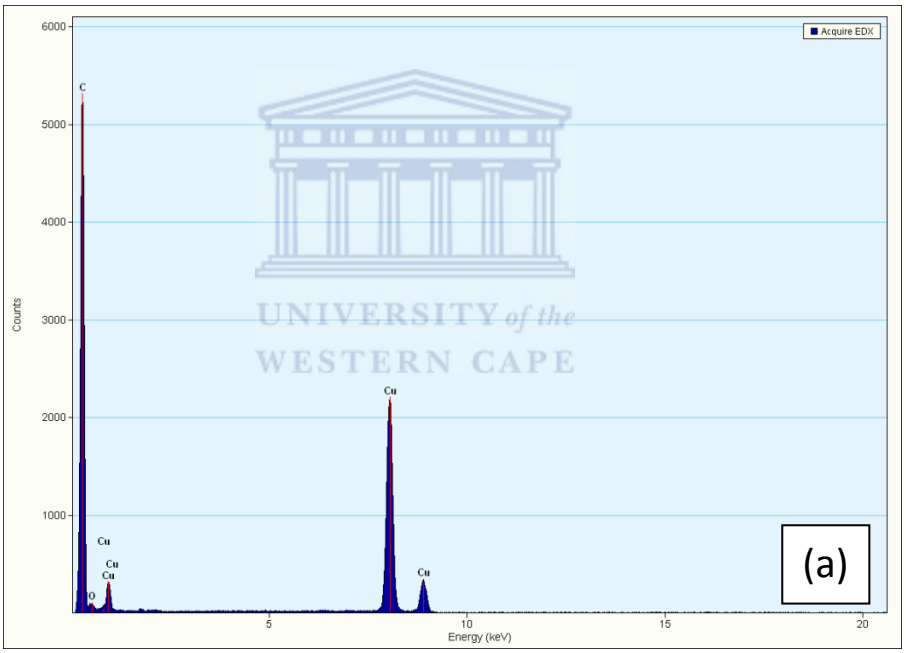

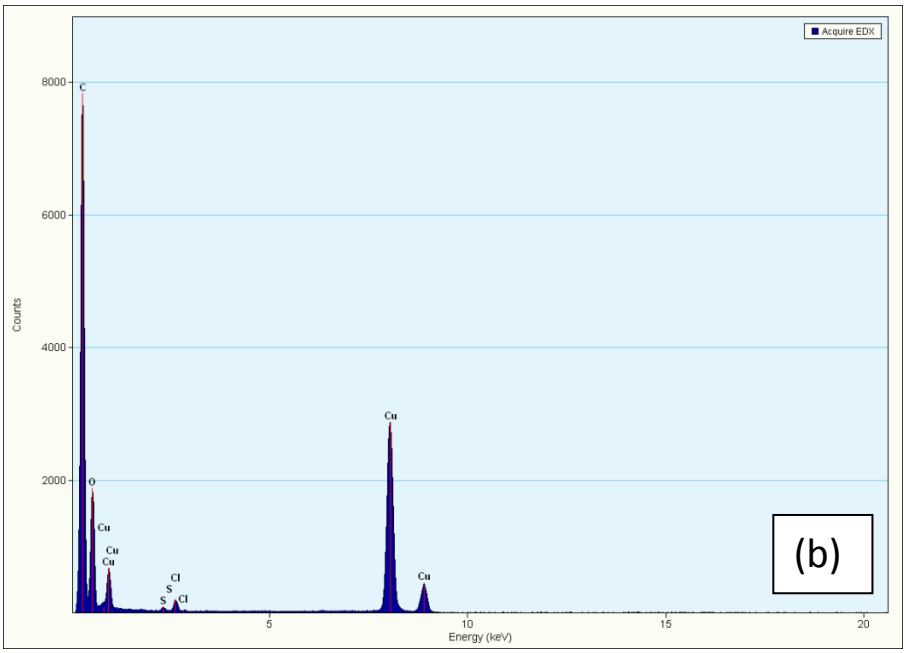

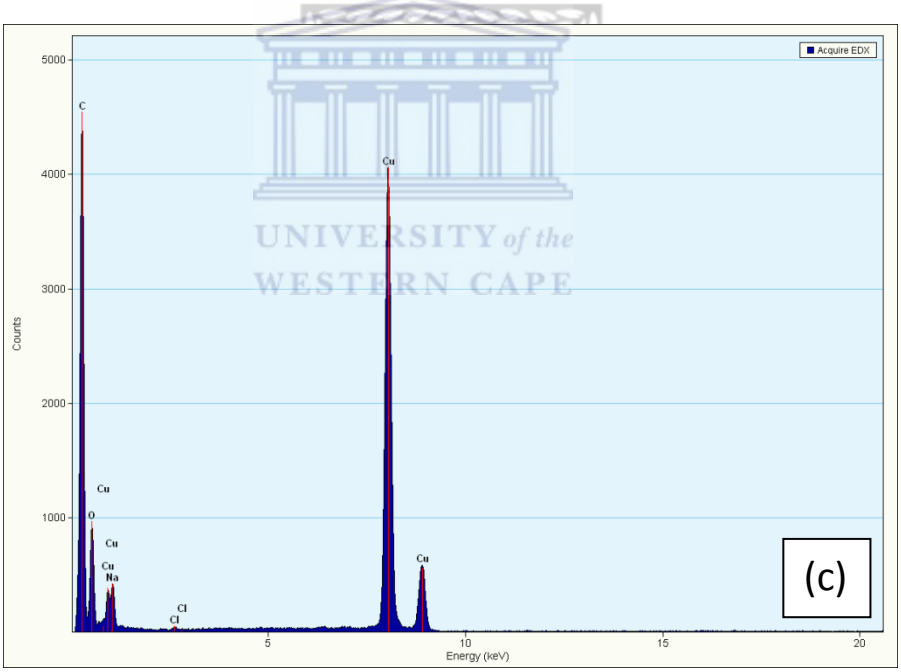

Figure 4.2: EDS spectra of (**a**) graphite, (**b**) graphene oxide and (**c**) graphene on standard copper-hole grids from HRTEM in conjunction with EDS detector.

4.4. Raman Spectroscopy

The change in structure, after the chemical transformation, from pure graphite to graphene oxide and graphene was investigated by Raman spectroscopy and represented by Figure 4.3 (a), (b) and (c) respectively. The Raman spectrum for graphite in Figure 4.3 (a) reveals a strong G band at 1575 cm^{-1}, a significantly weaker D band at 1350 cm^{-1} and a moderate 2D band at 2721 cm^{-1}. The G band occurs as a consequence of the symmetry which allows first order scattering of the E2g mode (of sp^3 hybridized carbon atoms) to occur in the neatly ordered graphite structure [47]. The ratio of the intensities of the D and G bands (I_D/I_G), used as a measure of disorder or defects within the structure [126, 127] was calculated as 0.25 for graphite, demonstrating the highly ordered structure.

Graphene oxide [Figure 4.3 (b)] on the other hand shows a significant decrease, broadening and Raman shift to 1600 cm^{-1} for the G band while the D band at 1360 cm^{-1} is considerably larger than in Figure 4.3 (a). This increase is attributed to the reduction in size of the in-plane sp^2 domains caused by the insertion of the epoxy, carboxyl, carbonyl and hydroxyl groups between the individual layers of the graphite [44]. A calculated I_D/I_G ratio of 0.975 was obtained, depicting an increase in structural disorder.

The Raman spectrum of graphene [Figure 4.3 (c)] includes the D peak located at 1345 cm^{-1}, G peak at 1589 cm^{-1} and 2D peak at 2867 cm^{-1}. The D band is attributed to the disorder or defects within the graphene structure or as a result of edge effects [128, 129]. The G band arises due to in-plane vibration of the sp^2 carbon atoms. The 2D band appears at almost double the frequency of the D band

and originates from second order Raman scattering processes. An increase in I_D/I_G ratio from 0.975, for GO to 1.17 for graphene is observed.

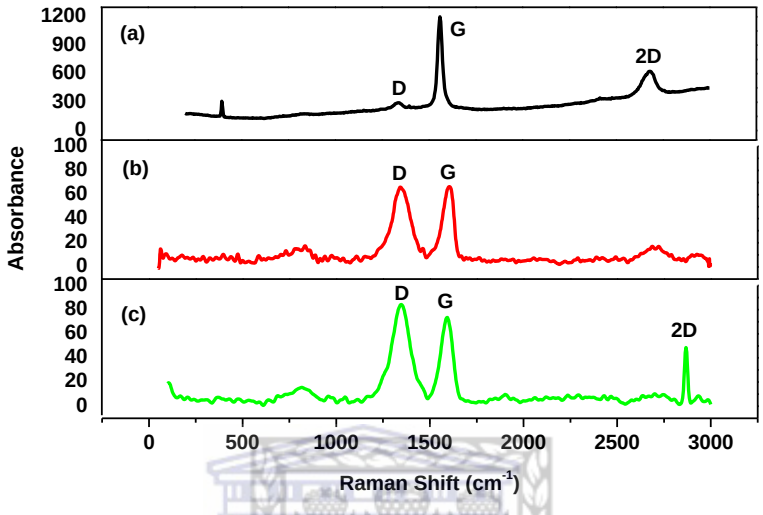

Figure 4.3: Raman spectra of (**a**) Graphite, (**b**) Graphene Oxide and (**c**) Graphene.

4.5. X-ray Diffraction (XRD)

The XRD patterns of graphite, graphene oxide (GO) and graphene are shown in Figures 4.4(a), 4.4(b) and 4.4(c) respectively. The peaks indexed as 100 at 44.58^o and 004 at 54.61^o are indicative of the crystalline structure of graphite [130] while the strong, distinguishable 002 peak at 26.56^o with inter-planar distance of 0.34 nm imply a highly ordered carbon structure [131]. In the XRD spectrum of GO the presence of a 001 peak at 9.81^o corresponds to an interlayer spacing of approximately 0.7 nm and confirms the presence of oxygen containing functional groups which in turn, facilitates the hydration and exfoliation of the graphene oxide sheets in aqueous media [132]. After reduction of graphene oxide

the peak at 9.81^{o} disappeared. A broad peak centered at 25^{o} occurred as a result of increased disorder and structural defects due to sonication [129].

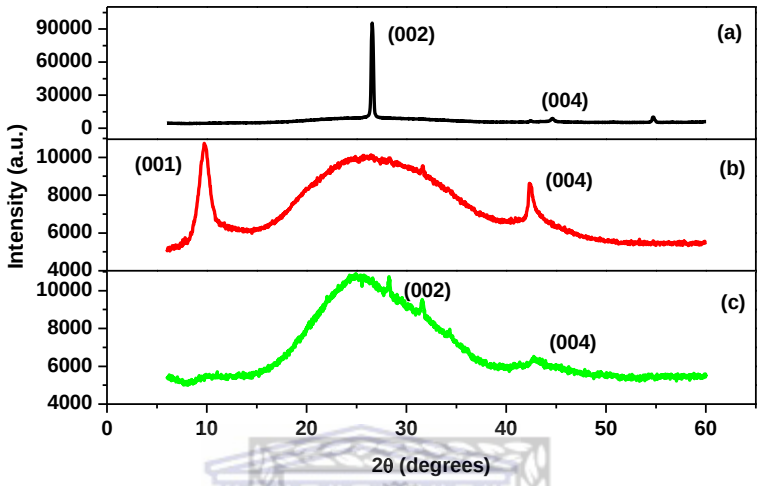

Figure 4.4: X-Ray Diffraction Patterns for (**a**) Graphite, (**b**) Graphene Oxide and (**c**) Graphene.

4.6. High Resolution Transmission Electron Microscopy (HRTEM)

Samples for HRTEM analysis were prepared by ultrasonication in pure ethanol and then drop-casted onto Cu grids. The HRTEM image, Figure 4.5(a) of pure graphite is portrayed as thick dark flakes with distinct sharp, straight edges demonstrating its crystalline nature. At higher magnification highly ordered packing of graphene sheets are observed as highlighted by the arrows in Figure 4.5(b). The GO image, Figure 4.5(c), however is significantly different in graphitic structure when compared to that of graphite. Here, large transparent "wavy" sheets having soft edges are seen with entanglement and folding being

portrayed as large wrinkles within sheets. An increase in transparency suggests regions of monolayer graphene [133]. Upon examination, at higher magnification of flake edges [Figure 4.5(d)] small regions of individual graphene sheets are observed. A lack of complete separation in non-aqueous media, such as ethanol is observed. This behaviour can presumably be attributed to the strong interlayer hydrogen bonds between the oxygen functional groups of adjacent graphene oxide layers in GO [134]. The HRTEM image for graphene in Figure 4.5(e) shows similar to GO [Figure 4.5(c)]. Lighter sheets with increased transparency, indicating decreased thickness as well as fewer wrinkles are observed. Figure 4.5(f) represents high magnification imaging of graphene. Exfoliation of individual sheets is observed but incomplete.

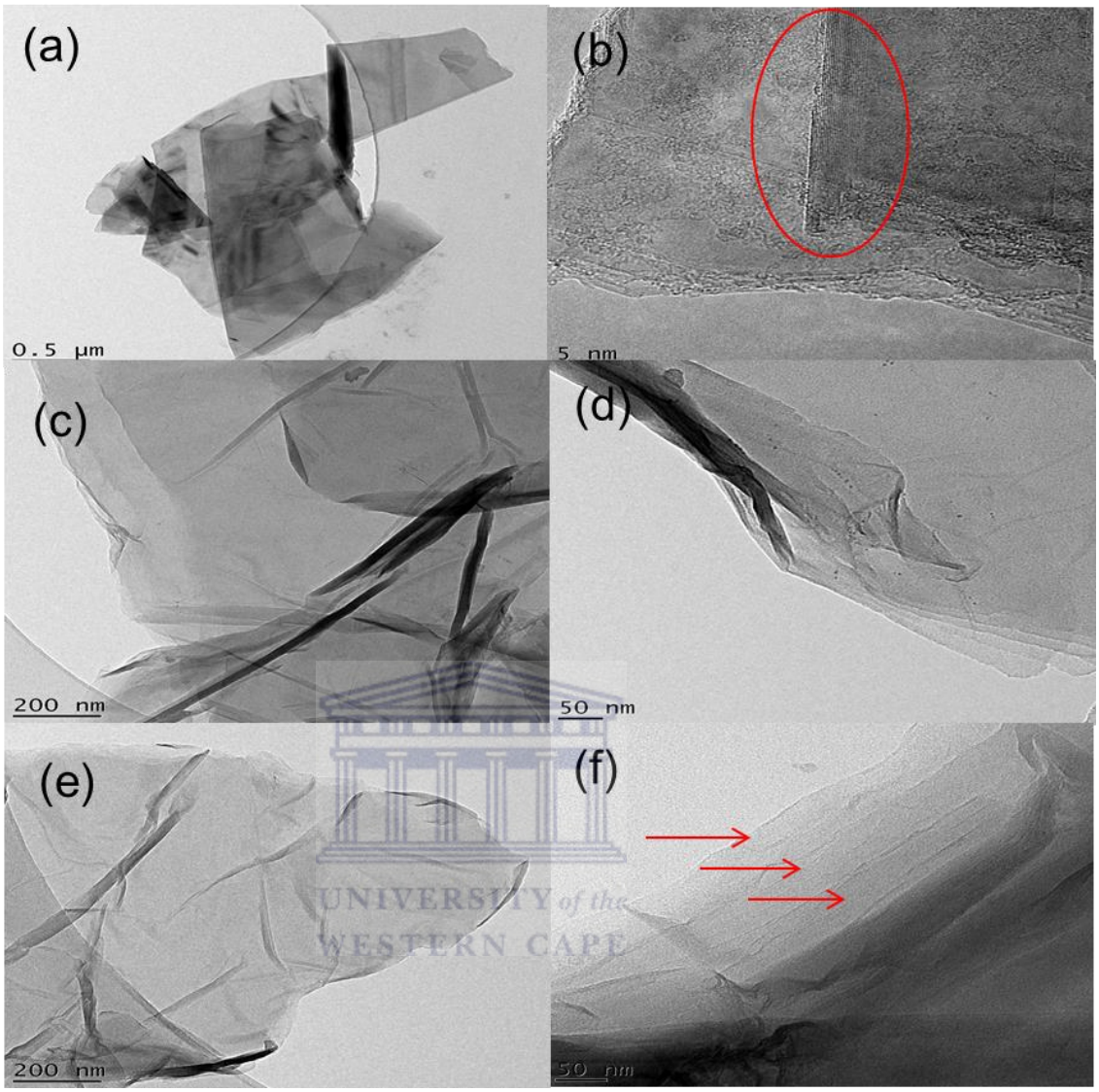

Figure 4.5: HRTEM images showing selected features of Graphite [(**a**) and (**b**)], Graphene Oxide [(**c**) and (**d**)] and Graphene [(**e**) and (**f**)].

4.7. High Resolution Scanning Electron Microscopy (HRSEM)

The surface morphologies of graphite, GO and graphene were investigated by high resolution scanning electron microscopy (HRSEM) according to the procedures stipulated in Chapter 3 and represented in Figure 4.6 below. The HRSEM image of graphite demonstrates a feather-like, "crumpled tissue paper"

texture with harsh lines indicating packing of graphene sheets on one another. A SEM image of feathery GO powder Figure 4.6(b), shows an agglomeration of the platelets. It is noticed that the GO shows an uneven surface probably owing to the oxidation of sheets [135]. The SEM image of graphene in Figure 4.6(c) reveals that the material consists of thin, haphazardly aggregated, wrinkly sheets closely linked with each other forming a lawless solid [47]. A comparison of the three surface morphologies does not reveal any significant differences as a result of lack of exfoliation of platelets in sample preparation.

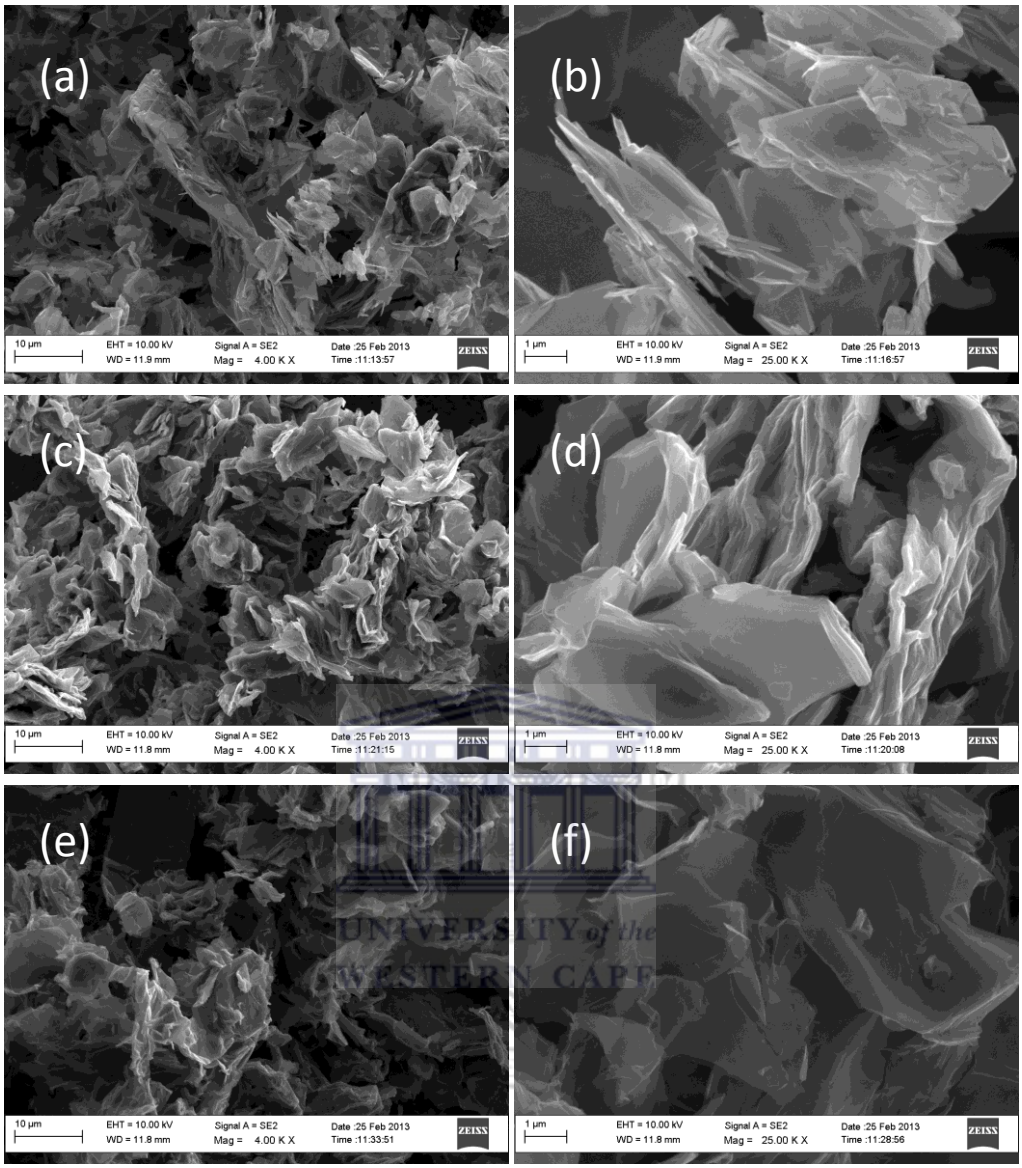

Figure 4.6: HRSEM images representing surface morphologies of Graphite [(**a**) and (**b**)], Graphene Oxide [(**c**) and (**d**)] and Graphene [(**e**) and (**f**)].

4.8. Atomic Force Microscopy (AFM)

Individual GO sheets were imaged using tapping mode AFM in order to estimate the dimensions of sheets. Figure 4.7(a) shows the image of a single flake of GO drop casted from graphene oxide dispersion (1 mg mL^{-1}) onto a silicon substrate. The cross-sectional view across the plain of the GO flake gave an

estimated vertical distance (thickness) ranging from 1.78 - 2.10 nm and flake lengths of approximately 0.6 µm. Typically the thicknesses of individual GO sheets are in the range of 0.7 - 1.0 nm [136, 47] hence, the flake shown in Figure 4.7(a) corresponds to two GO sheets stacked together and is consistent with that reported by Marcano *et al*. [123]. Similar imaging was performed for graphene and shown in Figure 4.7(b). Flakes of graphene and graphene oxide appear similar under AFM imaging. The cross-sectional view of graphene shows estimated vertical distance or thickness averaging at 2.00 nm. From literature, the inter-planar distance of graphene is approximately 3.5 nm [136, 47]. A vertical distance of 2.00 nm corresponds to the stacking of approximately 5 individual graphene sheets.

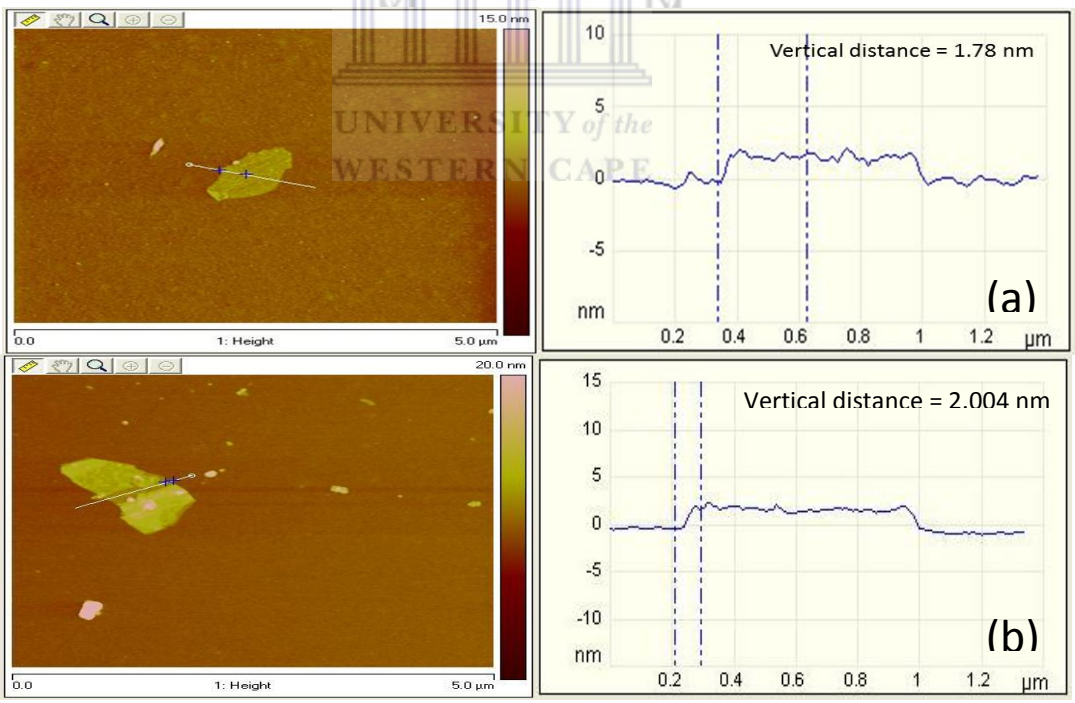

Figure 4.7: Tapping-mode AFM images and corresponding cross-sectional views of (**a**) graphene oxide and (**b**) graphene on silicon substrates.

CHAPTER FIVE:

Electrodeposited Graphene Pencil Graphite Bismuth-Film Electrodes (EG-PG-BiE)

5.1. Introduction

Graphene, a one-atom-thick 2D allotrope of carbon, is a very important material in fundamental scientific and technological research. It has its carbon atoms arranged in a honeycomb structure of hexagons with sp^2 hybridisation [8]. Graphene has attracted a lot of attention since it was first produced in 2004 and has shown to significantly improve the sensitivity in various applications [40]. In addition to the possibility of low- power, high density, and high-speed switches, graphene- based devices may also be applied to other areas as a storm- thick membrane for sensing pressure as components in nanoelectrochemical systems or in chemical sensing because of their high surface area [37].

Methods of developing active materials on electrode surfaces are crucial in the creation of sensitive sensors with high performance. Commonly used coating methods include drop casting [8], dip coating [40] and passive adsorption [43, 42] of graphene solutions, prepared via the chemical reduction of graphene oxide. The lack of control of film thickness and harsh reagents, which contaminate samples are a major downfall. Electrochemical reduction has been seen as a promising alternative due to its fast and green synthesis approach [50, 51, 52, 49]. Guo *et al*. and Chen *et al*. have proposed a direct electrochemical reduction method of

preparing reduced-graphene films at electrode surfaces in order to control film thickness and limit structural defects in graphene sheets [50, 49].

In this chapter, a one-step direct electrochemical reduction technique was utilised to prepare graphene modified pencil graphite electrodes from colloidal graphene oxide solutions. The modified pencil graphite electrodes were applied for the determination of trace metals (Zn^{2+}, Cd^{2+} and Pb^{2+}) by anodic stripping voltammetry (ASV) in conjunction with an *in situ* plated bismuth film.

5.2. Electrochemical Reduction of graphene oxide (GO)

Repetitive cyclic voltammograms obtained from the direct electrochemical reduction of a GO colloidal solution (1.0 mg mL^{-1}) onto PGEs are shown in Figure 5.1 and shows two anodic (I and II) and one cathodic (III) peak. The deposition of conducting graphene onto the PGE surface is confirmed by the redox couple (II and III). An increase in anodic peak (II) at 0.2 V and cathodic peak (III) at -0.6 V with increasing number of scans is observed [49]. The increase in peak currents (II and III) with increasing number of scans can be attributed to the deposition of graphene sheets that are formed by the reduction of GO sheets that are in direct contact with the electrode surface [49]. Furthermore, the large anodic peak I at -1.1 V decreased rapidly after the first cycle suggesting the conversion of the GO sheets in direct contact with the electrode surface.

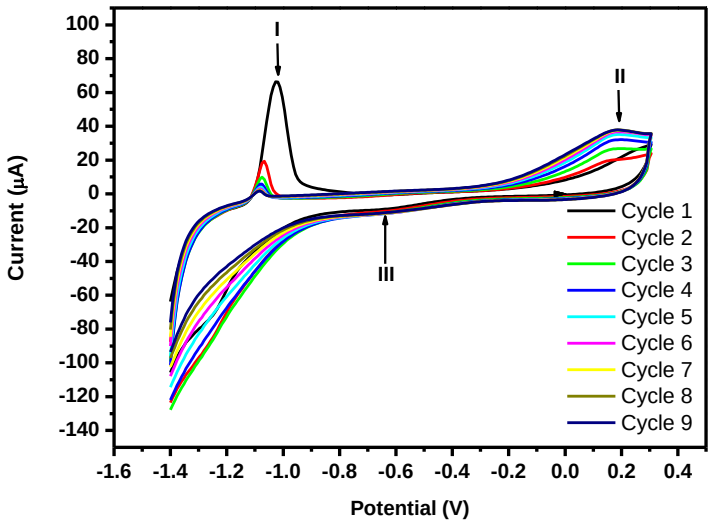

Figure 5.1: Cyclic voltammograms depicting the electrochemical reduction of 1.0 mg mL^{-1} GO in acetate buffer solution (0.1 M, pH 4.6) at the PGE using the following instrumental parameters: scan rate (10 $mV.s^{-1}$), deposition time (120 s); frequency (50 Hz); amplitude (0.04 V) and voltage step (0.004 V).

Figure 5.2, below represents the characteristic cyclic voltammograms of (a) a bare PGE and (b) an EG-PGE in 0.1 M acetate buffer solution. The absence of the peaks at -1.1 V, +0.2 V and -0.6 V, shown in Figure 6 confirm that they are due to red-ox actions of the GO solutions. A larger current range is observed for graphene-modified PGEs due to the enhanced electron transfer and conductivity at the electrode surface.

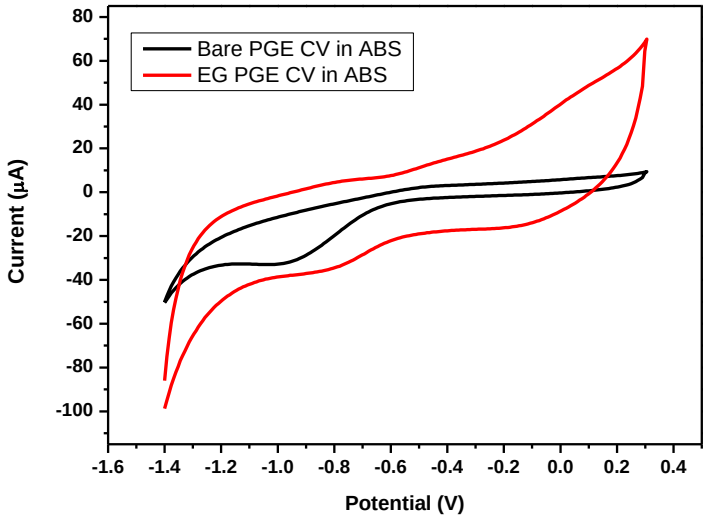

Figure 5.2: Cyclic voltammograms of (**a**) a bare PGE and (**b**) an EG-PGE in acetate buffer solution (0.1 M, pH 4.6) at the following instrumental parameters: scan rate (10 mV s^{-1}), deposition time (120 s), frequency (50 Hz), amplitude (0.04 V) and voltage step (0.004 V).

5.3. Characteristic oxidation potentials of Bi^{3+} and target metal ions (Zn^{2+}, Cd^{2+}, and Pb^{2+})

Figure 5.3 shows well-resolved, symmetrical characteristic stripping peaks for Zn^{2+}, Cd^{2+}, Pb^{2+} and Bi^{3+} at the EG-PG-BiEs in 0.1 M acetate buffer solution (pH 4.6). The oxidation potentials of the metal ions appear at -1.10 V, -0.75 V, -0.50 V and -0.06 V, respectively and arise from the redox reactions (equations 5.1 and 5.2) intrinsic to the anodic stripping analysis technique.

Mn^{n+} + né + Bi^{3+} → M (Bi) deposition step (reduction reaction) (Eqn. 5.1)

M (Bi) → M^{n+} + né + Bi^{3+} stripping step (oxidation reaction) (Eqn. 5.2)

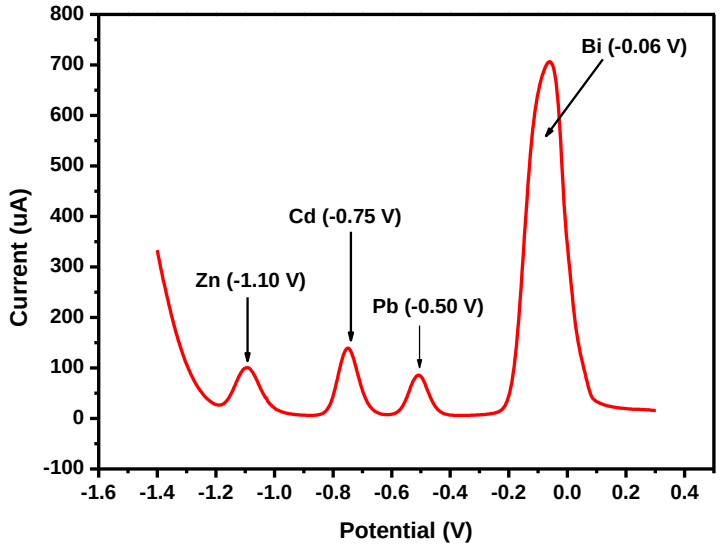

Figure 5.3: Anodic stripping voltammogram of characteristic oxidation stripping potentials of Zn^{2+} (1.10 V), Cd^{2+} (-0.75 V), Pb^{2+} (-0.50 V) and Bi^{3+} (-0.06 V) in 0.1 M acetate buffer solution (pH 4.6).

5.4. Influence of the number of electrodeposition cycles.

The speed and ease of electron transfer through a film is of paramount importance to the performance and sensitivity of any electrode. Figure 5.4 show that the number of electrochemical reduction cycles influences the stripping peak currents of Zn^{2+}, Cd^{2+} and Pb^{2+}. A general increase in peak currents is observed for all three metal ions up to 7 cycles after which, the thickness of the graphene film impedes the flow of electrons to the electrode surface. A deposition of seven cycles was selected as the optimum number of cycles for the detection of heavy metals at the EG-PG-BiE.

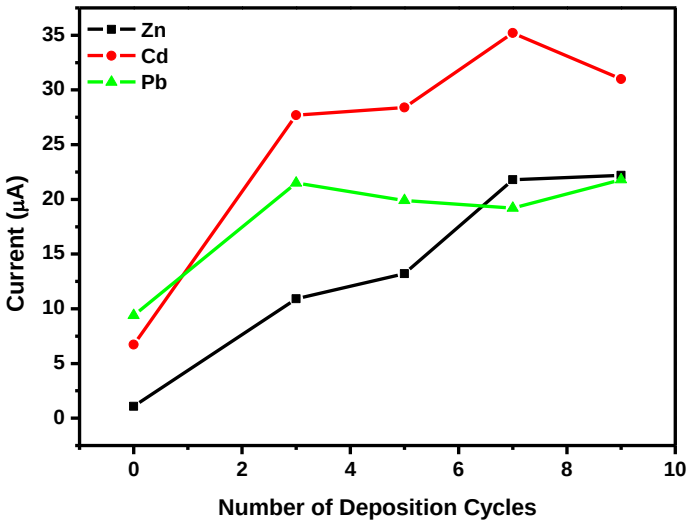

Figure 5.4: Effect of number of cycles on the stripping peak currents of Zn^{2+}, Cd^{2+} and Pb^{2+} at the EG-PG-BiE in 0.1 M acetate buffer (pH 4.6) at 120 s deposition time.

5.5. Microscopic Characterisation of Electrodeposited Graphene Modified Pencil Graphite Electrode (EG-PGE)

High resolution scanning electron microscopy (HRSEM) images of the bare PGE and EG-PGE surface morphologies are shown in Figure 10. The bare PGE surface shows surface roughness with grooves along the surface in the direction of machining, Figures 5.5(a) and 5.5(b). Following the electrodeposition, patterning was observed at the PGE surface at low magnification, Figure 5.5(c) while at higher magnification, Figure 5.5(d) flakes of graphene sheets are observed at the electrode surface. Erdem *et al*. reported similar microscopic images for the single walled carbon nanotube (SWCNT) modified graphite electrodes [42].

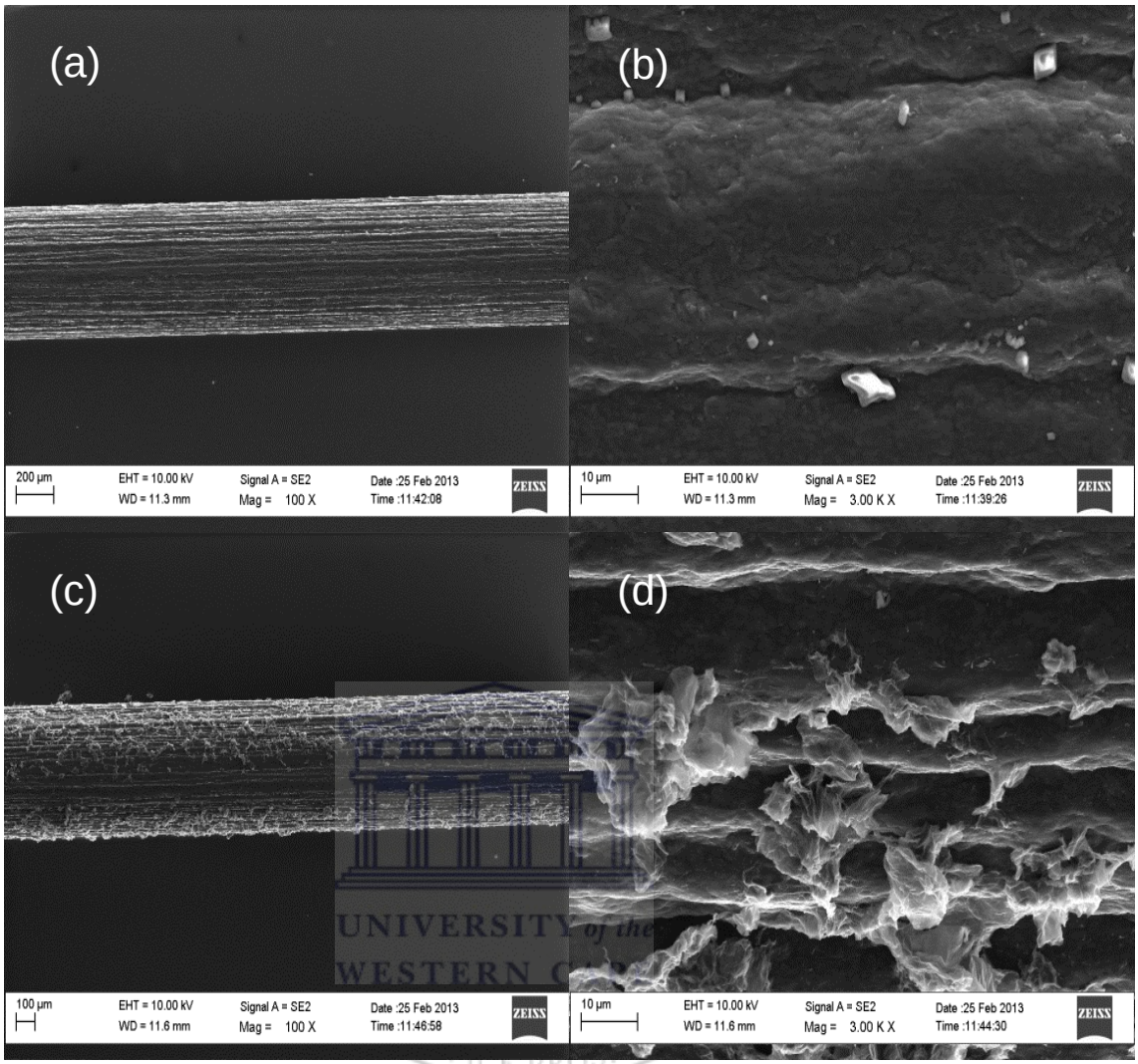

Figure 5.5: HRSEM images of bare PGEs (**a**) 100 times magnification, (**b**) 3000 times magnification and electrodeposited graphene PGEs (**c**) 100 times magnification, (**d**) 3000 times magnification.

5.6. Effect of Graphene Modified PGEs

The peak current responses of the bare PGE, EG-PGE and EG-PG-BiE platforms towards Zn^{2+}, Cd^{2+} and Pb^{2+} in 0.1 M acetate buffer solution (pH 4.6) are compared in Figure 5.6. A considerable increase in peak current is observed at

the EG-PGE in comparison to the bare PGE indicating improved sensitivity towards the heavy metal ions. The higher surface area-to-volume ratio, enhanced electron transfer and conductivity due to quantum confinement of graphene in the nanometer range (1-100 nm) [137, 116, 97, 138] all contribute towards the increase in stripping peak current. Furthermore, use of metal-films as part of the electrochemical platform for heavy metal ion detection is confirmed by the enhancement in stripping peak current and peak symmetry from EG-PGE to EG-PG-BiE. The fused alloys formed with bismuth-films allows for improved selectivity and sensitivity

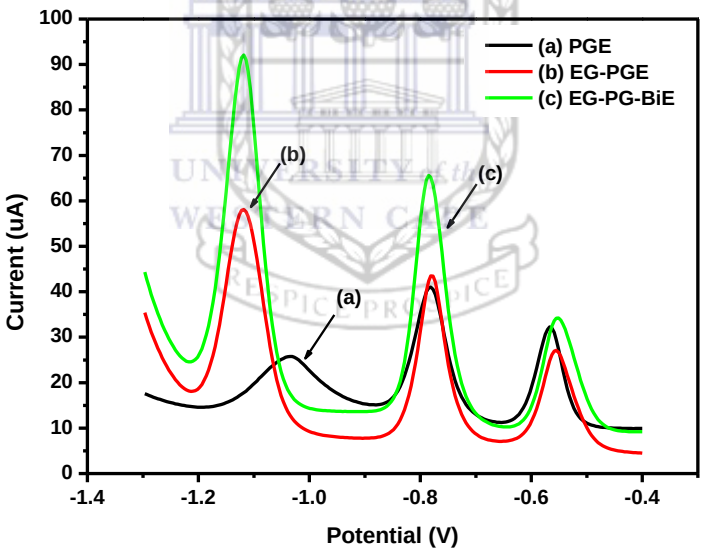

Figure 5.6: SWASV of 30 µg L^{-1} Zn^{2+}, Cd^{2+} and Pb^{2+} at (a) bare PGE, (b) EG-PGE and (c) EG-PG-BiE. Supporting electrolyte: 0.1 M acetate buffer (pH 4.6), deposition potential (-1.4 V), deposition time (120 s), frequency (50 Hz), amplitude (0.025 V) and voltage step (0.005 V).

5.7. Film Stability and Reproducibility

The stripping peak currents of Zn^{2+}, Cd^{2+} and Pb^{2+} showed little or no change during the preparation of the modified electrodes as well as its application to the detection of 20 μg L^{-1} of target metal ions in 0.1 M of acetate buffer (pH 4.6), at the same conditions. Relative standard deviation (RSD %) for the oxidation peaks were calculated to be in the range of 1 – 3.5 % for all three target metal ions. The low standard deviation provides evidence as to the good reproducibility in preparing the EG-PG-BiEs.

5.8. Effect of Supporting Electrolyte

The EG-PG-BiE was evaluated in different electrolyte solutions; 0.1 M acetate buffer solution (pH 4.6), 0.1 M HCl solution (pH 2) and 0.1 M phosphate buffer solution (pH 7.1) containing 30 μg L^{-1} each of Zn^{2+}, Cd^{2+} and Pb^{2+} ions. Figure 5.7 shows the stripping voltammograms recorded in the various electrolyte solutions. HCl (0.1 M, pH 2) shows small broad peaks for Cd^{2+} and Pb^{2+} with no Zn^{2+} peak. A large hydrogen evolution peak which extends to -1.1 V (the oxidation potential of Zn^{2+}) is observed and interferes with the Zn^{2+} signal. Phosphate buffer solution (0.1 M, pH 7.1) demonstrates small broad peaks for Zn^{2+} and Cd^{2+} with very broad peak for Pb^{2+}. The acetate buffer solution (0.1 M, pH 4.6) showed the best responses towards the three metal ions yielding tall peaks with good resolution and was thus selected as the preferred electrolyte.

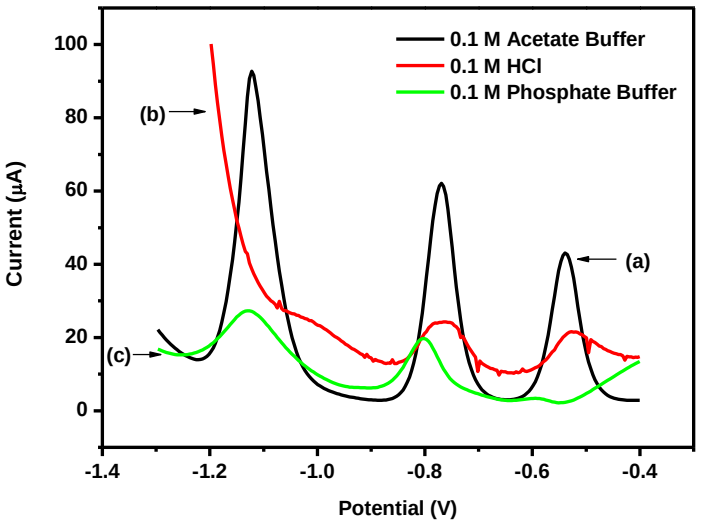

Figure 5.7: SWASV of 30μg L^{-1} of Zn^{2+}, Cd^{2+} and Pb^{2+} at EG-PG-BiE with supporting electrolyte: (**a**) 0.1 M acetate buffer (pH 4.6), (**b**) 0.1 M HCl and (**c**) 0.1 M phosphate buffer (pH 7.1). Deposition potential: -1.4 V; deposition time: 120 s; frequency: 50 Hz; amplitude: 0.025 V and voltage step: 0.005 V

5.9. Effect of the bismuth ion (Bi^{3+}) concentration

The effect of the bismuth ion concentration on the stripping peak currents of Zn^{2+}, Cd^{2+} and Pb^{2+} at the unmodified pencil graphite electrode (PGE) in Figure 5.8, was investigated in a 0.1 M acetate buffer solution (pH 4.6) containing 20 μg L^{-1} of each Zn^{2+}, Cd^{2+} and Pb^{2+} using Bi^{3+} concentrations varying from 200 to 5000 μg L^{-1}. In this controlled situation, the concentration of the bismuth solution was directly proportional to the thickness of the Bi-film [40]. The stripping current for all three metals showed similar behavior in the range of 200 – 800 μg L^{-1} where the stripping currents increased to a maximum with increasing concentration followed by the decrease in peak current with increasing Bi^{3+}

concentration. As a consequence of this behavior a bismuth ion concentration of 800 µg L^{-1} was selected for the developing the *in situ* deposited bismuth film.

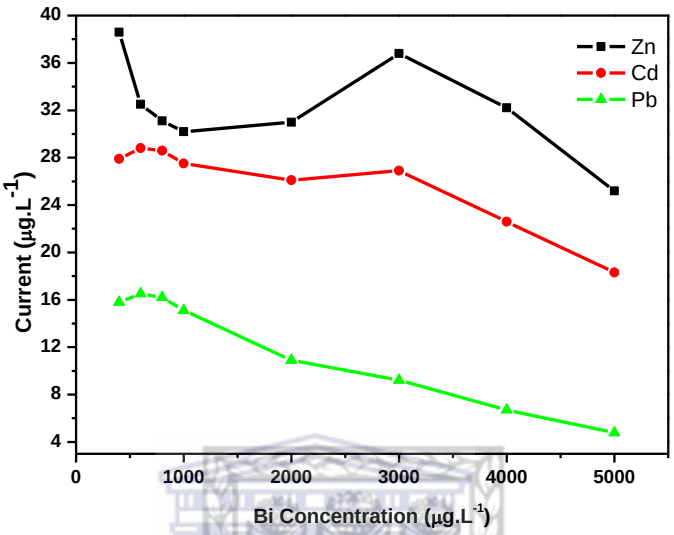

Figure 5.8: Effect of bismuth ion concentration on the stripping peak current of Zn^{2+}, Cd^{2+} and Pb^{2+} at electrodeposited graphene pencil graphite bismuth film electrode (EG-PG-BiE) in a 0.1 M acetate buffer solution (pH 4.6) containing 20 µg L^{-1} of each metal.

5.10. Optimisation of Instrumental Parameters

Amongst the various stripping waveforms (differential pulse, cyclic and square-wave), the square-wave modulation combines high sensitivity with high speed. In addition, square-wave voltammetry shows insensitivity towards dissolved oxygen and is advantageous since analysis can be performed without the time-consuming deoxygenating step [2, 40]. The square-wave parameters affecting the analytical response at the EG-PG-BiE are amplitude, deposition

potential, deposition time, frequency and rotation speed and are shown in Figure 5.9.

The amplitude in Figure 5.9(a) was varied from 10 to 100 mV and showed an increase in stripping peak currents (for all three metals) with increasing amplitude up to a maximum, followed by a gradual decrease. Cadmium and zinc show steeper rising slopes demonstrating their enhanced dependence on amplitude. A 40 mV amplitude was selected for subsequent experiments based on the information that any further amplitude increases does not result in a significant increase in peak current.

The influence of deposition potential on the peak currents of Zn^{2+}, Cd^{2+} and Pb^{2+} at the EG-PG-BiE was investigated in the potential range from +0.2 V to -1.7 V [(Figure 5.9(b)]. At potentials more positive than the oxidation potentials of individual metal ions no stripping peaks were observed due to the suppression of the reduction reaction responsible for the deposition of metal ions from solution onto the electrode surface. A general increase for all three metal ions is observed with increasing negative potentials up to -1.4 V, due to the preferential reduction and deposition of metal ions at the electrode surface. Electrode saturation results in the decrease in stripping response between -1.4V and -1.7V. A potential of -1.4 V was chosen as the optimal deposition potential.

The effect of deposition time on the peak currents of the target metal ions [(Figure 5.9(c)] was studied over the time interval from 30 to 600 seconds. As the deposition time increased so does the stripping peak current for each metal ion since, a longer time allowed for more metal to be deposited onto the electrode surface. At deposition times greater than 540 seconds the peak heights level off

suggesting surface saturation of the electrode, hence a deposition time of 120 s was used for further analysis.

Figure 5.9(d) shows the dependence of peak currents on the square wave frequency over the 12.5 Hz to 125 Hz range. The peak current for all three metals exhibit a linear increase with increasing frequency and is attributed to the increase in scan rate with increasing frequency [139]. A frequency of 50 Hz was chosen since distinct peaks with good resolution obtained.

Effect of rotation speed during the pre- concentration step was studied from 200 to 2000 rpm [Figure 5.9(e)]. As the rotation speed increased, so does the peak currents of the metal ions being analyzed. Rotation speed enhances sensitivity of stripping analysis as it facilitates the movement of metal ions from the bulk solution to the electrode surface. A rotation speed of 1000 rpm was chosen in.

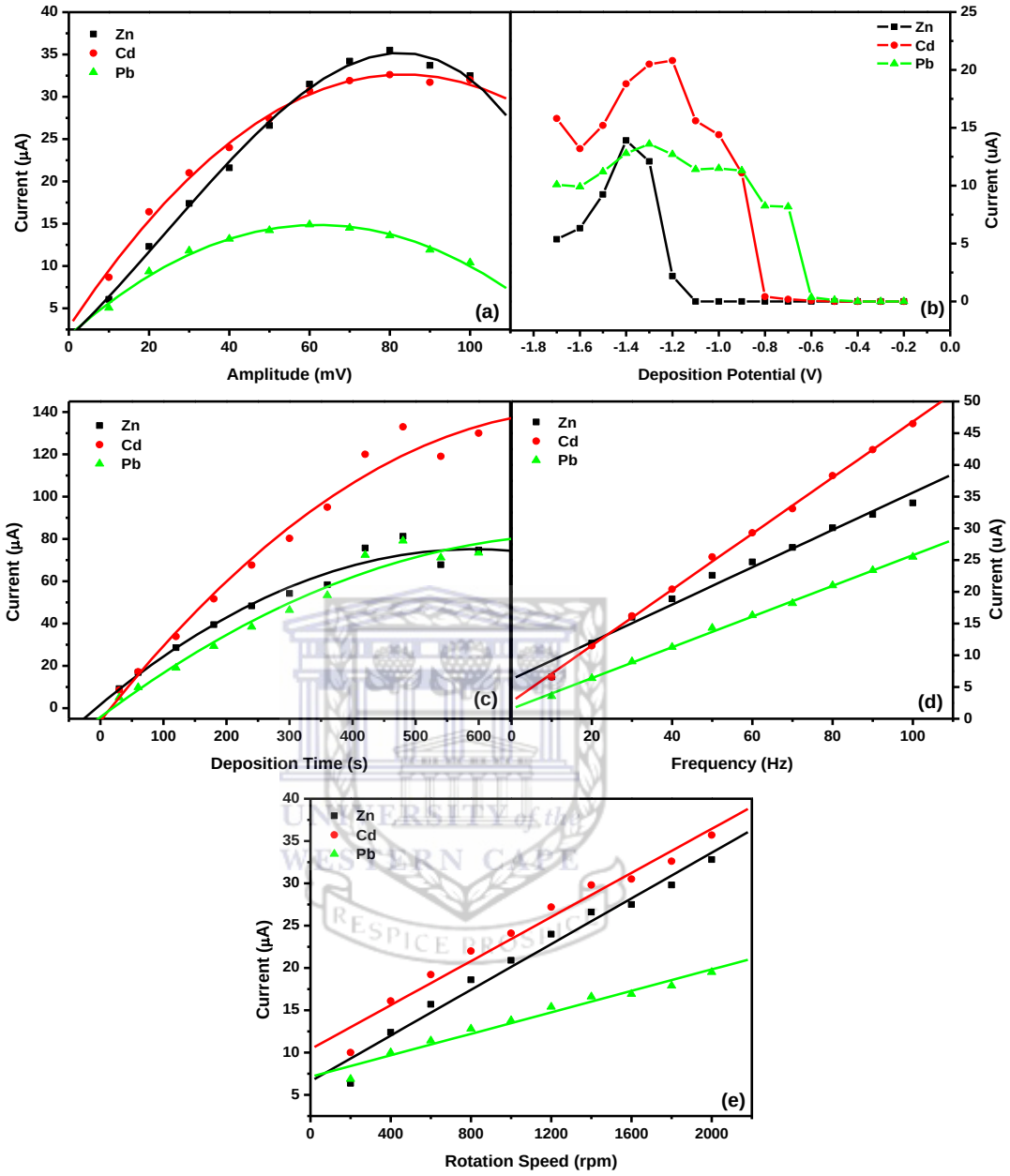

Figure 5.9: Effect of amplitude (**a**), deposition potential (**b**), deposition time (**c**), frequency (**d**) and rotation speed (**e**) on the stripping peak current of Zn^{2+}, Cd^{2+} and Pb^{2+} at electrodeposited graphene pencil graphite bismuth film electrode (EG-PG-BiE) in a 0.1 M acetate buffer solution (pH 4.6) containing 20 µg L^{-1} of each metal and 800 µg L^{-1} of bismuth.

5.11. Analytical Performance of Electrodeposited Graphene modified Pencil Graphite Bismuth-film Electrodes

The analytical performance of EG-PG-BiEs were investigated by simultaneous and individual analysis of Zn^{2+}, Cd^{2+} and Pb^{2+} over a low (2 – 20 µg L^{-1}) and a high (10 – 100 µg L^{-1}) concentration range. A slight shift in the peak potentials towards more positive potentials was observed for all three metal ions due to the IR-drop effect [8] since the oxidation of the metals became less reversible [139]. Figures 5.10 and 5.11 show the voltammograms and calibration plots for simultaneous and individual analyses, respectively. Calibration plots constructed from data obtained from voltammograms were used to calculate the detection limits and are presented in Table 5.1. Only the voltammograms and calibration curves for simultaneous and individual analyses at EG-PG-BiE over 10 – 100 µg L^{-1} range are presented in Figures 5.10 and 5.11.

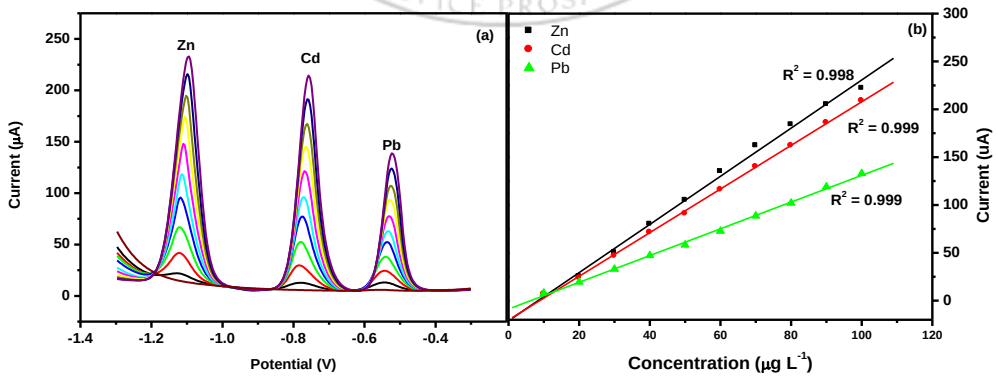

Figure 5.10: SWASV and corresponding calibration plots of simultaneous analysis of Zn^{2+}, Cd^{2+} and Pb^{2+} obtained at EG-PG-BiE over 10 – 100 µg L^{-1}. Supporting electrolyte: 0.1 M acetate buffer (pH 4.6), deposition time: 120,

deposition potential: -1.3 V, rotation speed: 1000 rpm, frequency: 50 Hz, amplitude: 0.04 V and sweep rate: 0.2975 V. s^{-1}.

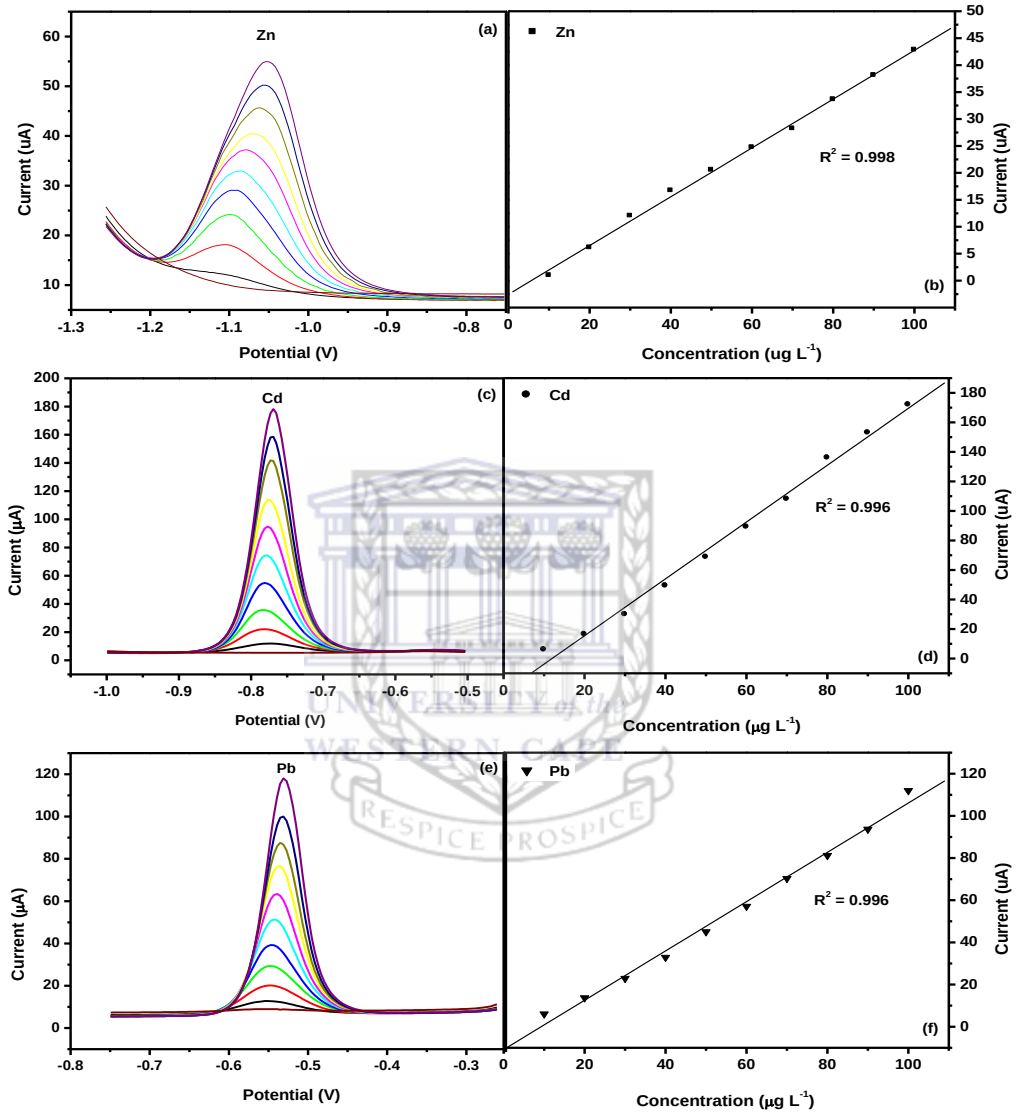

Figure 5.11: SWASV and corresponding calibration plots for individual analysis of (**a** and **b**) Zn^{2+}, (**c** and **d**) Cd^{2+} and (**e** and **f**) Pb^{2+} obtained at EG-PG-BiE over 10 – 100 µg L^{-1}. Supporting electrolyte: 0.1 M acetate buffer (pH 4.6), deposition time (120), deposition potential (-1.3 V), rotation speed (1000 rpm), frequency (50 Hz), amplitude (0.04 V) and sweep rate (0.2975 V s^{-1}).

The standard deviation of the blank was calculated from ten replications in the presence of Bi^{3+} ions. Detection limits (3σ blank/slope) of the target metals for both individual and simultaneous analysis were determined using a deposition time of 120 s and are summarized in Table 5.1. A summary of previously reported analyses for Zn^{2+}, Cd^{2+} and Pb^{2+} on Bismuth-film electrodes are shown in Table 5.2. Comparison of results obtained for simultaneous and individual analysis (Figure 5.10) showed improved sensitivity and detection limits for individual analysis at EG-PG-BiEs over all three concentration ranges. The increase in analytical performance was attributed to the lack of competition for available active sites on the electrode surface in individual analysis; more target metal ions could form alloys with the bismuth-film and bind to the electrode surface in the deposition step. For simultaneous analysis, the opposite was observed. Metal ions co-deposited to form the fused alloys. The EG-PG-BiEs prepared in this study showed similar results to literature and even improved sensitivities and detection limits in some cases.

Table 5.1: Calibration data representing Simultaneous and Individual Analysis of Zn^{2+}, Cd^{2+} and Pb^{2+} at EG-PG-BiEs in 0.1 M acetate buffer solution (pH 4.6) at 120s.

Analytical Parameter	**Simultaneous Analysis (2 – 20 µg L^{-1})**			**Individual Analysis (2 – 20 µg L^{-1})**		
	Zn^{2+}	Cd^{2+}	Pb^{2+}	Zn^{2+}	Cd^{2+}	Pb^{2+}
Sensitivity (µA L μg^{-1})	1.30 (±0.093)	1.09 (±0.104)	0.823 (±0.044)	0.549 (±0.021)	0.855 (±0.037)	0.673 (±0.019)
Correlation Coefficient (R^2)	0.991	0.985	0.993	0.965	0.988	0.993
Detection Limits (µg L^{-1})	0.255 (±0.046)	0.108 (±0.009)	0.127 (±0.008)	0.199 (±0.029)	0.099 (±0.002)	0.115 (±0.012)
Analytical Parameter	**Simultaneous Analysis (10 – 100 µg L^{-1})**			**Individual Analysis (10 – 100 µg L^{-1})**		
	Zn^{2+}	Cd^{2+}	Pb^{2+}	Zn^{2+}	Cd^{2+}	Pb^{2+}
Sensitivity (µA L μg^{-1})	2.74 (±0.039)	2.43 (±0.027)	1.52 (±0.021)	0.503 (±0.009)	1.80 (±0.023)	0.115 (±0.029)
Correlation Coefficient (R^2)	0.995	0.998	0.997	0.996	0.992	0.995
Detection Limits (µg L^{-1})	0.262 (±0.035)	0.103 (±0.009)	0.159 (±0.009)	0.209 (±0.005)	0.097 (±0.011)	0.115 (±0.005)

A summary of previously reported detection limits for Zn^{2+}, Cd^{2+} and Pb^{2+} at various Bismuth-film electrodes presented in Table 5.2 shows that the detection limits obtained at the EG-PG-BiE compare well with the modified electrodes in this category.

Table 5.2: A selected summary of previously reported detection limits for Zn^{2+}, Cd^{2+} and Pb^{2+} at various Bismuth-film electrodes (BiFE)

Metals Detected	Electrode Substrate	Measurement Technique	Deposition Time (s)	Detection Limit (µg L^{-1})	Reference
Pb^{2+}, Cd^{2+}, Zn^{2+}	BiF-PGE	SWASV	120	Pb^{2+} = 0.40 Cd^{2+} = 0.30 Zn^{2+} = 0.40	[40]
Pb^{2+} , Cd^{2+}	Nafion-G BiFE	DPASV	300	Pb^{2+} = 0.02 Cd^{2+} = 0.02	[22]
Pb^{2+}, Cd^{2+}, Zn^{2+}	NC(Bpy)BiFE	SWASV	120	Pb^{2+} = 0.08 Cd^{2+} = 0.12	[140]
Pb^{2+} , Cd^{2+}	Bi film C-paste	SWASV	120	Pb^{2+} = 0.80 Cd^{2+} = 1.00	[75]
Pb^{2+} , Cd^{2+}	Bi/GNFs-Nafion/GCE	DPASV	300	Pb^{2+} = 0.02 Cd^{2+} = 0.09	[141]
Pb^{2+}, Cd^{2+}, Zn^{2+}	Bi-CNT/GCE	SWASV	300	Pb^{2+} = 1.30 Cd^{2+} = 0.70 Zn^{2+} = 12.0	[142]
Pb^{2+} , Cd^{2+}	Bi nanopowder on carbon	SWASV	180	Pb^{2+} = 0.15 Cd^{2+} = 0.07	[143]
Pb^{2+}, Cd^{2+}, Zn^{2+} Simultaneous Analysis	EG-PG-BiE	SWASV	120	Pb^{2+} = 0.13 Cd^{2+} = 0.10 Zn^{2+} = 0.25	This Work
Pb^{2+}, Cd^{2+},Zn^{2+} Individual Analysis	EG-PG-BiE	SWASV	120	Pb^{2+} = 0.12 Cd^{2+} =0.09 Zn^{2+} =0.19	This Work

5.12. Recovery Studies of EG-PG-BiE

Recovery studies on test solutions of Zn^{2+}, Cd^{2+} and Pb^{2+} were investigated at EG-PG-BiE by a standard addition method. 10 mL portions of 0.1 M acetate buffer solution were spiked with known concentrations of target metals. Recovery

data obtained are reported in Table 5.3. Lower recoveries were obtained for simultaneous analysis. Individual analysis showed improved recoveries, indicating better quantitation for all three metals. The reported results prove the use of EG-PG-BiE as voltammetric sensor for the quantitation of trace metal samples. Figure 5.12 shows selected standard addition plots for the simultaneous analysis of target metals at EG-PG-BiEs.

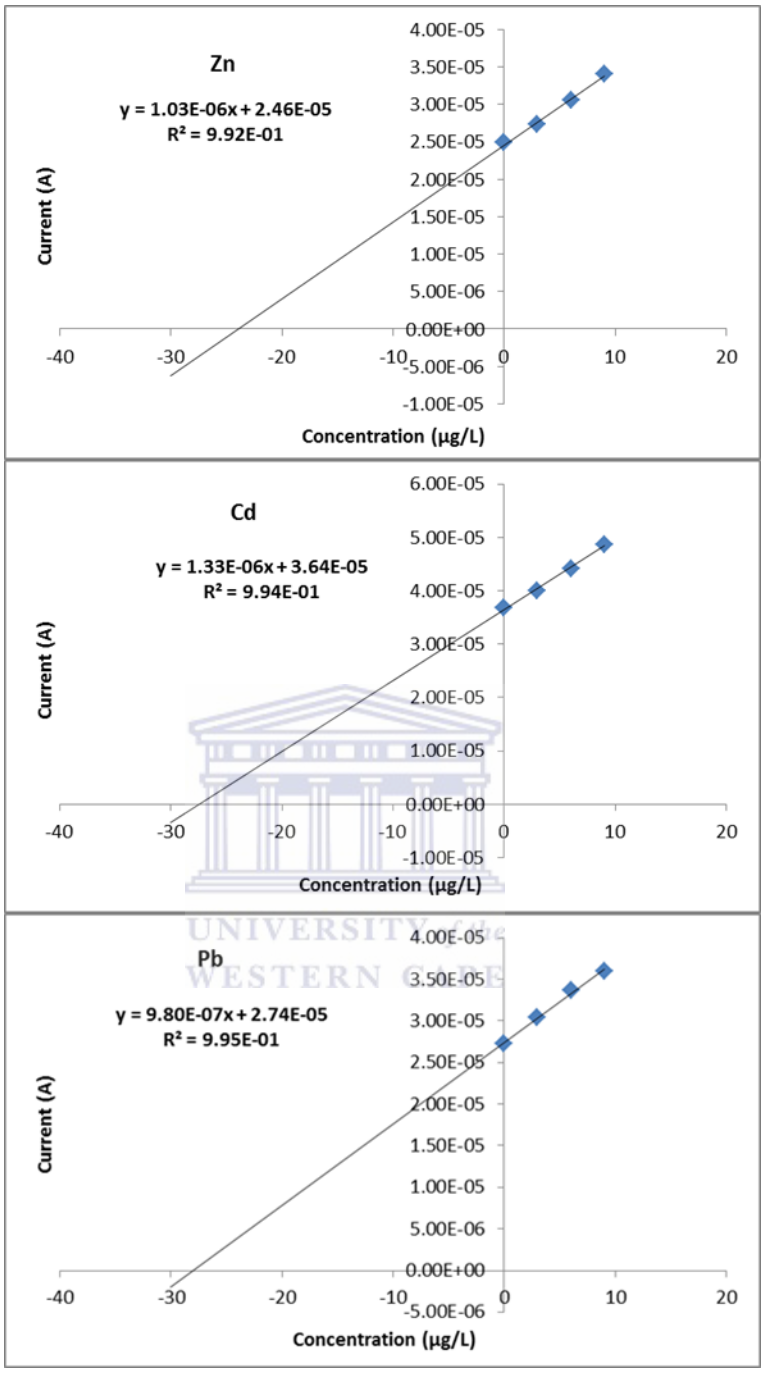

Figure 5.12: Standard Addition plots for the simultaneous determination of (**a**) Zn^{2+}, (**b**) Cd^{2+} and (**c**) Pb^{2+} at EG-PG-BiE in test solutions.

Table 5.3: Recovery data for the simultaneous and individual determination of Zn^{2+}, Cd^{2+} and Pb^{2+} at EG-PG-BiEs in test solutions

Recovery Studies of Zn^{2+}, Cd^{2+} and Pb^{2+} in Test Solutions			
Simultaneous Analysis			
	Zn^{2+}	**Cd^{2+}**	**Pb^{2+}**
Original ($\mu g\ L^{-1}$)	ND	ND	ND
Added ($\mu g\ L^{-1}$)	30	30	30
Found ($\mu g\ L^{-1}$)	19.18	21.62	23.15
RSD (%)	1.44	4.59	5.15
Recovery (%)	76.713	89.49	92.58
Individual Analysis			
	Zn^{2+}	**Cd^{2+}**	**Pb^{2+}**
Original ($\mu g\ L^{-1}$)	ND	ND	ND
Added ($\mu g\ L^{-1}$)	30	30	30
Found ($\mu g\ L^{-1}$)	30.94	28.77	29.37
RSD (%)	4.36	3.24	4.26
Recovery (%)	103.12	95.89	97.89

5.13. Effect of the pH value on Zn^{2+} Recovery

The ability of BiFEs to be utilised in both acidic and basic media is a major advantage in electrochemical stripping analysis. In this research, EG-PG-BiEs have been applied for the determination of trace amounts of heavy metals at pH 4.6. As seen from the recovery studies in 0.1 M acetate buffer solution (pH 4.6), low recoveries are observed for Zn^{2+} for both simultaneous and individual analysis. The plating of the bismuth film is discussed in section 3.17. The film thickness is governed by the concentration of the Bi^{3+} solution [27] and indicated that the background current at negative potentials, where the Zn^{2+} peak appeared, increased with the amount of Bi deposited resulting in a more sloping baseline for

the Zn^{2+} peak. This contradicts previous assumptions that the Bi-film would cause a negative shift of the hydrogen overpotential [27]. As a result there is a difficulty in determining Zn^{2+} in acidic solutions due to the masking of the Zn^{2+} reduction peak by Hydrogen ions [144]. Figure 5.13 shows the dependence of Zn^{2+} recovery (25 µg L^{-1}) on the pH value of the supporting electrolyte. It is shown that the stripping peak current at low pH values is seriously repressed and shows low recoveries as a result. Increased recoveries are shown with increased pH values as hydrogen ions in solution are decreased. At pH values greater than 9.1 no Zn^{2+} reduction peak can be seen. For further individual analysis of Zn^{2+}, ± pH 9.1 was selected.

Table 5.4: Recovery test of a 25 µg L^{-1} solution of Zn^{2+} in a 0.1 M acetate buffer solution; deposition time of 120 s at (**a**) pH 3, (**b**) pH 4.6, (**c**) pH 9.1 and (**d**) pH 12.5

Zn^{2+} pH Recovery Test (25 µg L^{-1})*				
	pH 3	**pH 4.6**	**pH 9.1**	**pH 12.5**
Recovery (µg L^{-1})	12.39	20.5	25.92	N/D
Recovery (%)	49.577	82.13	103.67	N/D

N/D, Not detected

*n = 3, where n is number of repetitions

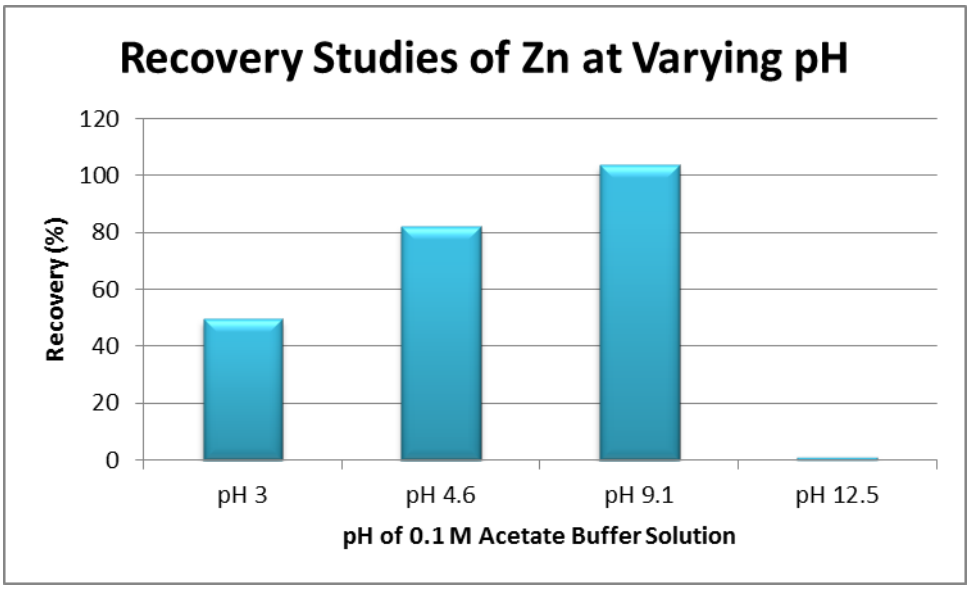

Figure 5.13: Effect of pH on Recovery of Zn^{2+} in 0.1 M acetate buffer solution with deposition time of 120 s.

5.14. Application to Tap Water Samples

Tap water samples were collected in our laboratory and analysed for Zn^{2+}, Cd^{2+} and Pb^{2+} ions using the electrodeposited graphene modified bismuth film electrode (EG-PG-BiE). Both individual and simultaneous analysis was performed and the amount of metal ions present in the water samples were quantified by the standard additions method. None of the heavy metal ions were detected in the original tap water samples when using a deposition potential of 120 seconds suggesting that the concentration of the metal ions were below their detection limits. However, upon spiking tap water samples with 20 µg L^{-1} and 30 µg L^{-1} of each metal ion yielded good recovery percentages (Table 5.5) for the individual analysis of all three metals ions.

Table 5.5: Recovery percentages for $Zn^{2+,}$ $Cd^{2+,}$ and $Pb^{2+,}$ at the EG-PG-BiE in tap water samples using a deposition time of 120 seconds.

Simultaneous Analysis					
Metal Ion	**Original ($\mu g\ L^{-1}$)**	**Added ($\mu g\ L^{-1}$)**	**Found ($\mu g\ L^{-1}$)**	**RSD (%)**	**Recovery (%)**
Zn^{2+}	ND	20	11.97	10.00	59.87
	ND	30	20.61	1.49	68.69
Cd^{2+}	ND	20	16.83	6.03	84.13
	ND	30	28.51	2.17	95.03
Pb^{2+}	ND	20	16.51	1.98	82.55
	ND	30	34.79	4.02	96.32
Individual Analysis					
Metal Ion	**Original ($\mu g\ L^{-1}$)**	**Added ($\mu g\ L^{-1}$)**	**Found ($\mu g\ L^{-1}$)**	**RSD (%)**	**Recovery (%)**
Zn^{2+}	ND	20	21.15	6.48	89.11
	ND	30	28.40	3.23	94.69
Cd^{2+}	ND	20	17.89	5.57	89.43
	ND	30	28.41	3.23	94.69
Pb^{2+}	ND	20	17.43	2.63	87.17
	ND	30	29.01	2.67	96.70

n = 3, where n is number of repetitive cycles performed

ND, not detected

The recovery percentages for Cd^{2+} and Pb^{2+} obtained with simultaneous analysis were comparable those obtained with individual analysis however, the recoveries for Zn^{2+} ions was much lower. The lower recoveries for Zn^{2+} can be

largely attributed to errors arising from the distortion of the zinc oxidation peak current caused by hydrogen gas evolution.

A pertinent observation in Table 5.5 is the improved recovery percentages for metal ions obtained in tap water samples spiked with 30 µg L^{-1} compared with those spiked with 20 µg L^{-1} and, highlights the fact that errors are enhanced when working with concentrations closer to the detection limit of the metal ions; these findings are similar to those reported by Yi *et al*. [139].

The results in Table 5.5 are satisfactory for water samples containing 20 – 30 µg L^{-1} of the metal ions whilst using a deposition potential of 120 seconds. However, in order to meet the United States Environmental Protection Agency's (USEPA) maximum contaminant level (MCL) for zinc (5 mg L^{-1}), cadmium (0.005 mg L^{-1}) and lead (0.015 mg L^{-1}) in drinking water a longer deposition time of 360 seconds was required. Typical voltammograms obtained during the simultaneous analysis of heavy metal ions together with their corresponding standard addition curves is shown in Figure 5.14.

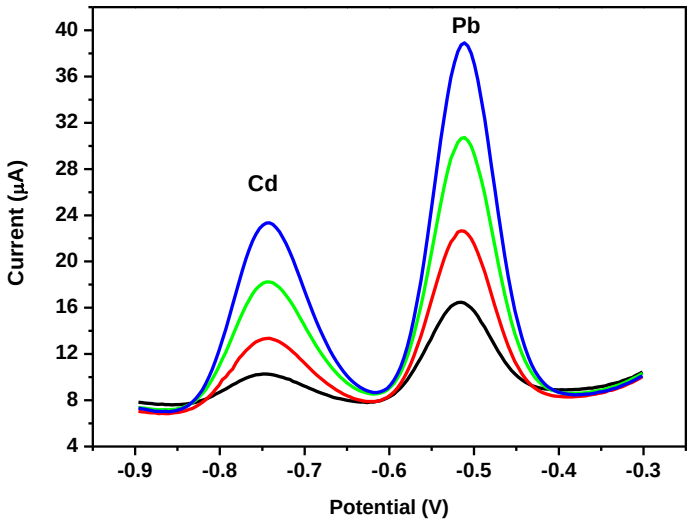

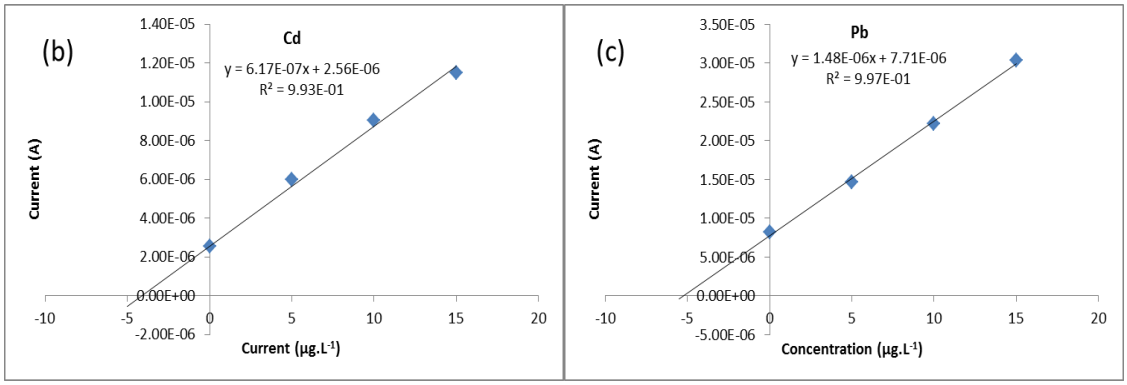

Figure 5.14: Simultaneous analysis of tap water (pH 4.6) spiked with 5 µg L^{-1} of each of metal ion using a deposition time of 360 seconds. Square-wave stripping voltammograms (**a**) and their corresponding standard addition calibration curves for Cd^{2+} (**b**) and (**c**) Pb^{2+}.

Table 5.6 shows the percentage recovery obtained when using a deposition time of 360 seconds during simultaneous and individual analysis. As expected, the longer pre-concentration time allows for more metal ions to be deposited at the electrode surface resulting in improved sensitivity.

Table 5.6: Recovery for the determination of Zn^{2+}, Cd^{2+} and Pb^{2+} in tap water samples using EG-PG-BiE at 360 seconds

Recovery for the determination of Zn^{2+}, Cd^{2+} and Pb^{2+} in tap water samples					
Simultaneous Analysis					
Sample	Original (µg L^{-1})	Added (µg L^{-1})	Found (µg L^{-1})	RSD (%)	Recovery (%)
Zn^{2+}	ND	5	ND	ND	ND
Cd^{2+}	ND	5	4.15	1.38	82.98
Pb^{2+}	ND	5	5.21	2.02	104.19
Individual Analysis					
Sample	Original (µg L^{-1})	Added (µg L^{-1})	Found (µg L^{-1})	RSD (%)	Recovery (%)
Zn^{2+}	ND	5	ND	ND	ND
Cd^{2+}	ND	5	5.19	2.74	103.80
Pb^{2+}	ND	5	5.13	1.89	102.60

n = 3, where n is number of repetitive cycles performed

ND, not detected

The recovery percentages obtained for the heavy metal ions ranged from 83 % and 104 % for Cd^{2+} and Pb^{2+}, respectively with relative standard deviations within 5%. No Zn^{2+} was detected in the tap water sample at the 5 µg L^{-1} level nevertheless the EG-PG-BiE is capable of detecting Zn^{2+} well below the USEPA maximum contaminant level of 5 mg L^{-1}. Furthermore, the results in Table 6 shows that the EG-PG-BiE in combination with square-wave anodic stripping

voltammetry is suitable for monitoring the levels of Zn^{2+}, Cd^{2+} and Pb^{2+} in drinking water.

5.15. Conclusions

A highly enhanced sensing platform based on the direct electrochemical reduction of colloidal graphene oxide at pencil graphite electrodes was developed for the determination of Zn^{2+}, Cd^{2+} and Pb^{2+} by square-wave anodic stripping voltammetry. The electrodeposited graphene pencil graphite bismuth-film electrode (EG-PG-BiE) showed improved sensitivities and detection limits to bismuth-film electrodes utilised in literature due to the combination of enhanced electron transfer rate, surface-to-volume ratio and improved sensitivity due to the graphene and metal-film. The analytical application of the EG-PG-BiE was assessed by recovery studies and real sample analysis within a 10 % error. The low detection limits obtained showed results well below the USEPA standards of 5 ppm, 5 ppb and 15 ppb for Zn^{2+}, Cd^{2+} and Pb^{2+} respectively.

CHAPTER SIX:

Nafion-Graphene Pencil Graphite Bismuth-film Electrodes (NG-PG-BiE)

6.1. Introduction

Surface-active substances which absorb onto the working electrode during analysis impede the electrode activity and performance [145, 146] and is a major downfall to the stripping voltammetric process. Conducting polymers and binders can alleviate these interferences [147].

Coating the pencil graphite electrodes with Nafion has shown to increase the detection sensitivity and alleviate the interferences from surfactants at bismuth film electrodes [33]. Nafion is a perfluorinated ionomer containing negatively charged sulfonic groups and has many applications as proton-conducting membrane material for fuel cells and electrochemical applications [34, 35]. The Teflon like hydrophobic backbone and highly hydrophilic ionisable sulfonic groups are responsible for its excellent chemical stability and ionic conductivity [38].

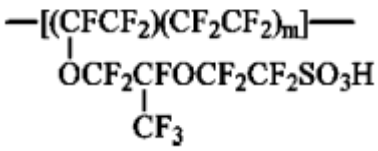

The unique ion- exchange, discriminative and biocompatibility properties have made Nafion- films useful for modification of electrode surfaces. The polar

side chain of Nafion allows for CNTs and Graphene to be easily suspended in solutions of Nafion in phosphate buffer and alcohols [39].

In previous work by our research group the use of binder-free [48] as well as Nafion-modified [8] electrodes have been proposed. Nafion, which acts as a binding agent has shown to improve the sensitity of electrodes towards heavy metal detection [8, 37].

In this chapter the use of SWASV together with a Nafion-Graphene nanocomposite in combination with an *in situ* bismuth-film at a pencil graphite electrode was investigated for the detection of Zn^{2+}, Cd^{2+} and Pb^{2+} in water samples.

6.2. Characteristic oxidation potentials of Bi^{3+} and target metal ions (Zn^{2+}, Cd^{2+}, and Pb^{2+})

Characteristic stripping peaks at modified Nafion-graphene pencil graphite bismuth-film electrodes (NG-PG-BiE) was investigated in 0.1 M acetate buffer solution (pH 4.6). Figure 6.1 shows a typical anodic stripping voltammograms (ASV) at the NG-PG-BiE. Well-defined oxidative stripping peaks with no inter-metallic interferences and good resolution were observed at -1.1, 0.75, 0.50 and -0.06 V for Zn^{2+}, Cd^{2+}, Pb^{2+} and Bi^{3+} respectively. Equations 6.1 and 6.2 describe the redox processes involved in deposition and stripping steps of the ASV procedure.

$Mn^{n+} + né + Bi^{3+} \rightarrow M\ (Bi)$ deposition step (reduction reaction) (Eqn. 6.1)

$M\ (Bi) \rightarrow M^{n+} + né + Bi^{3+}$ stripping step (oxidation reaction) (Eqn. 6.2)

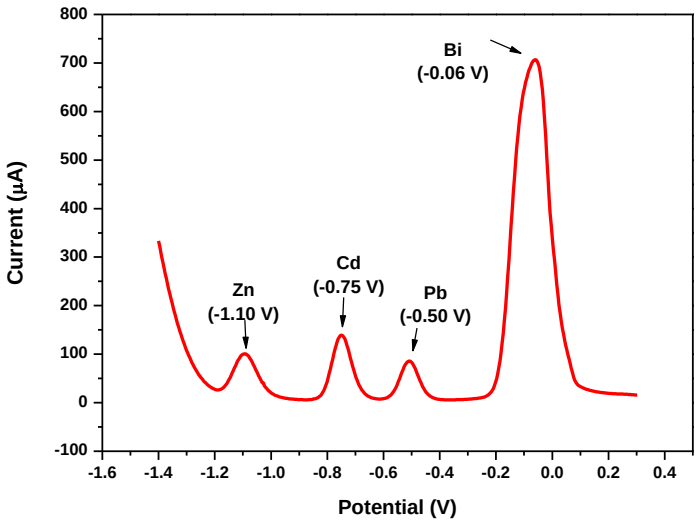

Figure 6.1: Anodic stripping voltammogram of Zn^{2+} (1.10 V), Cd^{2+} (-0.75 V), Pb^{2+} (-0.50 V) and Bi^{3+} (-0.06 V) in 0.1 M acetate buffer solution (pH 4.6) at the NG-PG-BiE.

6.3. Effect of Supporting Electrolyte

The supporting electrolyte which is usually an acid [148] or acid buffer solution [149] is pivotal in the formation of well-resolved peaks and good quantitation. The electrochemical responses of the NG-PG-BiE towards the target metal ions in different electrolyte solutions namely, 0.1 M acetate buffer (pH 4.6), 0.1 M HCl solution (pH 2) and 0.1 M phosphate buffer (pH 7.1) were investigated and are shown in Figure 6.2.

In 0.1 M HCl (pH 2.1) solution small broad peaks were observed for Cd^{2+} and Pb^{2+} whilst hydrogen evolution severely distorted at the Zn^{2+} signal to the extent that no well-defined peak was observed. On the other hand the stripping peaks recorded in Phosphate buffer (0.1 M, pH 7.1) showed small, resolved peaks

for Zn^{2+} and Cd^{2+} but, rather an extremely small Pb^{2+} peak. Considerably larger peaks with good resolution for all three metal ions are noted in acetate buffer solution (0.1 M, pH 4.6). Comparison of the stripping voltammograms of the EG-PG-BiE with the NG-PG-BiE showed similar results indicating the dependence of electrolyte solution on the metal-film used.

These results confirm the strong influence of electrolyte solution in anodic stripping voltammetric analysis.

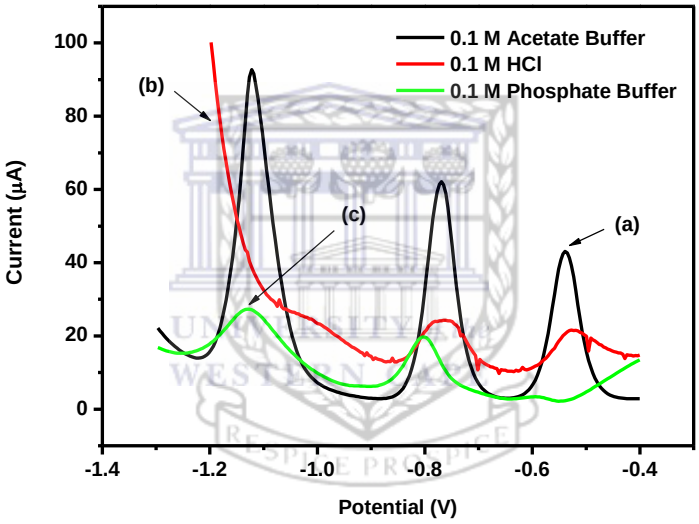

Figure 6.2: SWASV of 30 µg L^{-1} of Zn^{2+}, Cd^{2+} and Pb^{2+} at NG-PG-BiE with supporting electrolyte: (**a**) 0.1 M acetate buffer (pH 4.6), (**b**) 0.1 M HCl and (**c**) 0.1 M phosphate buffer (pH 7.1). Deposition potential: -1.4 V; deposition time: 120 s; frequency: 50 Hz; amplitude: 0.025 V and voltage step: 0.005 V.

6.4. Effect of the bismuth ion (Bi^{3+}) concentration

The procedure for depositing a bismuth film on an electrode substrate is crucial for obtaining good performance of the bismuth film electrode (BiE) [80].

Bismuth–film electrodes (BiEs) are either fabricated by *in situ* or *ex situ* electroplating of a bismuth film onto the surface of a conductive support. *In situ* plating is only suitable for the analysis of trace metals by anodic stripping voltammetry which involves cathodic electrolysis step [85]. The effect of bismuth ion concentration on the stripping responses of Zn^{2+}, Cd^{2+} and Pb^{2+} at Nafion-graphene pencil graphite electrodes (NG-PGE) is shown in Figure 6.3; here the Bi^{3+} concentrations were varied from 200 to 4000 µg L^{-1}. For all three target metal ions, similar increasing stripping currents were observed up to 800 µg L^{-1} after which the currents significantly decreased for Cd^{2+} and Pb^{2+} but starts to level off at 4000 µg L^{-1} for Zn^{2+}. Film thickness which is a consequence of Bi^{3+} ion concentration [40] results in the saturation of the electrode surface and causes a decrease in currents between 1000 and 5000 µg L^{-1}. A comparison of *in situ* and *ex situ* plating did not offer any major difference in peak heights; however *in situ* plating simplifies the analysis and shortens analysis time [80] henceforth, 800 µg L^{-1} was selected for all future experiments.

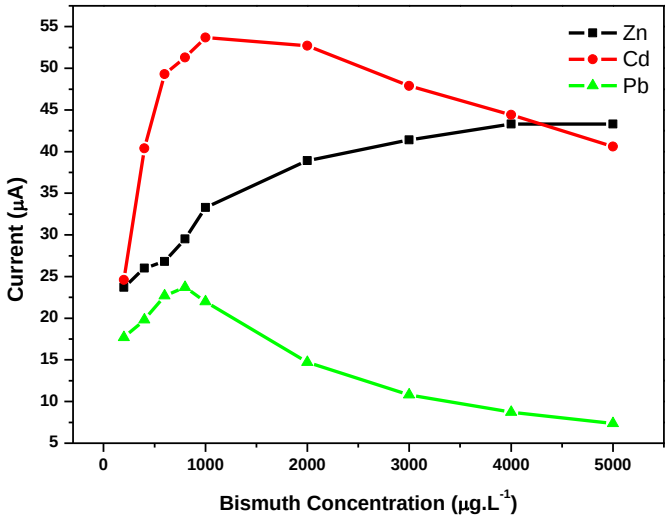

Figure 6.3: Effect of bismuth ion concentration on the stripping peak current of Zn^{2+}, Cd^{2+} and Pb^{2+} at Nafion-graphene pencil graphite bismuth film electrode (NG-PG-BiE) in a 0.1 M acetate buffer solution (pH 4.6) containing 20 µg L^{-1} of each metal.

6.5. Nafion-Graphene Pencil Graphite Bismuth-film Electrode Preparation (Electrode Coating Methods)

Over the years a range of coating methods have been developed and employed for modification or immobilization of electroactive compounds onto various electrode substrates. Drop-casting is commonly used for electrodes with flat surfaces which allow for drying or evaporation of solvent(s). For non-flat surfaces, the coating methods include dip-coating, passive adsorption, sputter coating etc.

6.5.1. Passive Adsorption Method

Graphene (5 mg) and Nafion-graphene was suspended in the organic solvent N,N-dimethylformamide (DMF) to prepare 1 mg mL^{-1} graphene and Nafion-graphene solutions. The mixture was then sonicated for an hour at room temperature. Each un-pretreated pencil graphite electrode was immersed into Eppendorf tubes containing 1 mL of G-based solutions for an hour in order to form a thin graphene layer on the surface of electrodes. Each of the electrodes was rinsed with ABS for 10 seconds, and then the G-PGEs and NG-PGEs were allowed to dry for 15 min in an upside down position [42]. Interrogation of the passive adsorption method for graphene modification of PGEs was demonstrated by the SWASVs in Figure 6.4 below. The N-PG-BiE and NG-PG-BiE showed increased stripping peak currents over the bare PG-BiEs. No significant enhancement in stripping peak currents is observed with the Nafion-graphene modification compared to the N-PG-BiE hence, it was deduced that no graphene stuck to the electrode surface.

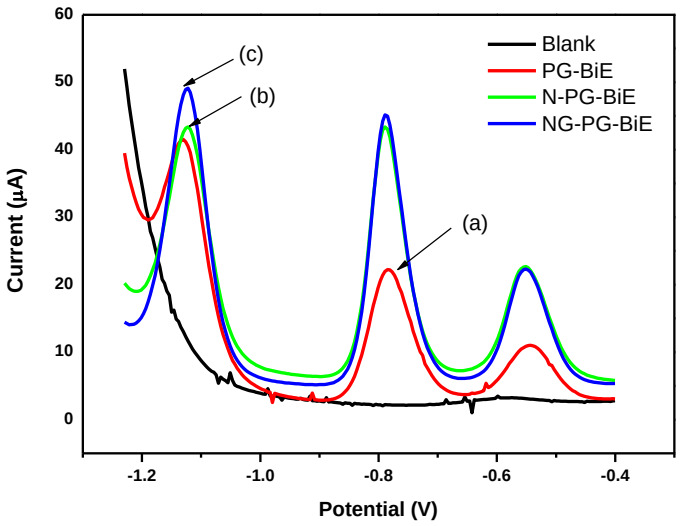

Figure 6.4: SWASV of 30 μg L^{-1} Zn^{2+}, Cd^{2+} and Pb^{2+} at (**a**) bare PG-BiE, (**b**) N-PG-BiE and (**c**) NG-PG-BiE prepared by passive adsorption. Supporting electrolyte: 0.1 M acetate buffer (pH 4.6), deposition potential (-1.4 V), deposition time (120 s), frequency (50 Hz), amplitude (0.025 V) and voltage step (0.005 V).

6.5.2. Dip-Coating without Pre-treatment

Bare pencil graphite electrodes were immersed; in 0.2 % Nafion, 0.25 mg mL^{-1} NG and 1 mg mL^{-1} NG solutions for 1 minute followed by drying to allow excess solvent to evaporate. This procedure was repeated three times to prepare uniformly modified pencil graphite electrodes.

Figure 6.5 shows square-wave anodic stripping voltammograms of Zn^{2+}, Cd^{2+} and Pb^{2+} at (a) bare PG-BiE, (b) NG-PG-BiE (c) 0.25 mg mL^{-1} NG-PG-BiE and (d) 1 mg mL^{-1} NG-PG-BiE without electrode pre-treatment in 0.1 M acetate buffer solution (pH 4.6). The bare PG-BiE shows well-defined sharp peaks for all three metal ions of interest. In addition the stripping peak currents of the target

metal ions are significantly enhanced when modified with dilute Nafion solutions. Comparison of N-PG-BiE and 0.25 mg mL^{-1} NG-PG-BiE showed no considerable increase in stripping peak currents for Cd^{2+} and Pb^{2+}. The lack of enhancement showed preferential binding to the Nafion solution than the electrode surface. The use of more concentrated NG solutions (1 mg mL^{-1}) resulted in broadening and reduction in size of stripping peaks. 0.25 mg mL^{-1} NG solutions were used.

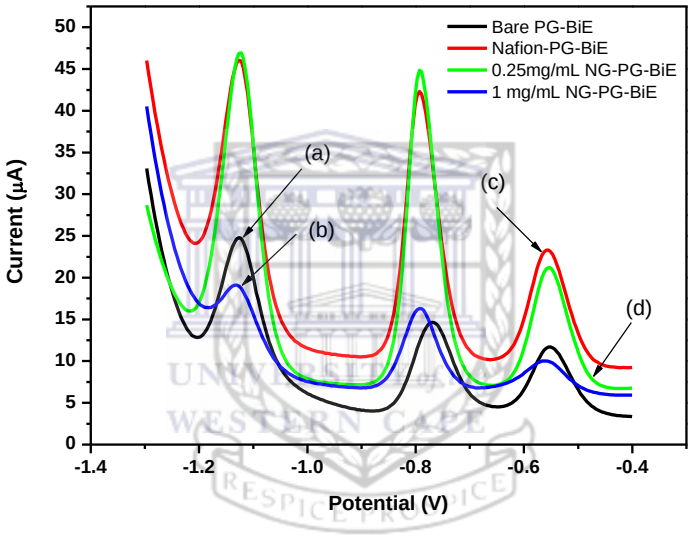

Figure 6.5: SWASV of 30 µg L^{-1} Zn^{2+}, Cd^{2+} and Pb^{2+} at (**a**) bare PG-BiE, (**b**) Nafion-PG-BiE (**c**) 0.25 mg mL^{-1} NG-PG-BiE and (**d**) 1 mg mL^{-1} NG-PG-BiE without electrode pre-treatment. Supporting electrolyte: 0.1 M acetate buffer (pH 4.6), deposition potential (-1.4 V), deposition time (120 s), frequency (50 Hz), amplitude (0.025 V) and voltage step (0.005 V).

6.5.3. Dip-Coating with Pre-treatment

Each pencil graphite electrode was place in the blank supporting electrolyte (0.1 M acetate buffer solution) and pretreated by applying a potential of +1.4 V

for 30 s to the electrode without stirring the solution. Pretreatment was performed in order to increase the hydrophilic properties of the electrode surface through the introduction of oxygenated functionalities as demonstrated in the work by Levent *et al* [122]. The pre-treated electrodes were then modified with 0.2 % Nafion and 0.25 mg mL^{-1} NG solutions as described in section 6.5.2 above. A comparison of voltammograms of Nafion-PG-BiE with NG-PG-BiE in Figure 6.6 shows that the modification of the Nafion-PG-BiE with graphene to give the NG-PG-BiE gave larger stripping peak signals due to the enhanced surface-to-volume ratio and quantum confinement of the graphene nanosheets [137]. In addition further peak signal enhancement is achieved and sharper well-resolved stripping peak are obtained when using an *in situ* plated bismuth-film.

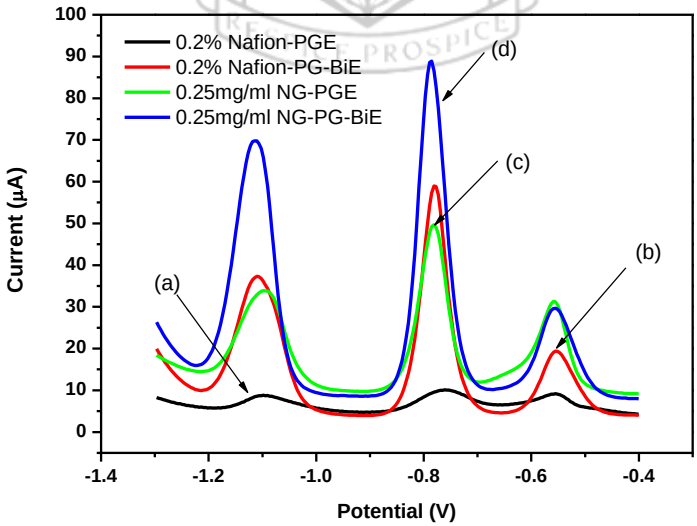

Figure 6.6: SWASV of 30 µg L^{-1} Zn^{2+}, Cd^{2+} and Pb^{2+} at (**a**) N-PGE, (**b**) N-PG-BiE (**c**) 0.25 mg mL^{-1} NG-PGE and (**d**) 0.25 mg mL^{-1} NG-PG-BiE with

electrochemical electrode pre-treatment. Supporting electrolyte: 0.1 M acetate buffer (pH 4.6), deposition potential (-1.4 V), deposition time (120 s), frequency (50 Hz), amplitude (0.025 V) and voltage step (0.005 V).

6.6. Microscopic Characterisation of Nafion Graphene Modified Pencil Graphite Electrode (NG-PGE)

High resolution scanning electron microscopy (HRSEM) images of the bare PGE and NG-PGE surface morphologies are shown in Figure 6.7. The bare PGE surface shows surface roughness with grooves along the surface in the direction of machining, Figures 6.7(a) and 6.7(b). Modification with a Nafion-graphene Nanocomposite was interrogated under various magnifications in Figure 6.7(c) and 6.7(d). A thin sheet of Nafion-graphene is observed at the electrode surface confirming modification with graphene sheets. Similar results are shown in work by Erdem *et al*. [42].

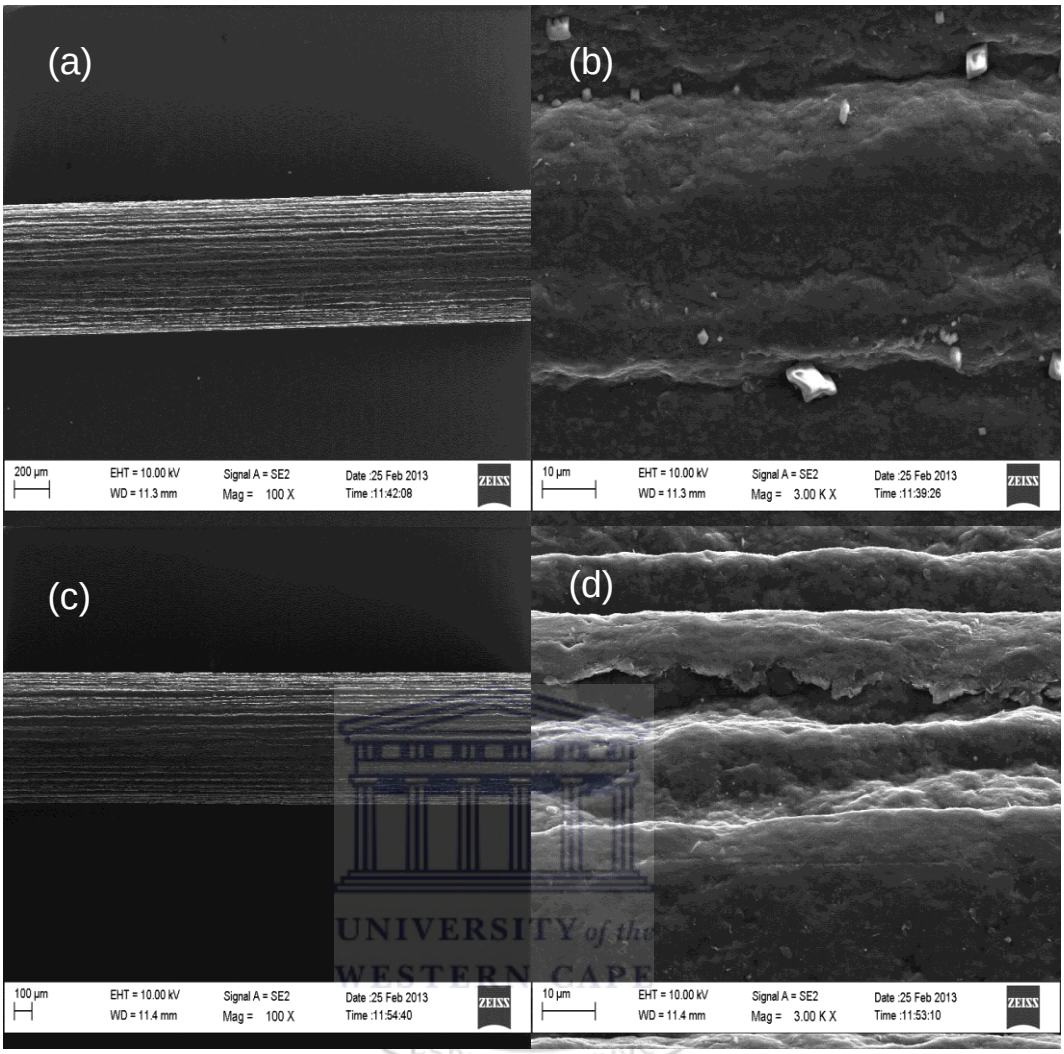

Figure 6.7: HRSEM images of bare PGEs (**a**) 100 times magnification, (**b**) 3000 times magnification and Nafion-graphene PGEs (**c**) 100 times magnification, (**d**) 3000 times magnification.

6.7. Optimisation of Instrumental Parameters at NG-PG-BiE

6.7.1. Nafion Graphene Pencil Graphite Bismuth-film Electrode (NG-PG-BiE)

Optimisation of the square-wave instrumental parameters: amplitude, deposition potential, deposition time, frequency and rotation speed at the NG-PG-BiE were performed and shown in Figure 6.8 below.

Interrogation of stripping peak currents of target metal ions as a function of amplitude was performed in the range of 10 to 100 mV and shown in Figure 6.8(a). A general increase in peak current is observed with increasing amplitude. Cadmium and zinc show steeper rising slopes demonstrating their enhanced dependence on amplitude. Lead, however increases to a maximum at 60 mV before stabilizing. Amplitude of 40 mV was selected for subsequent experiments based on the information that any further amplitude increases does not result in a significant increase in peak current.

The deposition step, which governs the loading of metal ions onto the working electrode, is a crucial step in any form of stripping analysis. An investigation of the effect of deposition potential on the peak currents of Zn^{2+}, Cd^{2+} and Pb^{2+} at the NG-PG-BiE is demonstrated in Figure 6.8(b). The potential was studied in the range from +0.2 V to -1.7 V. The stripping peak currents of all three metal ions increased with increasing negative potentials as the characteristic redox potentials of the ions was reached. Maximum stripping peak currents were observed at -1.4 V for all ions of interest at the BiE. This occurs as a result of preferential reduction and deposition of metal ions at the electrode surface.

Electrode saturation occurs after -1.4 V and the peak currents continuously decrease. A deposition potential of -1.4 V was utilized in further analysis.

The response of stripping peak currents of Zn^{2+}, Cd^{2+} and Pb^{2+} on deposition time was investigated and summarized in Figure 6.8(c). The peak currents for all three metal ions increased linearly with increased deposition times in the range of 30 to 600 seconds. Longer analysis times are unfavorable and not recommended. A deposition time of 120 s was selected for metal ion analysis.

Figure 6.8(d) shows the dependence of peak currents on the square wave frequency over the 12.5 Hz to 125 Hz range. Increasing the frequency showed increased peak currents as a result of increased scan rate [139]. A frequency of 50 Hz was chosen since distinct peaks with good resolution obtained.

Rotation speed which facilitates the movement of free metal ions at the electrode surface during the pre-concentration step was studied from 200 to 2000 rpm. In Figure 6.8(e) it is shown that with increasing rotation speed, the stripping peak currents of all three target metal ions are increased. A rotation speed of 1000 rpm was chosen.

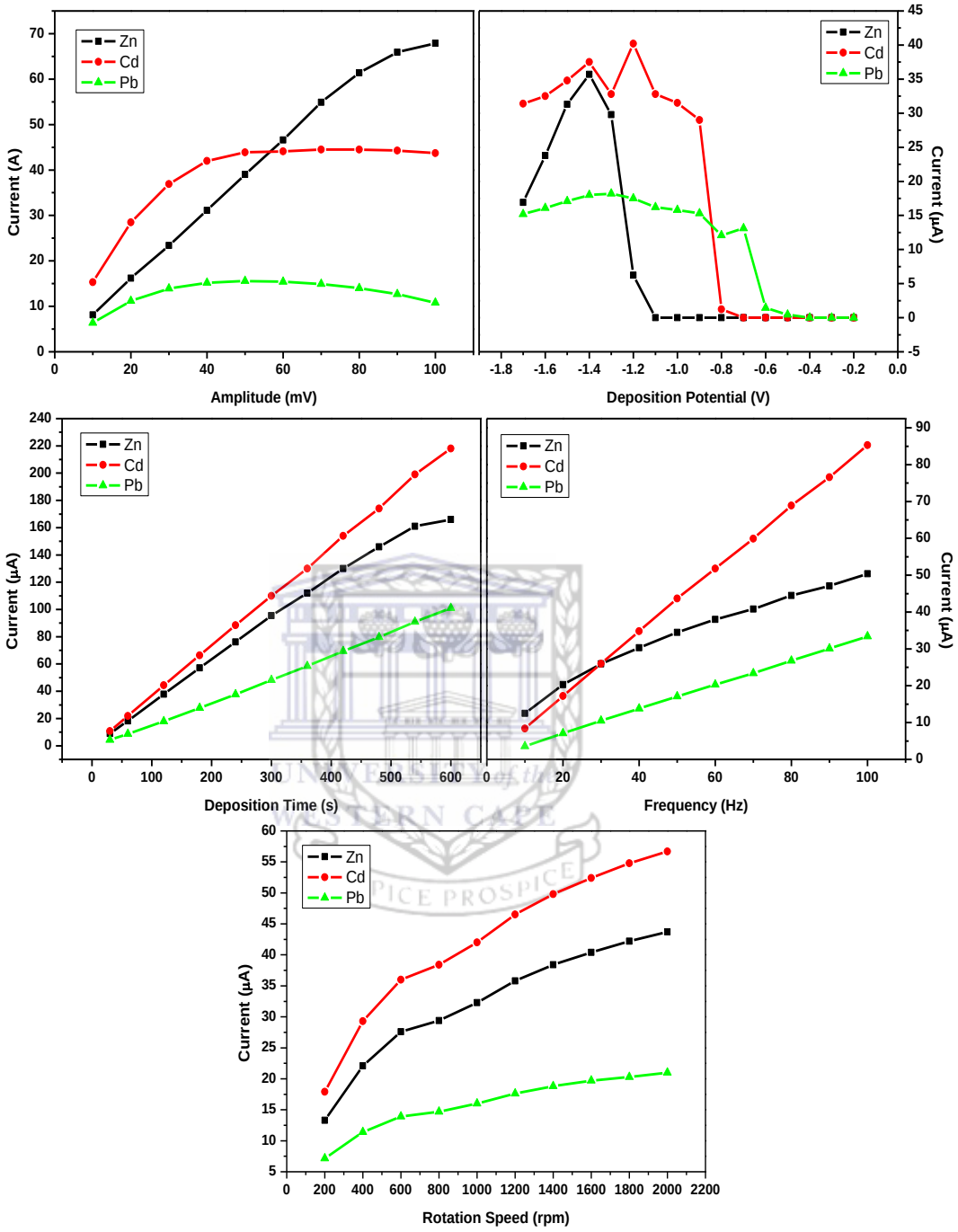

Figure 6.8: Effect of amplitude (**a**), deposition potential (**b**), deposition time (**c**), frequency (**d**) and rotation speed (**e**) on the stripping peak current of Zn^{2+}, Cd^{2+} and Pb^{2+} at Nafion-graphene pencil graphite bismuth film electrode (NG-PG-BiE)

in a 0.1 M acetate buffer solution (pH 4.6) containing 20 µg L^{-1} of each metal and 800 µg L^{-1} of bismuth.

6.8. Analytical Performance of Nafion-Graphene modified Pencil Graphite Bismuth-film Electrodes (NG-PG-BiEs)

Figure 6.9 and 6.10 below, show square-wave anodic stripping voltammograms and corresponding calibration plots for the simultaneous and individual analysis of Zn^{2+}, Cd^{2+} and Pb^{2+} in 0.1 M acetate buffer solution (pH 4.6) at NG-PG-BiE. Two concentration ranges, namely: 2 – 20 µg L^{-1} and 10 – 100 µg L^{-1} were used to investigate the analytical performance of the NG-PG-BiE. Well-defined, sharp peaks are observed for all target metal ions with slight positive shift due to oxidation of the metals becoming less reversible [139].

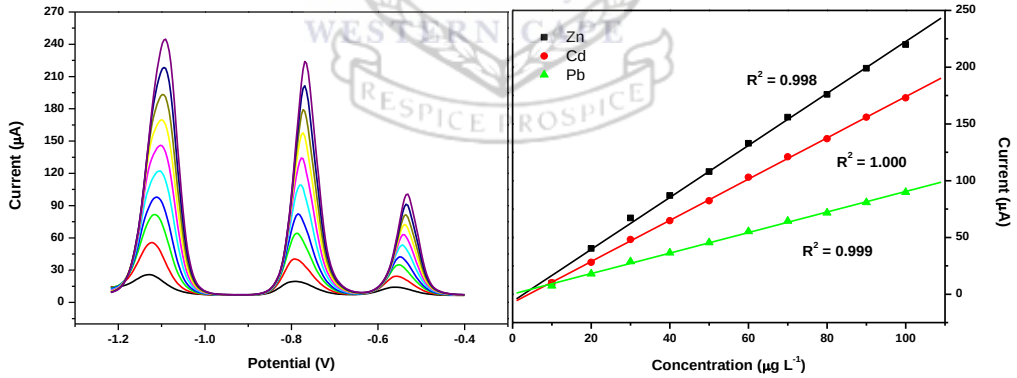

Figure 6.9: SWASV and corresponding calibration plots of simultaneous analysis of Zn^{2+}, Cd^{2+} and Pb^{2+} obtained at NG-PG-BiE over 10 – 100 µg L^{-1}. Supporting electrolyte: 0.1 M acetate buffer (pH 4.6), deposition time: 120, deposition potential: -1.4 V, rotation speed: 1000 rpm, frequency: 50 Hz, amplitude: 0.04 V and sweep rate: 0.2975 V. s^{-1}.

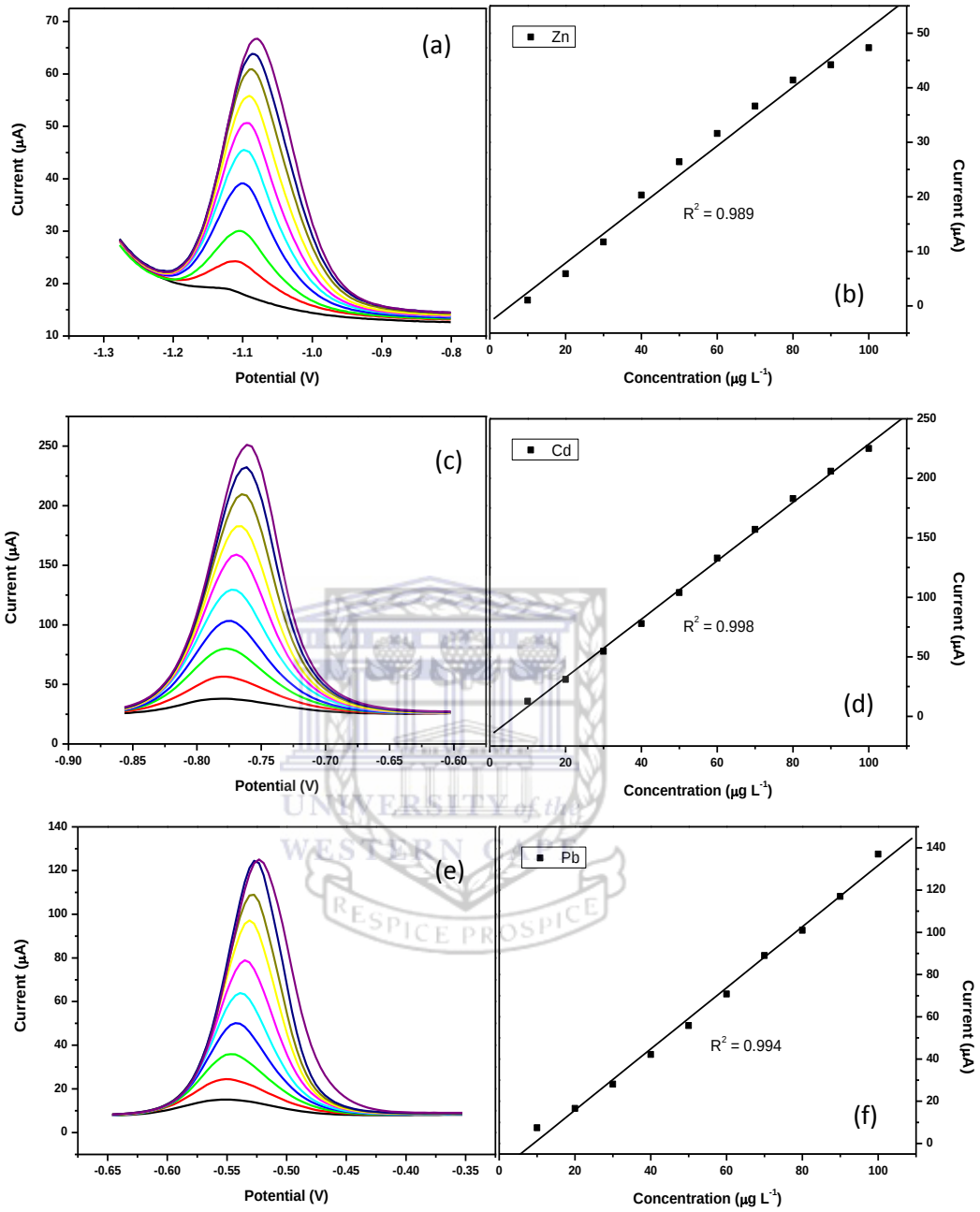

Figure 6.10: SWASV and corresponding calibration plots for individual analysis of (**a** and **b**) Zn^{2+}, (**c** and **d**) Cd^{2+} and (**e** and **f**) Pb^{2+} obtained at NG-PG-BiE over 10 – 100 µg L^{-1}. Supporting electrolyte: 0.1 M acetate buffer (pH 4.6), deposition time (120), deposition potential (-1.4 V), rotation speed (1000 rpm), frequency (50 Hz), amplitude (0.04 V) and sweep rate (0.2975 V s^{-1}).

$$D.L. = \frac{3\sigma}{slope} \qquad \text{(Eqn. 6.3)}$$

Where,

D.L, is the limit of detection

3σ, is three times the standard deviation of the blanks

Slope, is the gradient (slope) of the calibration curve

Detection limits were determined using equation 6.3 above. The standard deviation of the blanks was calculated based on ten replications of the electrode's response in the electrolyte solution. Table 6.1 summarises detection limits obtained for the simultaneous and individual analysis carried out at a deposition time of 120 s over two concentration ranges namely, 2 -20 µg L^{-1} and 10 – 100 µg L^{-1}. The calculated detection limits for Zn^{2+}, Cd^{2+} and Pb^{2+} were 0.224 µg L^{-1}, 0.098 µg L^{-1} and 0.204 µg L^{-1} for simultaneous analysis while individual analysis gave detection limits of 0.167 µg L^{-1}, 0.098 µg L^{-1} and 0.125 µg L^{-1} for Zn^{2+}, Cd^{2+} and Pb^{2+} respectively. Furthermore, the improved detection limits observed for individual analysis above simultaneous analysis is due to the lack of competition for available sites at the electrode surface. A ccomparison of detection limits with other previously reported bismuth-film electrodes are tabulated in Table 6.2 and shows that the NG-PG-BiE compares well with the electrodes in this table when a deposition time of 120 seconds is used.

Table 6.1: Calibration data representing Simultaneous and Individual Analysis of Zn^{2+}, Cd^{2+} and Pb^{2+} at NG-PG-BiEs in 0.1 M acetate buffer solution (pH 4.6) at 120s.

Analytical Parameter	**Simultaneous Analysis (2 – 20 µg L^{-1})**			**Individual Analysis (2 – 20 µg L^{-1})**		
	Zn^{2+}	Cd^{2+}	Pb^{2+}	Zn^{2+}	Cd^{2+}	Pb^{2+}
Sensitivity (µA L μg^{-1})	2.08 (±0.113)	1.89 (±0.071)	0.992 (±0.064)	0.432 (±0.021)	1.61 (±0.017)	0.747 (±0.032)
Correlation Coefficient (R^2)	0.989	0.998	0.993	0.998	0.995	0.989
Detection Limits (µg L^{-1})	0.257 (±0.032)	0.098 (±0.017)	0.204 (±0.009)	0.167 (±0.028)	0.151 (±0.004)	0.125 (±0.013)
Analytical Parameter	**Simultaneous Analysis (10 – 100 µg L^{-1})**			**Individual Analysis (10 – 100 µg L^{-1})**		
	Zn^{2+}	Cd^{2+}	Pb^{2+}	Zn^{2+}	Cd^{2+}	Pb^{2+}
Sensitivity (µA L μg^{-1})	2.29 (±0.021)	1.82 (±0.037)	0.904 (±0.019)	0.531 (±0.005)	2.431 (±0.035)	1.457 (±0.029)
Correlation Coefficient (R^2)	0.998	1.000	0.999	0.990	0.998	0.994
Detection Limits (µg L^{-1})	0.224 (±0.021)	0.099 (±0.006)	0.177 (±0.022)	0.168 (±0.005)	0.098 (±0.005)	0.141 (±0.001)

Table 6.2: A selected summary of previously reported detection limits for Zn^{2+}, Cd^{2+} and Pb^{2+} at various Bismuth-film electrodes (BiFE)

Metals Detected	Electrode Substrate	Measurement Technique	Deposition Time (s)	Detection Limit (µg L^{-1})	Reference
Pb^{2+}, Cd^{2+}, Zn^{2+}	BiF-PGE	SWASV	120	Pb^{2+} = 0.40 Cd^{2+} = 0.30 Zn^{2+} = 0.40	[40]
Pb^{2+} , Cd^{2+}	Nafion-G BiFE	DPASV	300	Pb^{2+} = 0.02 Cd^{2+} = 0.02	[22]
Pb^{2+}, Cd^{2+}, Zn^{2+}	NC(Bpy)BiFE	SWASV	120	Pb^{2+} = 0.08 Cd^{2+} = 0.12	[140]
Pb^{2+} , Cd^{2+}	Bi film C-paste	SWASV	120	Pb^{2+} = 0.80 Cd^{2+} = 1.00	[75]
Pb^{2+} , Cd^{2+}	Bi/GNFs-Nafion/GCE	DPASV	300	Pb^{2+} = 0.02 Cd^{2+} = 0.09	[141]
Pb^{2+}, Cd^{2+}, Zn^{2+}	Bi-CNT/GCE	SWASV	300	Pb^{2+} = 1.30 Cd^{2+} = 0.70 Zn^{2+} = 12.0	[142]
Pb^{2+} , Cd^{2+}	Bi nanopowder on carbon	SWASV	180	Pb^{2+} = 0.15 Cd^{2+} = 0.07	[143]
Pb^{2+}, Cd^{2+}, Zn^{2+} Simultaneous Analysis	NG-PG-BiE	SWASV	120	Pb^{2+} = 0.22 Cd^{2+} = 0.09 Zn^{2+} = 0.20	This Work
Pb^{2+}, Cd^{2+},Zn^{2+} Individual Analysis	NG-PG-BiE	SWASV	120	Pb^{2+} = 0.17 Cd^{2+} =0.09 Zn^{2+} =0.13	This Work

6.9. Recovery Studies of NG-PG-BiE

The NG-PG-BiE was used in recovery studies to determine the target metal ions in test solutions. Known concentrations of target metal ions were used to spiked 10 mL portions of 0.1 M acetate buffer solutions and determined using the

standard addition method (Figure 6.11). An advantage of this method is that it compensates for interferences caused by the sample matrix. Recovery percentages of the metal ions from test solutions spiked with 30 µg L^{-1} Zn^{2+}, Cd^{2+} and Pb^{2} values of 77.56 %, 94.35 % and 92.83 % for simultaneous analysis while for individual analysis the recovery percentages were 97.36 %, 99.24 % and 97.62 % for Zn^{2+}, Cd^{2+} and Pb^{2+}, respectively. The percentage recoveries for simultaneous and individual analysis are shown in Table 6.3; slightly higher recovery percentages were obtained for individual analysis due to the lack of competition for available sites at the electrode surface.

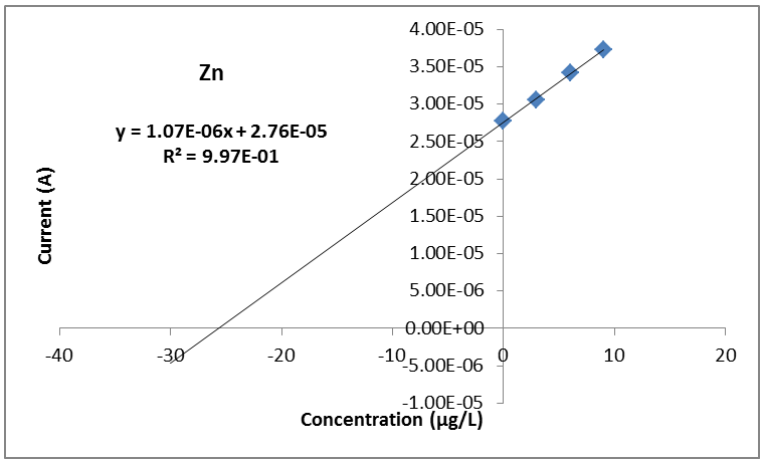

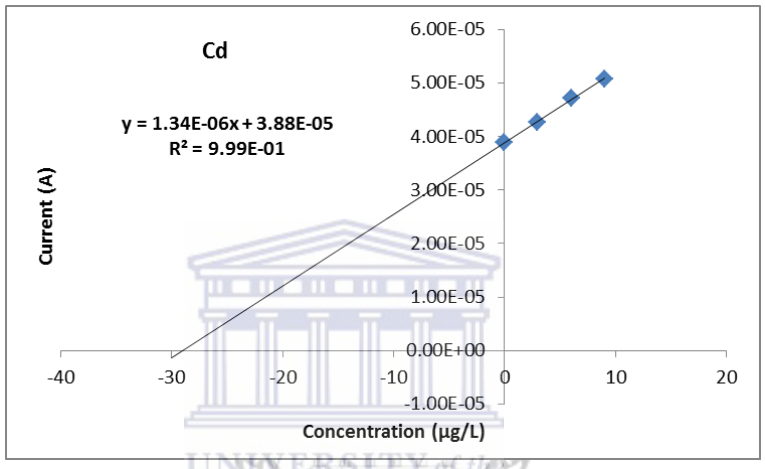

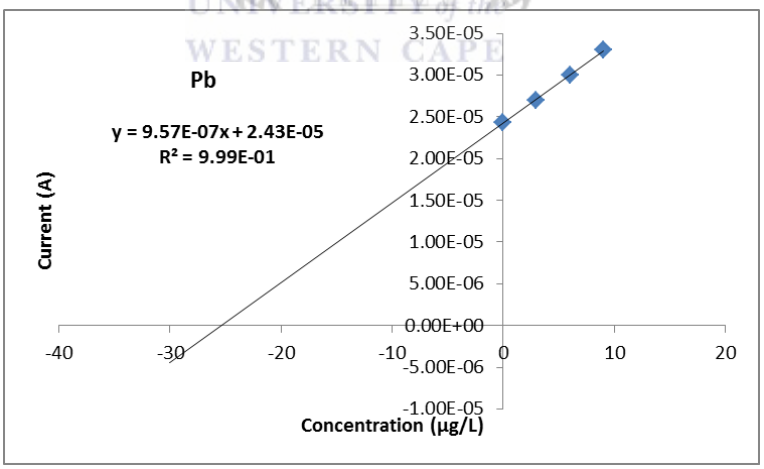

Figure 6.11: Standard Addition plots for the simultaneous determination of (**a**) Zn^{2+}, (**b**) Cd^{2+} and (**c**) Pb^{2+} at NG-PG-BiE in test solutions.

Table 6.3: Recovery data for the simultaneous and individual determination of Zn^{2+}, Cd^{2+} and Pb^{2+} at NG-PG-BiEs in test solutions

Recovery Studies of Zn^{2+}, Cd^{2+} and Pb^{2+} in Test Solutions			
Simultaneous Analysis			
	Zn^{2+}	Cd^{2+}	Pb^{2+}
Original (µg L^{-1})	ND	ND	ND
Added (µg L^{-1})	30	30	30
Found (µg L^{-1})	23.27	28.31	27.85
RSD (%)	2.89	3.74	4.21
Recovery (%)	77.56	94.35	92.83
Individual Analysis			
	Zn^{2+}	Cd^{2+}	Pb^{2+}
Original (µg L^{-1})	ND	ND	ND
Added (µg L^{-1})	30	30	30
Found (µg L^{-1})	29.21	29.77	29.29
RSD (%)	3.17	2.81	3.75
Recovery (%)	97.36	99.24	97.62

6.10. Effect of the pH value on Zn^{2+} Recovery

The ability of BiFEs to be utilised in both acidic and basic media is a major advantage in electrochemical stripping analysis. In this research, NG-PG-BiEs have been applied for the determination of trace amounts of heavy metals at pH 4.6. As seen from the recovery studies in 0.1 M acetate buffer solution (pH 4.6), low recoveries are observed for Zn^{2+} for both simultaneous and individual analysis. The plating of the bismuth film is discussed in section 6.4. The film thickness is governed by the concentration of the Bi^{3+} solution [27] and indicated that the background current at negative potentials, where the Zn^{2+} peak appeared, increased with the amount of Bi^{3+} deposited resulting in a more sloping baseline for the Zn^{2+} peak. This contradicts previous assumptions that the Bi-film would

cause a negative shift of the hydrogen overpotential [27]. As a result there is a difficulty in determining Zn^{2+} in acidic solutions due to the masking of the Zn^{2+} reduction peak by Hydrogen ions [144]. Figure 6.12 shows the dependence of Zn^{2+} recovery (25 µg L^{-1}) on the pH value of the supporting electrolyte. It is shown that the stripping peak current at low pH values is seriously repressed and shows low recoveries as a result. Increased recoveries are shown with increased pH values as hydrogen ions in solution are decreased. At pH values greater than 9.1 no Zn^{2+} reduction peak can be seen. For further individual analysis of Zn^{2+}, ± pH 9.1 was selected.

Table 6.4: Recovery test of a 25 µg L^{-1} solution of Zn^{2+} in a 0.1 M acetate buffer solution; deposition time of 120 s at (**a**) pH 3, (**b**) pH 4.6, (**c**) pH 9.1 and (**d**) pH 12.5

Zn^{2+} pH Recovery Test (25 µg L^{-1})*				
	pH 3	**pH 4.6**	**pH 9.1**	**pH 12.5**
Recovery (µg L^{-1})	12.03	21.68	25.30	ND
Recovery (%)	48.123	86.72	101.21	ND

N/D, Not detected

*n = 3, where n is number of repetitions

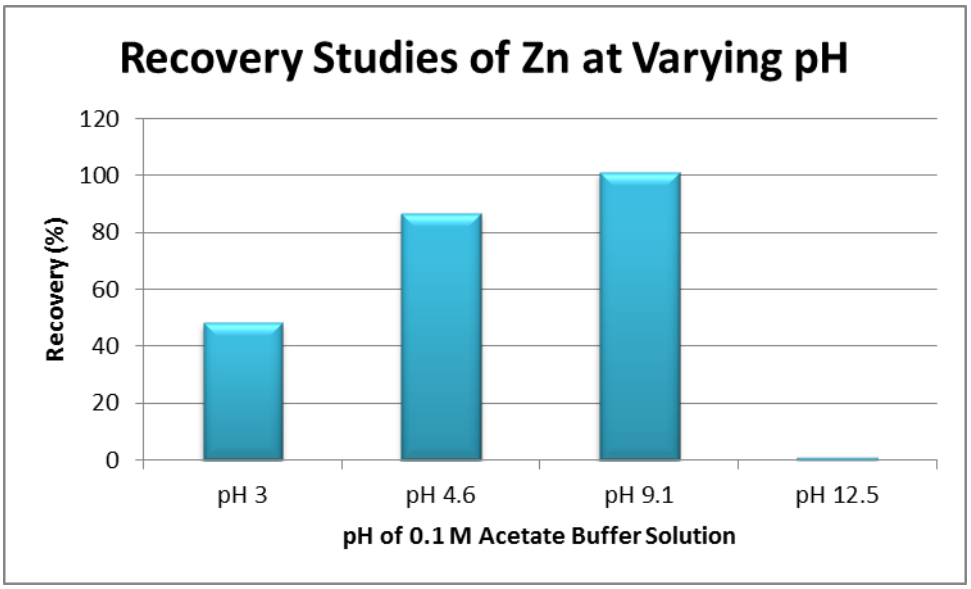

Figure 6.12: Effect of pH on Recovery of Zn^{2+} in 0.1 M acetate buffer solution with deposition time of 120 s.

6.11. Application to Tap Water Samples

The NG-PG-BiE developed was employed as an electrochemical sensing platform for the analysis of tap water samples. Tap water was collected in our laboratory and analysed for Zn^{2+}, Cd^{2+} and Pb^{2+}, detected by the standard addition method. None of the target metal ions were detected at a pre-concentration time of 120 s for either simultaneous or individual analysis due to their low concentrations. Spiking tap water samples with 20 µg L^{-1} and 30 µg L^{-1} of the target metal ions respectively yielded good recoveries as shown in Table 6.5. Increasing concentrations from 20 to 30 µg L^{-1} as well as performing individual analysis improved the percentage recoveries for all three metal ions. The lower recoveries for Zn^{2+} can be largely attributed to errors arising from the distortion of the zinc oxidation peak current caused by hydrogen gas evolution. The lower recoveries obtained for tap water samples spiked with 20 µg L^{-1} can be attributed

to the fact that errors are generally greater when working closer at the detection limits of the metal ions [139]. As reported for test solutions, good recoveries were achieved at elevated concentrations.

Table 6.5: Recovery percentages for $Zn^{2+,}$ $Cd^{2+,}$ and $Pb^{2+,}$ at the NG-PG-BiE in tap water samples using a deposition time of 120 seconds.

Simultaneous Analysis					
Metal Ion	**Original ($\mu g\ L^{-1}$)**	**Added ($\mu g\ L^{-1}$)**	**Found ($\mu g\ L^{-1}$)**	**RSD (%)**	**Recovery (%)**
Zn^{2+}	ND	20	12.52	2.84	62.59
	ND	30	20.52	3.83	68.42
Cd^{2+}	ND	20	18.03	5.43	90.14
	ND	30	30.73	4.19	102.43
Pb^{2+}	ND	20	18.69	5.36	93.47
	ND	30	29.44	1.46	98.12
Individual Analysis					
Metal Ion	**Original ($\mu g\ L^{-1}$)**	**Added ($\mu g\ L^{-1}$)**	**Found ($\mu g\ L^{-1}$)**	**RSD (%)**	**Recovery (%)**
Zn^{2+}	ND	20	17.84	5.77	89.23
	ND	30	28.60	2.38	95.34
Cd^{2+}	ND	20	17.29	4.85	86.45
	ND	30	29.94	1.22	99.79
Pb^{2+}	ND	20	20.30	1.11	101.51
	ND	30	29.53	2.84	98.43

n = 3, where n is number of repetitive cycles performed

ND, not detected

To meet the United States Environmental Protection Agency's (USEPA) maximum contaminant level (MCL) for zinc (5 mg L^{-1}), cadmium (0.005 mg L^{-1}) and lead (0.015 mg L^{-1}) in drinking water, a longer deposition time of 360 seconds

was used. Typical voltammograms obtained during the simultaneous analysis of heavy metal ions together with their corresponding standard addition curves is shown in Figure 6.13.

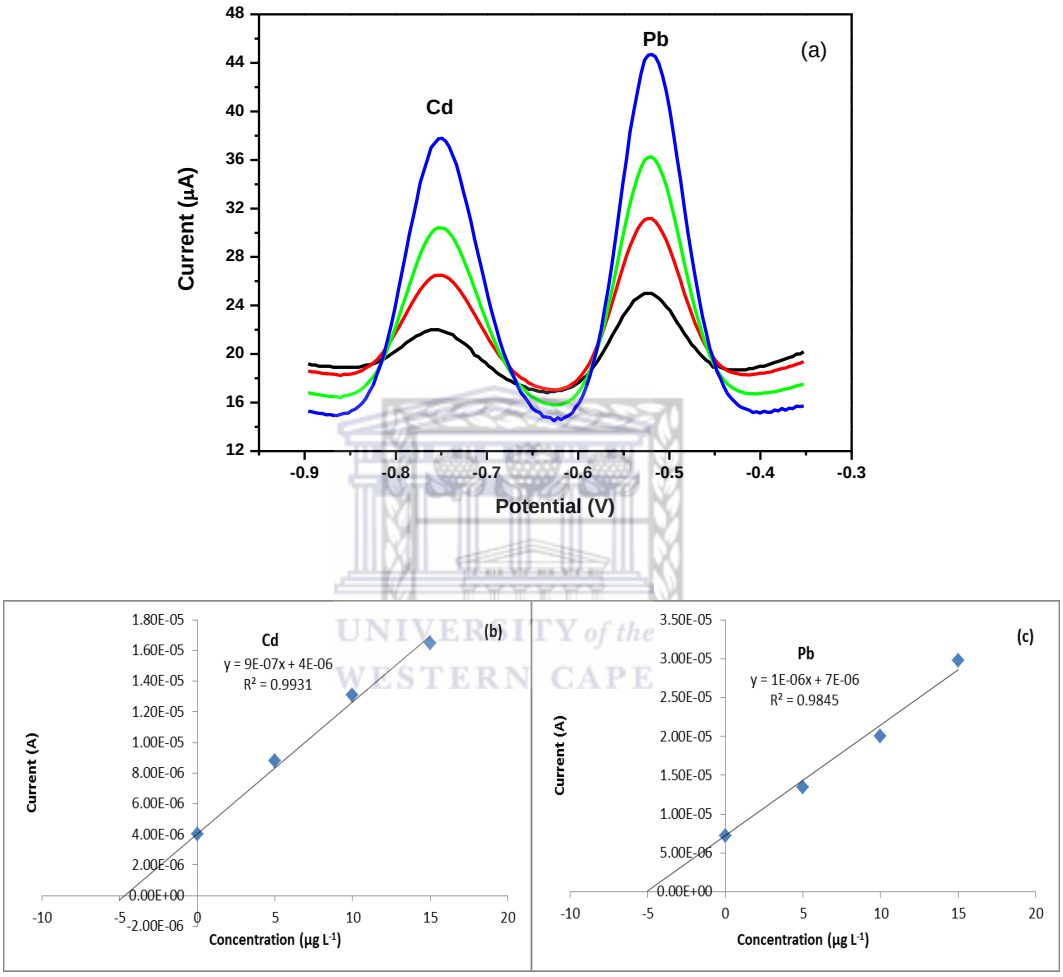

Figure 6.13: Simultaneous analysis of tap water (pH 4.6) spiked with 5 µg L^{-1} of each of metal ion using a deposition time of 360 seconds. Square wave voltammograms (**a**) and corresponding standard addition calibration curves for Cd^{2+} (**b**) and (**c**) Pb^{2+}.

Table 6.6 shows the percentage recovery obtained when using a deposition time of 360 seconds during simultaneous and individual analysis. As expected, the longer pre-concentration time allows for more metal ions to be deposited at the electrode surface resulting in improved sensitivity.

Table 6.6: Recovery for the determination of Zn^{2+}, Cd^{2+} and Pb^{2+} in tap water samples using NG-PG- BiE at pre-concentration time of 360 seconds

Recovery for the determination of Zn^{2+}, Cd^{2+} and Pb^{2+} in tap water samples					
Simultaneous Analysis					
Metal Ion	Original (µg L^{-1})	Added (µg L^{-1})	Found (µg L^{-1})	RSD (%)	Recovery (%)
Zn^{2+}	ND	5	ND	ND	ND
Cd^{2+}	ND	5	4.72	2.11	94.36
Pb^{2+}	ND	5	5.18	1.93	103.52
Individual Analysis					
Metal Ion	Original (µg L^{-1})	Added (µg L^{-1})	Found (µg L^{-1})	RSD (%)	Recovery (%)
Zn^{2+}	ND	5	ND	ND	ND
Cd^{2+}	ND	5	5.08	1.90	101.68
Pb^{2+}	ND	5	4.95	1.87	98.91

n = 3, where n is number of repetitive cycles performed

ND, not detected

Recovery percentages summarised in Table 6.6 show improved recoveries for individual analysis at 102 % and 99 % for Cd^{2+} and Pb^{2+} respectively. The accurate quantitation of heavy metals at concentration below the USEPA

standards proves the effective use of the NG-PG-BiE in conjunction with SWASV for detection of trace amounts of metals in drinking water.

6.12. Conclusions

Modification of pencil graphite electrodes with a Nafion-graphene nanocomposite and *in situ* plated bismuth film resulted in an ultra-sensitive sensing platform (NG-PG-BiE) for the detection of trace amounts of Zn^{2+}, Cd^{2+} and Pb^{2+} by square-wave anodic stripping voltammetry. Improved detection limits at values comparable to other known bismuth-film electrodes and below the USEPA standards, as well as accurate detection of metal ions in drinking water with a 5 % error prove the enhanced sensing capabilities of the binder-graphene platform.

CHAPTER SEVEN:

Conclusions and Future Work

A highly enhanced sensing platform based on the direct electrochemical reduction of colloidal graphene oxide at pencil graphite electrodes was developed for the determination of Zn^{2+}, Cd^{2+} and Pb^{2+} by square-wave anodic stripping voltammetry. The electrodeposited graphene pencil graphite bismuth-film electrode (EG-PG-BiE) showed improved sensitivities and detection limits to bismuth-film electrodes utilised in literature due to the combination of enhanced electron transfer rate, surface-to-volume ratio and improved sensitivity due to the graphene and metal-film. The analytical application of the EG-PG-BiE was assessed by recovery studies and real sample analysis within a 10 % error. The low detection limits obtained showed results well below the USEPA standards of 5 ppm, 5 ppb and 15 ppb for Zn^{2+}, Cd^{2+} and Pb^{2+} respectively.

Modification of pencil graphite electrodes with a Nafion-graphene nanocomposite and *in situ* plated bismuth film resulted in an ultra-sensitive sensing platform (NG-PG-BiE) for the detection of trace amounts of Zn^{2+}, Cd^{2+} and Pb^{2+} by square-wave anodic stripping voltammetry. Improved detection limits at values comparable to other known bismuth-film electrodes and below the USEPA standards, as well as accurate detection of metal ions in drinking water with a 5 % error prove the enhanced sensing capabilities of the binder-graphene platform.

Future work includes the use of bismuth films on various substrate materials to offer green approaches to existing techniques. The results achieved in the study show encouraging proof that the electroanalytical use of bismuth electrodes is possible.

The pencil graphite substrate has proved to offer good comparable results to common electrode substrates. In future, investigating the pencil graphite substrate for a wide range of applications is possible at low costs. The use of pencil graphite as substrate could also be investigated for low cost point-of-care devices due to its ease of use, robustness and low cost.

Minimizing errors in recoveries of Zn^{2+} at BiEs is of vital importance. The investigation of increased pH water samples should also be further interrogated.

Lastly, the use of nanomaterials and functionalised graphene sheets could be further investigated at various metal-films.

Bibliography

[1] L. Sanita di Toppi and R. Gabbrielli, "Review: Response to Cadmium in Higher Plants," *Environ. Exp. Bot.*, vol. 41, pp. 105-130, **1999**.

[2] J. Wang, Stripping Analysis-Priciples, Instrumentation and Application, Deerfield Beach, FL, USA: VCH Publishers, Inc., **1985**.

[3] R. Sharma and M. Agrawal, "Biological Effects of Heavy Metals: An Overview," *J. Environ. Biol.*, vol. 26, pp. 301-313, **2005**.

[4] G. Tyler, A. M. Pahlsson, G. Bengtsson, E. Baath and L. Tranvik, "Heavy Metal Ecology and Terrestrial Plants, Micro-Organisms and Invertebrates: A Review.," *Water, Air and Soil Pollution*, vol. 47, pp. 189-215, **1989**.

[5] "Heavy Metals," LENNTECH, [Online]. Available: http://www.lenntech.com/heavymetals.htm. [Accessed 10 November **2011**].

[6] J. Buffle and M. Tercier-Waeber, "Voltammetric Environmental Trace-Metal Analysis and Speciation: From Laboratory to In Situ Measurement," *Trends in Anal. Chem.*, vol. 24, **2005**.

[7] X. Wang, T. Sato, B. Xing and S. Tao, "Health Risks of Heavy Metals to the General Public in Tianjin, China via Consumption of Vegetables and Fish.," *Sci. Tot. Environ.*, Vols. 350, pp. 28-37, **2005**.

[8] C. Willemse, K. Tlhomelang, N. Jahed, P. Baker and E. Iwuoha, "Metallo-Graphene Nanocomposite Electrocatalytic Platform for the Determination of Toxic Metal Ions," *Sensors*, vol. 11, pp. 3970-3987, **2011**.

[9] L. Patrick, "Lead Toxicity, A Review of the Literature. Part 1: Exposure, Evaluation, and Treatment," *Alt. Med. Rev.*, vol. 11, no. 1, **2006**.

[10] E. Brodkin, R. Copes, A. Mattman, J. Kennedy, R. Kling and A. Yassi, "Lead and Mercury Exposures: Interpretation and Action," *CMAJ.*, Vols. 176, pp. 59-63, no. 1, **2007**.

[11] M. Ahamed and M. Siddiqui, "Low Level Lead Exposure and Oxidative Stress: Current Opinions," *Clin. Chim. Acta*, Vols. 383, pp. 57-64, **2007**.

[12] B. Lanphear, R. Hornung, J. Khoury, K. Yolton, P. Baghurst, D. Bellinge, R. Canfield, K. Dietrich, R. Bornschein, T. Greene, S. Rothenberg, H.

Needleman, L. Schnaas, G. Wasserman, J. Graziano and R. Ro, "Low-Level Environmental Lead Exposure and Children's Intellectual Function: An International Pooled Analysis," *Environ. Health Perspect.,* Vols. 113, pp. 894-899, no. 7, **2005**.

[13] M. Waalkes, "Cadmium Carcinogenesis in Review," *J. Inorg. Biochem.,* vol. 79, pp. 241-244, **2000**.

[14] P. Das, S. Samantaray and G. Rout, "Studies on Cadmium Toxicity in Plants: A Review," *Environ. Pollut.,* vol. 98, no. 1, pp. 29-36, **1997**.

[15] "Water Services National Information System, WSNIS," DWA (Department of Water Affairs, South Africa), [Online]. Available: http://www.dwaf.gov.za/dir_ws/wsnis/default.asp?nStn=pg_Reports&SAID=207&SASID=539&curPerspectiveID=2. [Accessed 14 October **2013**].

[16] "United States Environmental Protection Agency (USEPA)," [Online]. Available: http://water.epa.gov/drink/index.cfm. [Accessed 14 October **2013**].

[17] J. Wang, B. Tian, J. Wang, J. Lu, C. Olsen, C. Yarnitsky, K. Olsen and D. Hammerstron, W. Bennett, "Stripping Analysis into the 21st Century: Faster, Smaller, Cheaper, Simpler and Better," *Anal. Chim. Acta,* vol. 385, pp. 429-435, **1999**.

[18] M.A. Janusa, J.N. Beck, "Recent Applications of Flame Atomic Absorption Spectroscopy to Environmental Measurements," *Appl. Spectrosc. Rev.,* vol. 37, no. 2, pp. 137-186, **2002**.

[19] T. Inaba, E. Kobayashi, Y. Suwazano, M. Uetani, M. Oishi, N. Nakagawa and K. Nogawa, "Estimation of Cumulative Cadmium Intake Causing Itai-Itai Disease.," *Toxicol. Lett.,* vol. 159, pp. 192-201, **2005**.

[20] L.Y. Vasyukov, "Potentials and Prospects of the Use of Voltammetry for the Analysis of Natural Waters," *J. Anal. Chem.,* vol. 51, pp. 432-442, **1996**.

[21] A. Ala, A. Walker, K. Ashkan, J. Dooley and M. Schilsky, *The Lanchet,* vol. 369, pp. 397-408, **2007**.

[22] J. Li, S. Guo, Y. Zhai and E. Wang, "High-sensitivity Determination of Lead and Cadmium Based on the Nafion-graphene Composite Film," *Anal. Chim. Acta,* vol. 649, pp. 196-201, **2009**.

[23] J. Wang, Analytical Electrochemistry, Hoboken, N.J.: Wiley-VCH, **2006**.

[24] M. Goldcamp, M. Underwood, J. Cloud and S. Harshman, "An Environmentally Friendly, Cost Effective Determination of Lead in Environmental Samples Using Anodic Stripping Voltammetry," *J. Chem. Edu.,* vol. 85, **2008**.

[25] H. Xu, L. Zeng, S. Xing, Y. Xian, G. Shi and L. Jin, "Ultrasensitive Voltammetric Detection of Trace Lead(II) and Cadmium(II) Using MWCNTs-Nafion/Bismuth Composite Electrodes," *Electroanalysis,* vol. 24, no. 20, pp. 2655-2662, **2008**.

[26] B. Claux and O. Vittori, "Bismuth Film Electrode as an Alternative for Mercury Electrodes: Determination of Azo Dyes and Application for Detection in Food Stuffs," *Electroanalysis,* vol. 21, no. 19, pp. 2243-2246, **2007**.

[27] G. Kefala, A. Economou, A. Voulgaropoulos and M. Sofoniou, "A Study Of Bismuth-Film Electrodes for the Detection of Trace Metals by Anodic Stripping Voltammetry and their Application to the Determination of Pb and Zn in Tapwater and Human Hair," *Talanta,* vol. 61, pp. 603-610, **2003**.

[28] G. Long, L. Freedman and G. Doak, "Bismuth and Bismuth Alloys," *Encycl.Chem. Technol.,* pp. 912-937, **1978**.

[29] V. Guzsvany, H. Nakajima, N. Soh, K. Nakano and T. Imato, "Antimony-Film Electrode for the Determination of Trace Metals by Sequential-Injection Analysis/Anodic Stripping Voltammetry," *Anal. Chim. Acta,* vol. 658, pp. 12-17, **2010**.

[30] S. Hocevar, "Antimony Film Electrode for the Electrochemical Stripping Analysis," *Anal. Chem.,* vol. 79, no. 22, pp. 8639-8643, **2007**.

[31] J. Wang, A. Kawde and E. Sahlin, "Renewable Pencil Electrodes for Highly Sensitive Stripping Potentiometric Measurements of DNA And RNA," *Analyst, The Royal Society of Chemistry,* vol. 125, pp. 5-7, **2000**.

[32] A. Ozcan, Y. Sahin, "Preparation of Selective and Sensitive Electrochemically Treated Pencil Graphite Electrodes for the Determination of Uric Acid in Urine and Blood Serum," *Biosens. Bioelectron.,* vol. 25, no. 11, pp. 2497-2502, **2010**.

[33] A. Bond, P. Mahona, J. Schiewe and V. Vicente-Beckett, "An Inexpensive

and Renewable Pencil Electrode for Use in Field-Based Stripping Voltammetry," *Anal. Chim. Acta,* vol. 345, pp. 67-74, **1997**.

[34] G. Wilkes, M. Tant and K. Mauritz, "Ionomers: Synthesis, Structure, Properties and Elasticity," *Eds.; Chapman and Hall: London,* **1997**.

[35] S. Schlick, "Characterization, Theory and Applications," *CRC Press: Boca Raton, FL,* **1996**.

[36] U. Sen, "Nafion/poly(1-vinyl-1,2,4-triazole) Blends as Proton Conducting Membranes for Polymer Electrolyte Membrane Fuel Cells," *J. Power Sources,* vol. 195, no. 23, pp. 7720-7726, **2010**.

[37] J. Li, S. Guo, Y. Zhai, E. Wang, "Nafion–graphene Nanocomposite Film as Enhanced Sensing Platform for Ultrasensitive Determination of Cadmium," *Electrochem. Comm.,* vol. 11, no. 5, pp. 1085-1088, **2009**.

[38] M. Bass, A. Berman, A. Singh, O. Konovalov and V. Freger, "Surface Structure of Nafion in Vapor and Liquid," *J. Phys. Chem.,* vol. 114, pp. 3784-3790, **2010**.

[39] J. Wang, M. Musameh and Y. Lin, "Solunilization of Carbon Nanotubes by Nafion toward the Preparation fo Amperometric Biosensors," *J. Am. Chem. Soc.,* vol. 125, pp. 2408-2409, **2003**.

[40] D. Demetriades, A. Economou and A. Voulgaropoulos, "A Study of Pencil-lead Bismuth-film Electrodes for the Determination of Trace Metals by Anodic Stripping Voltammetry," *Anal. Chim. Acta,* vol. 519, pp. 167-172, **2004**.

[41] T. Kakizaki, K. Hasebe and J. Fresnius, *Anal. Chem.,* vol. 360, pp. 175, **1998**.

[42] A. Erdem, H. Karadeniz and A. Caliskan, "Single-Walled Carbon Nanotubes Modified Graphite Electrodes for Electrochemical Monitoring of Nucleic Acids and Biomolecular Interactions," *Electroanalysis,* Vols. 21, pp. 464-471, no. 3-5, **2009**.

[43] M. Muti, S. Sharma, A. Erdem and P. Papakonstantiou, "Electrochemical Monitoring of Nucleic Acid Hybridization by Single-Use Graphene Oxide-Based Sensor," *Electroanalysis,* Vols. 23, pp. 272-279, no. 1, **2011**.

[44] J. Shen, Y. Hu, M. Shi, X. Lu, C. Qin, C. Li and M. Ye, "Fast and Facile Preparation of Graphene Oxide and Reduced Graphene," *Chem. Mater.,*

vol. 21, pp. 3514-3520, **2009**.

[45] X. Lu, M. Yu, H. Huang and R. Ruoff, "Tailoring Graphite with the Goal ofAchieving Single Sheets," *Nanotechnology,* vol. 10, no. 3, pp. 269-272, **1999**.

[46] C. Berger, Z. Song, X. Li, X. Wu, N. Brown and C. Naud, D. Mayou, T. Li, J. Hass, A.N. Marchenkov, E.H. Conrad, P.N. First, W.A. de Heer, "Electronic Confinement and Coherence in Patterned Epitaxial Graphene," *Science,* vol. 312, no. 5777, pp. 30-33, **2006**.

[47] S. Stankovich, D. Dikin, R. Piner, K. Kohlhaas, A. Kleinhammes, Y. Jia, Y. Wu, S. Nguyen and R. Ruoff, "Synthesis of Graphene-based Nanosheers via Chemical Reduction of Exfoliated Graphite Oxide," *Carbon,* pp. 1558-1565, **2007**.

[48] S. Zbeda, K. Pokpas, S. Titinchi, N. Jahed, P. Baker and E. Iwuoha, "Few-layer Binder Free Graphene Modified Mercury Film Electrode for Trace Metal Analysis by Square Wave Anodic Stripping Voltammetry," *Int. J. Electrochem. Sci.,* vol. 8, pp. 11125-11141, **2013**.

[49] L. Chen, Y. Tang, K. Wang, C. Liu and S. Luo, "Direct Electrodeposition of Reduced Graphene Oxide on Glassy Carbon Electrode and its Electrochemical Application," *Electrochem. Comm.,* vol. 13, pp. 133-137, **2011**.

[50] H. Guo, X. Wang, Q. Qian, F. Wang and X. Xia, "A Green Approach to the Synthesis of Graphene Nanosheets," *ACS Nano,* vol. 3, no. 9, pp. 2653-2659, **2009**.

[51] C. Su, A. Lu, Y. Xu, F. Chen, A. Khlobystov and L. Li, "High-Quality Thin Graphene Films from Fast Electrochemical Exfoliation," *ACS Nano,* vol. 5, no. 3, pp. 2332-2339, **2011**.

[52] Y. Shao, J. Wang, M. Engelhard, C. Wang and Y. Lin, "Facile and Controllable Electrochemical Reduction of Graphene Oxide and its Applications," *J. Mater. Chem.,*Vols. 20, pp. 743-748, **2010**.

[53] W. Weppner, R.A. Huggins, "Electrochemical Methods for Determining Kinetic Properties of Solids," *Annual Review of Mater. Sci.,* vol. 8, pp. 269-311, **1978**.

[54] P. Monk, Fundamentals of Electro-Analytical Chemistry, Chinchester:

John Wiley & Sons Ltd., **2001**.

[55] S. Otles, Handbook of Food Analysis Instruments: Electroanalytical Techniques and Instrumentation in Food Analysis, **2008**.

[56] C. Zoski, Handbook of Electrochemistry, Elsevier, **2007**.

[57] P. Kissinger and W. Heineman, Laboratory Techniques in Electroanalytical Chemistry: 2nd Edition, **1996**.

[58] A. Bard, Electrochemical Methods, New York: Wiley, **2001**.

[59] S. Kounaves, "Chapter 37: Voltammetric Techniques," in *Handbook of Instumental Techniques for Analytical Chemistry*, Settle. F., Prentice Hall PTR, **1997**.

[60] Unknonwn, "University of Cambridge, Department of Chemical Engineering and Biotechnology- Linear Sweep and Cyclic Voltammetry: The Principles," 2013. [Online]. Available: http://www.ceb.cam.ac.uk/pages/linear-sweep-and-cyclic-voltametry-the-principles.html. [Accessed 8 November **2013**].

[61] J.G. Osteryoung, M.M. Schreiner, "Recent Advances in Pulse Voltammetry," *CRC Crit. Rev. Anal. Chem.*, vol. S1, **1988**.

[62] G.E. Bately, T.M. Florence, "Evaluation and Comparison of Some Techniques of Anodic-stripping Voltammetry," *J. Electroanal. Chem.*, vol. 55, pp. 23-43, **1974**.

[63] J.P. Franke, R.A. De Zeeuw, "Differential Pulse Anodic Stripping Voltammetry as a Rapid Screening Technique for Heavy Metal Intoxications," *Arch. Toxicol.*, vol. 37, no. 1, pp. 47-55, **1976**.

[64] H. Kahlert, "Reference Electrodes," in *Electroanalytical Methods, Scholz, F.*, Berlin/Heidelberg/New York, Springer, 2001, p. Chapter 3.

[65] G. Barker, "Square Wave Polarography and Some Related Techniques," *Anal. Chim. Acta*, vol. 18, pp. 118, **1958**.

[66] M. Lovric and S. Komorsky-Lovric, A.M. Bond, "Theory of Square-wave Stripping Voltammetry and Chronoamperometry of Immobilized Reactants," *J. Electroanal. Chem. and Interfacial Electrochem.*, vol. 319, no. 1-2, pp. 1-18, **1991**.

[67] M.A. Janusa, J.N. Beck, "Recent Applications of Flame Atomic Absorption Spectrometry to Environmental Measurements," *Appl. Spectrosc. Rev.*, vol. 37, no. 2, pp. 137-186, **2002**.

[68] P. Protti, Introduction to Modern Voltammetric and Polarographic Analysis Techniques 4th Ed., AMEL Electrochemistry, **2001**.

[69] A. Merkoci, "Electrochemical Sensor Analysis," in *Comp. Anal. Chem.: Barcelo, D.*, UK, Elsevier, **2007**.

[70] E. Alvarez de Eulate and D. Arrigan, "Adsorptive Stripping voltammetry of Hen-egg-white-lysozyme iva Adsorptio-desorption at an Array of Liquid-Liquid Microinterfaces," *Anal. Chem.*, vol. 84, no. 5, pp. 2505-2511, **2012**.

[71] S. Abbasi and K. Khodarahmiyan, F. Abbasi, "Simultaneous Determination of Ultra Trace Amounts of Lead and Cadmium in Food Samples by Adsorptive Stripping Voltammetry," *Food Chemistry*, vol. 128, no. 1, pp. 254-257, **2011**.

[72] L. Piankova, N. Malakhova, N. Stozhko, K. Brainina and A. a. T. O. Murzakaev, "Bismuth Nanoparticles in Adsorptive Stripping Voltammetry of Nickel," *Electrochem. Comm.*, vol. 13, no. 9, pp. 981-984, **2011**.

[73] J. Wang, J. Lu, S.B. Hocevar, P.A.M. Farias, "Bismuth Coated Carbon Electrodes for Anodic Stripping Voltammetry," *Anal. Chem.*, vol. 72, pp. 3218-3222, **2000**.

[74] S. Hocevar, J. Wang and R.P. Deo, B. Ogorevc, "Potentiometric Stripping Analysis at Bismuth-Film Electrode," *Electroanalysis*, vol. 14, no. 2, pp. 112-115, **2002**.

[75] I. Svancara, L. Baldrianova, E. Tesarova, S. Hocevar, S. Elsuccary, A. Economou, S. Sotiropoulos, Ogorevc. and K. B. Vytras, "Recent Advances in Anodic Stripping Voltammetry with Bismuth-modified Carbon Paste Electrodes," *Electroanalysis*, vol. 18, pp. 177, **2006**.

[76] E. Hutton and S.B. Hocevar, B. Ogorevc, "Ex Situ Preparation of Bismuth Film Microelectrode for use in Electrochemical Stripping Microanalysis," *Anal. Chim. Acta*, vol. 537, no. 1-2, pp. 285-292, **2005**.

[77] J. Wang, "Stripping Analysis at Bismuth Electrodes: A Review," *Electroanalysis*, vol. 17, pp. 15-16, **2005**.

[78] F. Arduini, J. Calvo, G. Palleschi, D. Moscone, "Bismuth-Modified Electrodes for Lead Detection," *Trends in Anal. Chem.,* vol. 29, no. 11, pp. 1295-1304, **2010**.

[79] R. Pauliukaite, S. Hocevar and B. Ogorevc, J. Wang, "Characterization and Applications of a Bismuth Bulk Electrode," *Electroanalysis,* vol. 16, pp. 719, **2004**.

[80] A. Economou, "Bismuth-film Electrodes: Recent Developments and Potentialities for Electroanalysis," *Trends in Anal. Chem.,* vol. 24, no. 4, pp. 334-340, **2005**.

[81] T. Copeland and R. Osteryoung, R. Skogerboe, "Elimination of Copper-Zinc Intermetallic Interferences in Anodic Stripping Voltammetry.," *Anal. Chem.,* vol. 46, pp. 2093, **1974**.

[82] H. Huiliang and D. Jagner, L. Renman, "Flow Potentiometric and Constant-current Stripping Analysis for Arsenic(V) Without Prior Chemical Reduction to Arsenic(III): Application to the Determination of Total Arsenic in Seawater and Urine," *Anal. Chim. Acta,* vol. 207, pp. 37-46, **1988**.

[83] E. Hutton, J. van Elteren and B. Ogorevc, M. Smyth, "Validation of Bismuth Film Electrode for Determination of Cobalt and Cadmium in Soil Extracts using ICP–MS," *Talanta,* vol. 63, no. 4, pp. 849-855, **2004**.

[84] R. Kadara, I. Tothill, "Stripping Chronopotentiometric Measurements of Lead(II) and Cadmium(II) in Soils Extracts and Wastewaters using a Bismuth Film Screen-printed Electrode Assembly," *Anal. Bioanal. Chem.,* vol. 378, no. 3, pp. 770-775, **2004**.

[85] N. Lezi, V. Vyskocil and A. Economou, J. Barek, "Electroanalysis of Organic Compounds at Bismuth Electrodes: A Short Review," in *Sensing in Electroanalysis*, University Press Centre, **2012**, pp. 71-78.

[86] V. Guzsvany, Z. Papp, J. Zbiljic and O. Vajdle, M. Rodic, "Bismuth Modified Carbon-Based Electrodes for the Determination of Selected Neonicotinoid Insecticides," *Molecules,* vol. 16, no. 6, pp. 4451-4466, **2011**.

[87] G. Kreft and O. de Braga, A. Spinelli, "Analytical Electrochemistry of Vitamin B12 on a Bismuth-film Electrode Surface," *Electrochim. Acta,* vol. 83, pp. 125-132, **2012**.

[88] M. Kuno, “Introduction to Nanoscience and Nanotechnology: A Workbook,” 2005. [Online]. Available: http://nd.edu/~mkumo/Classdownloads/Chem647nanotext.pdf. [Accessed 15 October **2013**].

[89] SCENIHR, “The Appropriateness of Existing Methodologies to Assess the Potential Risks Associated with Engineered and Adventitious Products of Nanotechnologies.,” European Commision: Health and Consumer Protection Directorate-General.

[90] K. Klabunde, R. Richards, Nanoscale Materials in Chemistry: Second Edition, Hoboken, New Jersey: John Wiley & Sons, Inc., **2009**.

[91] T. Takagahara, K. Takeda, “Theory of the Quantum Confinement Effect on Excitons in Quantum Dots of Indirect-gap Materials.,” *Phys. Rev. B,* vol. 46, pp. 15578-15581, **1992**.

[92] O. Arsenault, Nanochemistry: A Chemical Approach to Nanomaterials, Cambridge: Royal Society of Chemistry, **2005**.

[93] B. Sharma, “Allotropes and Polymorphs,” *J. Chem. Edu.,* vol. 64, no. 5, pp. 404-407, **1987**.

[94] B. Pollard, “Growing Graphene via Chemical Vapor Deposition,” Department of Physics, Pomona College, **2011**.

[95] Unkown, “Reviews in Minerology and Geochemistry,” Geo Science World, [Online]. Available: http://rimg.geoscienceworld.org/content/75/1/47/F1.expansion.html. [Accessed 10 November **2013**].

[96] J. Bunch, S. Verbridge, J. Alden, A. van der Zande, J. Parpia and H. Craighead, P. McEuen, “Impermeable Atomic Membranes from Graphene Sheets,” *Nano Letters,* vol. 8, no. 8, pp. 2458-2462, **2008**.

[97] A. Geim and K. Novoselov, “The Rise of Graphene,” *Nat. Mater.,* vol. 6, pp. 183-191, **2007**.

[98] K. Novoselov, A. Geim, S. Morozov, D. Jiang, Y. Zhang, S. Dubonos and I. a. F. A. Grigorieva, “Electric Field Effect in Atomically Thin Carbon Films,” *Science 22,* vol. 306, no. 5696, pp. 666-669, **2004**.

[99] B. Partoens, F. Peeters, “From Graphene to Graphite: Electronic Structure

Around the K Point," *Phys. Rev. B*, vol. 74, **2006**.

[100] N. Mermin, "Crystalline Order in Two Dimensions," *Phys. Rev.*, vol. 176, pp. 250-254, **1968**.

[101] C. Schonenberger, Bandstructure of Graphene and Carbon Nanotubes: An Excercise in Condensed Matter Physics..

[102] O. Kharisov, "Graphenes, One of the Hottest Areas in the Nanotechnology: Attention of Chemists is Needed," *The Open Inorg. Chem. J.*, vol. 2, pp. 39-49, **2008**.

[103] A. Kuzmenko, E. van Heumen and F. Carbone, D. van der Marel, "Universal Infrared Conductance of Graphite," *Phys. Rev. Letters*, vol. 100, no. 11, pp. 117401, **2008**.

[104] B. Brodie, "Sur le poids atomique du graphite," *An. Chim. Phys.*, vol. 59, pp. 466-472, **1860**.

[105] W. Hummers and R. Offeman, "Preparation of Graphitic Oxide," *J. Anal. Chem. Soc.*, pp. 1339, **1958**.

[106] L. Staudenmaier, "Verfahren zur darstellung der graphitsaure," *Ber. Dtsch. Chem Ges.*, vol. 31, pp. 1481-1499, **1898**.

[107] A. Reina, S. Thiele, X. Jia, S. Bhaviripudi, M. Dresselhaus and J. Schaefer, J. Kong, "Growth of Large-area Single- and Bi-layer Graphene by Controlled Carbon Precipitation on Polycrystalline Ni Surfaces," *Nano Res.*, vol. 2, pp. 509-516, **2009**.

[108] H. Park, J. Meyer and S. Roth, V. Skakalova, "Growth and Properties of Few-layer Graphene Prepared by Chemical Vapor Deposition," *Carbon*, vol. 48, no. 4, pp. 1088-1094, **2010**.

[109] A. Chakrabarti, J. Lu, J. Skrabutenas, T. Xu, Z. Xiao and J. Maguire, N. Hosmane, "Conversion of Carbon Dioxide to Few-layer Graphene," *J. Mater. Chem.*, vol. 21, pp. 9493-9493, **2011**.

[110] G. Jo, M. Choe, S. Lee, W. Park and Y. Kahng, T. Lee, "The Application of Graphene as Electrodes in Electrical and Optical Devices," *Nanotechnology*, vol. 23, **2012**.

[111] M. Voutilainen, H. F. Nokia Res. Center, E. Seppala, P. Pasanen and M. Oksanen, "Graphene and Carbon Nanotube Applications in Mobile

Devices," *Electron Devices, IEEE Transactions,* vol. 59, no. 11, pp. 2876-2887, **2012**.

[112] H. Wang, L. Cui, Y. Yang, H. Casalongue, J. Robinson, Y. Liang and Y. Cui, H. Dai, "Mn3O4−Graphene Hybrid as a High-Capacity Anode Material for Lithium Ion Batteries," *J. Am. Chem. Soc.,* vol. 132, no. 40, pp. 13978-13980, **2010**.

[113] M. Stoller, S. Park, Y. Zhu and J. An, R. Ruoff, "Graphene-Based Ultracapacitors," *Nano Letters,* vol. 8, no. 10, pp. 3498, **2008**.

[114] N. Shang, P. Papakonstantinou, P. Wang and S. Ravi, P. Silva, "Platinum Integrated Graphene for Methanol Fuel Cells," *J. Phys. Chem.,* vol. 114, no. 37, pp. 15837-15841, **2010**.

[115] P. Reunchan, S. Jhi, "Metal-dispersed Porous Graphene for Hydrogen Storage," *Appl. Phys. Lett.,* vol. 98, no. 9, pp. 093103-093103-3, **2011**.

[116] Y. Shao, J. Wang, H. Wu, J. Liu, I. Aksay and Y. Lin, "Graphene Based Electrochemical Sensors and Biosensors: A Review," *Electroanalysis,* vol. 10, pp. 1027-1036, **2010**.

[117] J. Kariuki, "An Electrochemical and Spectroscopic Characterization of Pencil Graphite Electrodes," *J. Electrochem. Soc.,* vol. 159, no. 9, pp. 5, **2012**.

[118] "Analytical I, Characterization of Materials by FT-IR".

[119] P. Griffiths, "Fourier Transform Infrared Spectrometry," *Science,* vol. 222, no. 4621, pp. 297-302, **1983**.

[120] W. Zachariasen, "A General Theory of X-Ray Diffraction in Crystals," *Acta Cryst.,* vol. 23, pp. 558-564, **1967**.

[121] N. Colthup and L. Daly, S. Wiberley, Introduction to Infrared and Raman Spectroscopy, Elsevier, **1990**.

[122] A. Levent and Y. Yardim, Z. Sentruk, "Voltammetric Behaviour of Nicotine at Pencil Graphite Electrode and its Enhancement Determination in the Presence of Anionic Surfactant," *Electrochim. Acta,* vol. 55, pp. 190-195, **2009**.

[123] D. Marcano, D. Kosynkin, J. Berlin, A. Sinitskii, Z. Sun, A. Slesarev, L. Alemany, W. Lu, J. Tour, "Improved Synthesis of Graphene Oxide," *ACS*

Nano, vol. 4, no. 8, pp. 4806-4814, **2010**.

[124] W. Chen and L. Yan, "Preparation of Graphene by a Low-temperature Thermal Reduction at Atmosphere Pressure," *Nanoscale,* vol. 2, pp. 559-563, **2010**.

[125] A. Bourlinos, D. Gournis, D. Petridis, T. Szabo, A. Szeri and I. Dekany, "Graphite Oxide: Chemical Reduction to Graphite and Surface Modification with Primary Aliphatic Amines and Amino Acids," *Langmuir,* vol. 19, pp. 6050-6055, **2003**.

[126] A. Eckmann, A. Felten, A. Mishchenko, L. Britnell, R. Krupke, K. Noveslov, C. Casiraghi, "Probing the Nature of Defects in Graphene by Raman Spectroscopy," *ACS Nano,* Vols. 12, 3925-3930, **2012**.

[127] Y. Zhu, S. Murali, W. Cai, X. Li, J. Won Suk, J.R. Potts, R.S. Ruoff, "Graphene and Graphene Oxide: Synthesis, Properties and Applications," *Adv. Mater.,* vol. 22, pp. 3906-3924, **2010**.

[128] V. Singh, D. Joung, L. Zhai, S. Das and S. Khondaker, S. Seal, "Graphene based Materials: Past, Present and Future," *Science,* vol. 56, pp. 1178-1271, **2011**.

[129] Y. Zhu, "Exfoliation of Graphite Oxide in Propylene Carbonate and Thermal Reduction of the resulting Graphene Oxide Platelets.," *J. Chem. Soc.,* vol. 132, pp. 1227-1233, **2010**.

[130] F. Ban, S. Majid, N. Huang and H. Lim, "Graphene Oxide and Its Electrochemical Performance," *Int. J. Electrochem. Sci.,* vol. 7, pp. 4345-4351, **2012**.

[131] A. Nepal, G. Singh, B. Flanders and C. Sorensen, "One-Step Synthesis of Graphene via Catalyst-Free Gas-Phase Hydrocarbon Detonation," *Nanotechnology,* vol. 24, no. 24, **2013**.

[132] F. Thema, M. Moloto, E. Dikio, N. Nyangiwe, L. Kotsedi, M. Maaza and M. Khenfouch, "Synthesis and Characterization of Graphene Thin Films by Chemical Reduction of Exfoliated and Intercalated Graphite Oxide," *J. Chem.,* vol. 2013, p. 6 pages, **2013**.

[133] D. Zhang, X. Zhang, Y. Chen, C. Wang and Y. Ma, "An Environmentally-friendly Route to Synthesize Reduced Graphene Oxide as a Supercapacitor Electrode Material," *Electrochim. Acta,* vol. 69, pp. 364-370, **2012**.

[134] S. Stankovich, R. Piner and S. Nguyen, R. Ruoff, "Synthesis and Exfoliation of Isocyanate-treated Graphene Oxide Nanoplatelets," *Carbon,* vol. 44, pp. 3342-3347, **2006**.

[135] J. Shen, B. Yan, T. Li, Y. Long and Li, N., *Soft Mater.,* vol. 8, pp. 1831-1836, **2012**.

[136] D. Chen, H. Feng and J. Li, "Graphene Oxide: Preparation, Functionalization and Electrochemical Applications," *Chem. Rev.,* vol. 112, pp. 6027-6053, **2012**.

[137] J. Allen, V. Tung and R. Kaner, "Honeycomb Carbon: A Review of Graphene," *Chem. Rev.,* vol. 110, pp. 132-146, **2010**.

[138] W. Lu, P. Soukiassian and J. Boecki, "MRS Bulletin-Volume 37, Number 12," 2012. [Online]. Available: www.onlinedigeditions.com. [Accessed 15 August **2013**].

[139] W. Yi, Y. Li, G. Ran, H. Luo and N. Li, "A Glassy Carboon Electrode Modified with Antimony and Poly(p-aminobenzene sulfonic acid) for Sensing Lead(II) by Square Wave Anodic Stripping Voltammetry," *Microchim. Acta,* vol. 179, pp. 171-177, **2012**.

[140] F. Torma, M. Kadar, K. Toth and E. Tatar, "Nafion/2,2'-bipyridal-modified Bismuth Film Electrode for Anodic Stripping Voltammetry," *Anal. Chim. Acta,* vol. 619, pp. 173-182, **2008**.

[141] D. Li, J. Jia and J. Wang, "Simultaneous Determination of Cd(II) and Pb(II) by Differential Pulse Anodic Stripping Voltammetry Based on Graphite Nanofibers-Nafion Composite Modified Bismuth-Film Electrode," *Talanta,* vol. 83, pp. 332-336, **2010**.

[142] G. Hwang, W. Han, J. Park and S. Kang, "Determination of Trace Metals by Anodic Stripping Voltammetry using a Bismuth-modified Carbon Nanotube Electrode," *Talanta,* vol. 76, pp. 301-308, **2008**.

[143] G. Lee, H. Lee and C. Rhee, "Bismuth Nano-powder Electrode for Trace Analysis of heavy Metals using Anodic Stripping Voltammetry," *Electrochem. Comm.,* vol. 9, pp. 2514-2518, **2007**.

[144] S. Sounderajan, A. Singh and M. Palarecha, "Determination of Zinc in High Purity Gallium by Differential Pulse Anodic Stripping Voltammetry," *Indian J. Chem.,* vol. 41A, pp. 1433-1435, **2002**.

[145] M. Rahman and M. Won, Y. Shim, "Characterization of an EDTA Bonded Con-Ducting Polymer Modified Electrode: Its Application for the Simultaneous Determination of Heavy Metal Ions," *Anal. Chem.,* vol. 75, pp. 1123-1129, **2003**.

[146] L. Chen, Z. Li, Y. Meng, P. Zhang, Z. Su, Y. Liu, Y. Huang, Y. Zhou and Q. Xie, "Sensitive Square Wave Anodic Stripping Voltammetric Determination of Cd2+ And P2+ Ions at Bi/Nafion/Overoxidized 2-Mercaptoethanesulfonate-Tethered Polypyrrole/Glassy Carbon Electrode," *Sensors and Actuators B: Chemical,* vol. 191, pp. 94-101, **2014**.

[147] M. Imisides, R. John and P.Riley, G. Wallace, "The Use of Electropolymerization to Produce New Sensing Surfaces: A Review Emphasising Electrode Position Of Heteroaromatic Compounds," *Electroanalysis,* vol. 3, pp. 879-889, **1991**.

[148] H. Sopha, S. Hocevar, B. Pihlar and B. Ogorevc, "Bismuth Film Electrode For Stripping Voltammetric Measurement of Sildenafil Citrate," *Electrochim. Acta,* vol. 60, pp. 274-277, **2012**.

[149] K. Asadpour-Zeynali and P. Najafi-Marandi, "Bismuth Modified Disposable Pencil-Lead Electrode for Simultaneous Determination of 2-Nitrophenol and 4-Nitrophenol by Net Analyte Signal Standard Addition Method," *Electroanalysis,* vol. 23, no. 9, pp. 2241-2247, **2011**.

[150] J. Yang, S. Deng, J. Lei, H. Ju and S. Gunasekaran, "Electrochemical Synthesis Of Reduced Graphene Sheet-Aupd Alloy Nanoparticle Composites For Enzymatic Biosensing," *Biosens. Bioelectron.* Vols. 29, 159-166, **2011**.

[151] H. Yang, C. Shan, F. Li, Q. Zhang, D. Han and L. Niu, "Convenient Preparation Of Tunably Loaded Chemically Converted Graphene Oxide/Epoxy Resin Nanocomposites From Graphene Oxide Sheets Through Two-Phase Extraction," *J. Mater. Chem.,* vol. 19, pp. 8856-8860, **2009**.

[152] J. Hass, W. de Heer and E. Conrad, "The Growth And Morphology Of Epitaxial Multilayer Graphene," *J. Phys.: Condens. Matter,* vol. 20, p. 27 pages, **2008**.

[153] Unkown, “Electrochemical Methods of Analysis, Potentiometry”. [Online]. Available:http://intranet.tdmu.edu.ua/data/kafedra/internal/pharma_2.../classes_stud/en/pharm/prov_pharm/ptn/analytical%20chemistry/2%20course/23%20Electrochemical%20methods%20of%20analysis.htm. [Accessed 15 August **2013**].

[154] J. Gong, T. Zhou, D. Song and L. Zhang, “Monodispersed Au Nanoparticles Decorated Graphene as an Enhanced Sensing Platform for Ultasensitive Stripping Voltammetric Detection of Mercury(II),” *Sensors and Actuators B: Chemical,* Vol. 150, 2, pp. 491-497, **2010**.